UNIVERSITÀ DEGLI STUDI DI PADOVA

DIPARTIMENTO DI INGEGNERIA INDUSTRIALE DII

CORSO DI LAUREA MAGISTRALE IN INGEGNERIA MECCANICA

Numerical simulations of Running Specific Prostheses for the evaluation of their structural behaviour during running

Relatore: **Prof. Nicola Petrone**

Laureando: **Alessandro Luisi**
Matricola: **1179822**

Anno accademico 2019/2020

ABSTRACT

Carbon fiber Running Specific Prostheses (RSPs) have allowed athletes with lower extremity amputations to recover their functional capability of running. RSPs are designed to replicate the spring-like nature of biological legs: they are passive components that mimic the elastic potential energy storage and release of tendons during ground contact.

In order to improve performances and comfort, it is necessary to know the structural behaviour and characteristics of prostheses, in terms of mechanical stiffness and loads applied in different conditions during running. In this way it is possible to evaluate which is the most suitable prosthesis according to the athlete and the sport discipline considered.
In literature there are some study examples in which test benches were developed and used to carry out experimental tests with the aim of measuring the mechanical properties of prostheses.
However, there are very few publications concerning the use of numerical analyses that, in a virtual in-vitro environment, allow to perform engineering simulations starting from a CAD model of the examined component.
The main advantage of having a FEM (Finite Element Method) model is the possibility of predicting its mechanical behaviour in several load conditions, even different from what can be performed during laboratory tests, and without the risk of damaging or breaking the prosthetic foot. Furthermore, another advantage consists in the possibility to modify the geometry in few minutes, which is clearly not feasible in experimental reality, and to observe also in this case how the foot behaves under load.

The purpose of this thesis is precisely to define a method for developing a 3D FEM model of a running specific prosthesis, using the ANSYS Workbench software, through which it was possible to predict and study the mechanical behaviour of the foot for different constraint and load conditions.

In this study two typologies of Running Specific Feet (RSF) were evaluated: the Ottobock Runner Standard C-shaped Category 3 and Category 4. As is known, these RSPs are made of carbon fibre composite material. However, the internal layout of prostheses is unknown as manufacturers do not provide this information. In fact, materials, orientation of the sheets, lay-up and number of sheets are unknown. For this reason, the overall mechanical behaviour of the prosthesis was simplified by modelling it using an isotropic material.

Therefore, the first step was to develop a procedure that allowed the calibration of the numerical model using data collected during some in-vitro static bench tests. Thanks to the calibration it was feasible to determine a single equivalent elastic modulus value to be assigned to the material of the prosthesis, by which it was possible to find numerically, known the displacement imposed to the clamp, the reaction forces obtained during the various experimental tests.
Once the model was calibrated, the foot structural behaviour was determined by evaluating the mechanical stiffness of the RSF constrained in different ways: the classification is based on the clamp position, the load ratio value $\rho = F_{XC}/F_{YC}$ with respect the shank/clamp reference frame and

the orientation ϑ_G of Ground impact surface with respect the RSF, in order to simulate several instants of the running stance phase.

Then, the potentiality of the FEM analyses were used, always working in a static environment, to define another method (which, however, is not repeatable) that would guarantee to simulate the prosthesis behavior during a whole running step. The experimental data used to validate the numerical model were collected during an in-vivo outdoor running test session carried on by an elite paralympic athlete.

Finally, having a numerical running step available, that guaranteed a good convergence between FEM results and experimental data, it was assessed the effect on the mechanical behaviour produced by changing the clamp position and by virtual shaping of the prosthesis, modifying the original geometry and creating a new prototype.

INDEX

CHAPTER 1: INTRODUCTION

1.1 History of prostheses

For many years, people are searching for a mechanical solution for amputees, with the aim of enabling the amputees to walk with two legs. Across the years, different solutions were thought, from the first peg leg to the actual carbon fibers Running Specific Prostheses (RSP).

The simplest prototype, the peg leg, was a straight wooden stick harnessed to the thigh; it was focused only to connect the stump with the floor and did not consider ergonomic aspects. It was uncomfortable for the amputees and it could cause chafing or muscle and bone aches. [1]

Along the time, designers tried to build prostheses that resembled a human limb and that imitated a leg and even a foot, for hide the missing leg. In Figure 1.1 is possible to see the evolution of the prosthesis in different periods.

Figure 1.1: A mixture of simple function and mimesis of the human leg in different eras. (Ventura and Shvo, 2017) [1]

Designers and the amputees themselves tried to create and improve more ergonomics and functional prostheses, imitating the behavior of the health limb. For example, in 1957, Federal Government's Artificial Limb program converted various designs into one standard manufactured production model: the Solid Ankle and Cushioned Heel (SACH) foot. This model had a simple design and gives amputees many of foot and ankle functions that are required (Figure 1.2). [2]
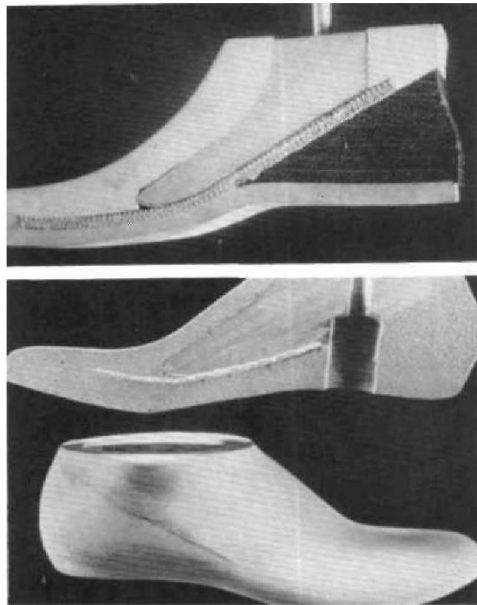
Figure 1.2: SACH Foot (solid-ankle, cushion-heel) [25]

Prosthetic foot designs and materials changed little for approximately 20-30 years after the invention of SACH foot. The big innovation and research improvements in the lower limb prostheses happened in the 1980s, when advances in carbon material flooded the prosthetics industry. Carbon composite materials allow to design prosthetic feet, pylons, and sockets providing lightness, durability, and strength. In 1984, Van Phillips, an American inventor of prostheses, created the "Flex-Foot®" made of carbon graphite (Figure 1.3). Using carbon fiber material, the innovative artificial foot allowed to store and then return elastic energy during the ground-contact phase of gait. [3]
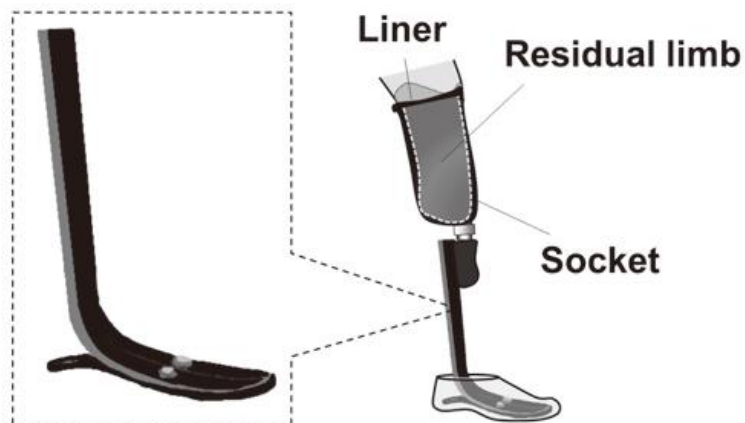
Figure 1.3: Schematic representation of "Flex-Foot®" and prosthetic
components (socket and liner) with representation of a residual limb.
The schema is based on transtibial (below-knee) amputees [3]

The Flex-Foot was the first Running Specific Prosthesis (RSP) used at the 1988 Paralympic Games. Four years later, the prosthetic heel was absent in some athlete's configuration, and this created the first sprint running prosthesis. In fact, the first specialized RSP was developed by eliminating the prosthetic heel and also the stiffness configuration was changed with the layup sequence of carbon fibres while still maintaining the J-shape outline of the carbon forefoot: the Running Prosthetic Foot was called Flex Sprinter I, manufactured by Össur (Reykjavik, Iceland). Nowadays there are several different sprint foot designs available (Figure 1.4).
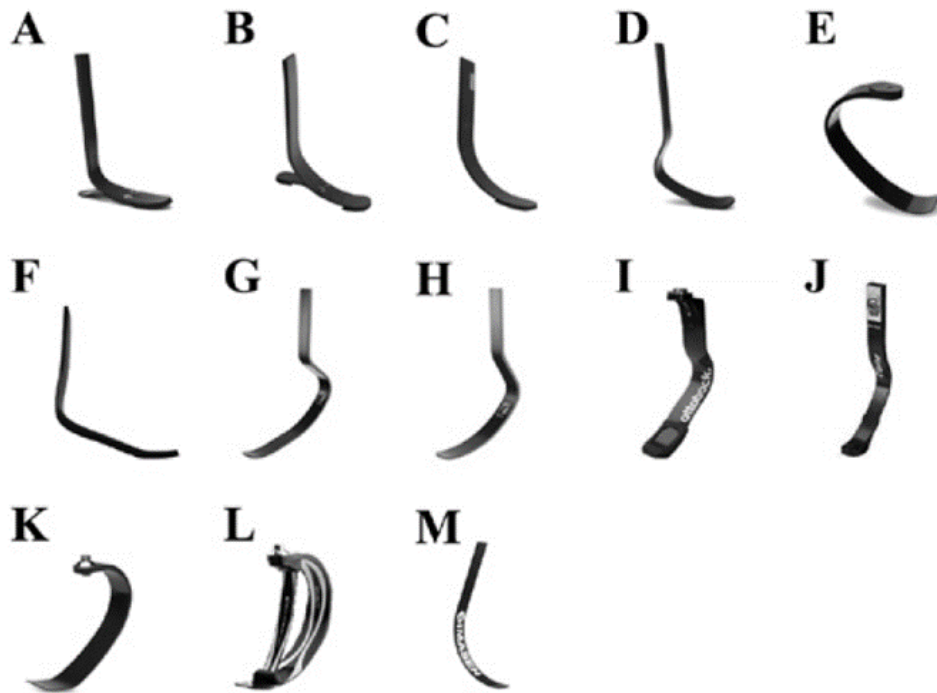
Figure 1.4: A: Flex-Foot® (Modular III; Össur), B: Flex-Sprint II (Össur), C: Flex-Sprint I (Össur), D: Flex-Sprint III® (Cheetah; Össur), E: Flex-RunTM (Össur), F: Symes-Sprint (Össur), G: Cheetah Xtreme®, H: Cheetah Xtend®, I:1E90 (Sprinter, Ottobock), J: 1C2 (C-Sprint®), K: Nitro (Freedom Innovation), L: CatapultTM (Freedom Innovation), M: SP1100 (KATANA, IMASEN Engineering Corporation), N: Rabbit (IMASEN Engineering Corporation). [3]

One of the best examples of the incredible performance improvements that these carbon fiber blades have brought, are the results obtained by Tony Volpentest, an American Paralympian athlete. When he initiated running using the walking prostheses in 1989, his personal record in a 100 m race was only 14.38 s. Later, when he started to use Flex-Foot prosthesis, he won the gold medal at the Atlanta Paralympic Games (1998) in the men's 100 m race by setting a world record with a time of 11.36 s. [3]

For the last 15 years, technical advances in prostheses were a main factor in the increased performance of athletes with lower-limb amputations. The use of materials such as carbon fibres, titanium, and graphite has provided added strength and energy storage capabilities to prostheses while decreasing the weight of prosthetic components. Today, carbon fibres prostheses are most popular in elite running and jumping events.

1.2 RSPs main components

The main components of prostheses are the following (Figure 1.5):

- Socket: portion of the prosthesis that fits around and envelopes the residual limb and to which the prosthetic components are attached. Socket is also important to guarantee performance and comfort at the same time.
- Connecting components: they can be fixed for transtibial amputees or with some degrees of freedom for transfemoral people (prosthetic knee).
- RSP-Running Specific Prosthesis: carbon fiber blade.
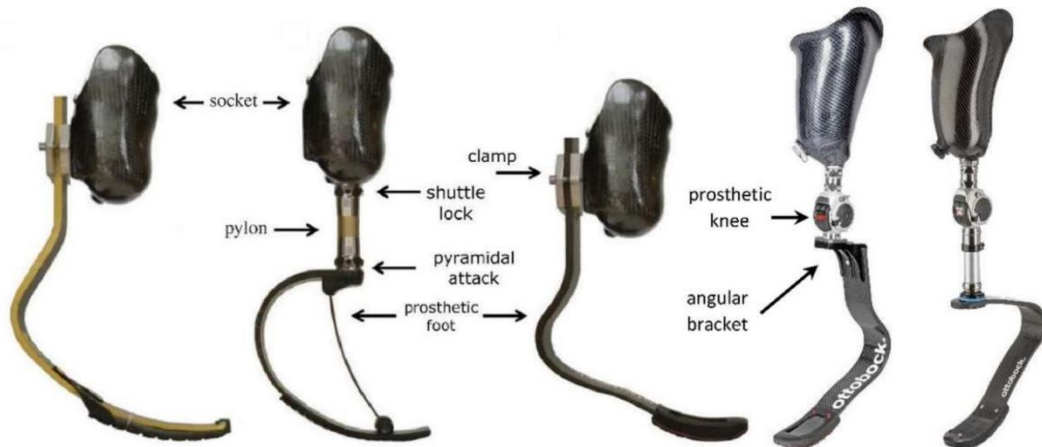
Figure 1.5: Example of main components of prostheses [4]

About the connecting components, there are mainly two types adopted:

- Ottobock® pyramid attack: the pyramidal attack consists of a pyramid receiver and a pyramid adapter in titanium. This system allows to quickly change the foot and allows adjustment of the angles of alignment in the sagittal plane and in the frontal plane, acting on the four screws. This method is usually implemented for C-shaped feet (Figure 1.6).
- Direct connection of the blade to the socket by screws (Figure 1.6). This method is used only on J-shaped prostheses. It is lighter because no adapter is necessary, but less adjustments can be made: sometimes angular wedges are put between the socket and the J-foot to vary the inclination angle in the sagittal plane.
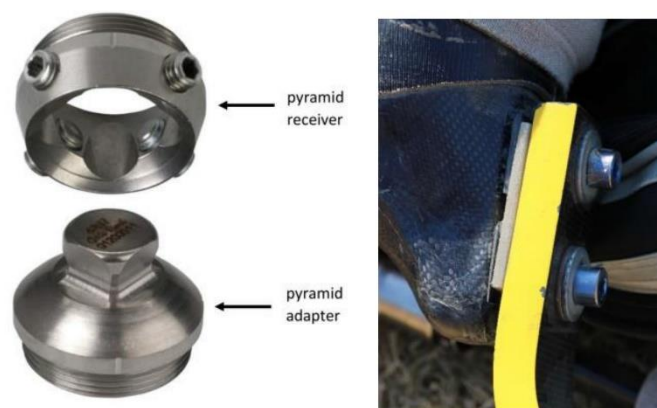
Figure 1.6: Ottobock® pyramid attack (on the left) and fixing with screws (on the right).

1.3: Mass-spring model and biomechanics of running with RSPs

During running, the vertical position of an athlete's centre of mass (COM) reaches its lower position at mid-stance and its highest position at the middle of the swing phase. [4]
This fundamental cyclic bouncing movement is due to the spring-like behaviour of the leg and is well described by a spring-mass model [5]. The model simplifies the leg system during running to a mass-less linear leg spring supporting a point mass that represents the athlete's COM (Figure 1.7). During the first half of stance phase, elastic potential energy is stored in the compressed leg spring. Then, the stored mechanical energy is released during the second half of the ground contact as the leg spring recoils. Therefore the COM can accelerate forward and upward into the swing phase [6]. For this reason the prosthetic foot can be considered as a passive carbon fiber component.
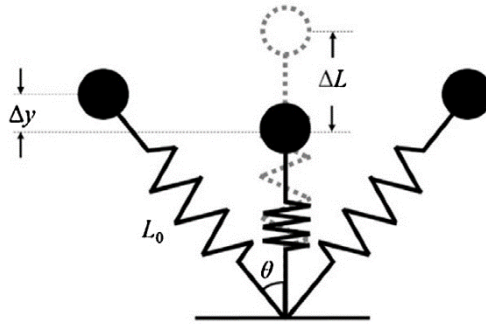
*Figure 1.7: Schematization of the leg during running
with the spring mass-model. (Blickhan, 1989)*

In this model the leg stiffness k_{leg} is defined as the ratio of maximal vertical ground reaction force ($vGRF_{peak}$) to maximum leg compression (ΔL) from touchdown to mid-stance (Figure 1.7).

$$k_{leg} = \frac{vGRF_{peak}}{\Delta L} \tag{1.1}$$

Maximum displacement of the virtual leg spring ΔL is calculated following Farley et al. [7] using the maximum vertical COM displacement (Δy), the length of the leg spring at touch-down, which is estimated to be equal to the standing leg length (L_0), and half of the angle swept by the leg spring while the foot was on the ground (θ):

$$\Delta L = \Delta y + L_0\,(1 - \cos\theta) \tag{1.2}$$

In order to account for differences in the athletes' size, leg stiffness can be made dimensionless by multiplying it by the ratio of L_0 and body weight (BW).

$$K_{leg} = k_{leg} * \left(\frac{L_0}{BW}\right) \tag{1.3}$$

In this model, the leg spring is completely elastic, however the structures of a biological leg are viscoelastic and therefore only a portion of the stored potential elastic energy is returned (due to hysteresis). The spring-like action of the leg conserves a portion of the runner's mechanical energy, theoretically mitigating the additional muscular force and mechanical energy input necessary to maintain running speed. The magnitude of the stored and returned mechanical energy is inversely related to leg stiffness (resistance to compression) and is influenced by the magnitude and orientation of the external force vector acting on the leg. [5] [6] [8]
Moreover, from literature [9], it is known that force isn't perfectly vertical at midstance and RSPs stiffness isn't linear as a linear spring: vGRF vs displacement curves are well interpolated by polynomial equations.

RSF is made in carbon fibre and is put in series with the residual limbs, attached to the socket. This material allows to the prosthesis to reproduce the mechanical energy storage and return of tendons during ground contact, but, conversely biological ankles, RSP can't generate mechanical power and, according to a previous study [10], the energy that is return goes only from 63% to 95%. Also, the prosthesis stiffness can't be varied during running. Instead, biological ankles generate mechanical power through muscles (elastic structures) and this allow to have a 241% of energy return during running at 2.8 m/s.

Y. Sano et al. [11] reported that, in *transfemoral* amputees, K_{leg} of the prosthetic leg was approximately 12% smaller than that of the intact leg. These results are congruent with previous finding [12] demonstrating that *transtibial* amputees wearing RSP have bilateral asymmetry in K_{leg} while running: K_{leg} in transtibial amputee sprinters remained constant or increased with speed in intact limbs, while it remained constant or decreased in limbs using RSPs.

These studies suggest that bilateral asymmetry in spring-like leg behavior may be a common biomechanical characteristic among lower extremity amputees wearing the RSPs while running. Although Y. Sano et al. [11] observed that there was no difference in ΔL, $vGRF_{peak}$ was significantly greater in the intact leg than in the prosthetic leg. These results indicate that asymmetric spring-like leg behavior in *transfemoral* amputees with RSP is mainly due to the bilateral differences in $vGRF$ (Figure 1.8).
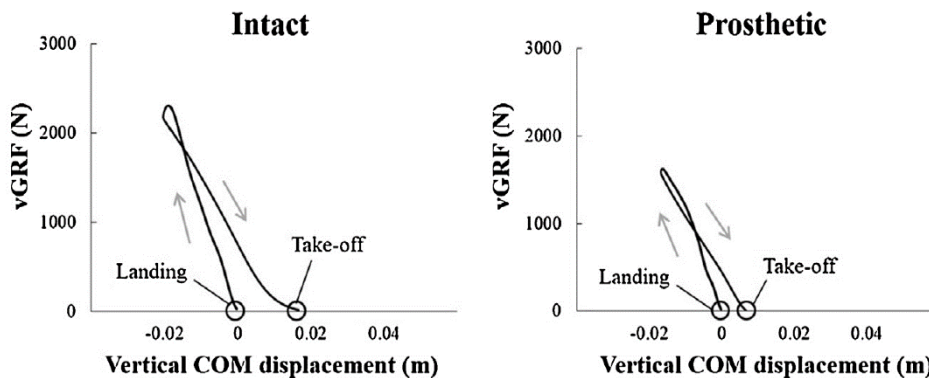
Figure 1.8: Typical examples of vGRF-COM displacement curves
recorded from one subject for the intact (left) and prosthetic leg (right).
Note the bilateral differences in vGRF (Sano et al., 2017) [11]

These results are also similar to those in C.P. McGowan at al. study [12]: in *transtibial* amputees the bilateral differences in K_{leg} during running was mainly due to the differences in $vGRF$. One potential explanation of less force production in prosthetic leg than intact leg in sprinters with amputations may be mechanical properties of RSP and/or muscle weakness due to muscle atrophy. Moreover, in the Grabowski's studies [13], during running, athletes with *transtibial* amputation generate a peak of ground reaction force with their affected leg (AL) that is 2.1/3.3 times body weight (BW) at speeds of 2.5 to 10.8 m/s. However, compared with their unaffected limb (UL), this peak is always lower, as mentioned before.

Similar considerations on *transfemoral* amputees were made by Makimoto at al. [14]: peak forces in vertical, braking, propulsive, and medial directions were significantly greater in intact limbs than those in prosthetic limbs, whereas there were no significant differences in peak lateral force between limbs. Further, the results shown in Figure 1.9 indicate that regardless of the amputation levels, amputee runners generate less braking and equivalent propulsive impulses in their prosthetic limbs wearing running-specific prostheses to the intact limbs during running.

6
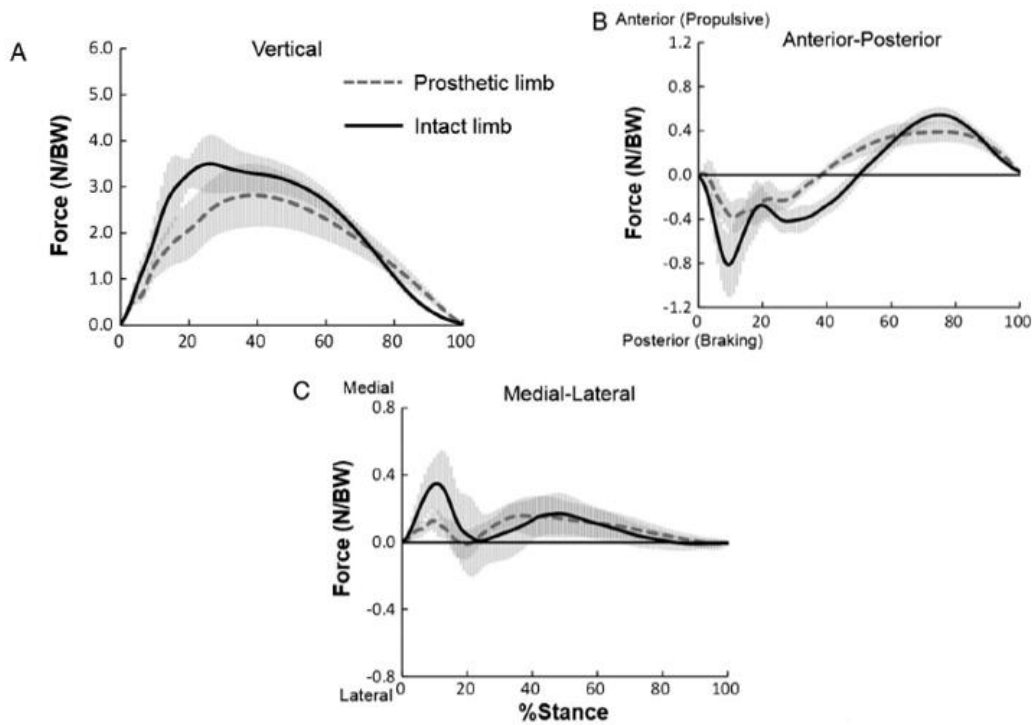
Figure 1.9: GRFs. Average time-course profiles of ground reaction forces (GRFs) of prosthetic (dashed line) and intact (continue line) limbs during maximal sprinting recorded from 9 participants. Shaded area indicates standard deviations. Positive values indicate the vertical (A) and anterior (B) component of the GRFs, respectively. GRFs are normalized with respect to the athlete's weight force, BW. (Makimoto et al., 2017) [14]

The medial and lateral GRFs were not reported in most studies about running and sprinting due to lower magnitude of forces and larger variability compared to the other components of forces. In the Makimoto's study (Figure 1.9), there were no significant differences in medial and lateral impulses between the limbs.

CHAPTER 2: CALIBRATION OF RSF FEM MODEL

2.1 Introduction

In May 2019, at the Laboratory of Mechanical Engineering of the University of Padua, static experimental tests on two C-shaped Ottobock Runner prostheses were performed using bench tests. In order to understand the aim of these experimental tests it is necessary to know that engineers and orthopaedic technicians, specialised in prostheses, are looking for the right foot-socket configuration that could improve performance for elite athletes. Due to the complexity and different shapes of prostheses, it is essential to discover if some alignment is better with respect to another.

For example, considering a prosthetic system used by a transfemoral athlete with a mechanic monocentric knee and a C shape Ottobock RSF, the orthopaedic technician (O.T.) performs the so-called "static alignment". The latter is made on a perch, simulating the midstance, by aligning the athlete's greater trochanter (GT), the centre of the mechanical knee (K) and a distal reference marker placed on the prosthesis. The static alignment can also be guaranteed by changing five main parameters that can allow the athlete to reach the maximum level of performance. [15]
These parameters (Figure 2.1) are:

- Socket flexion angle γ: the angle between the line passing through the GT and the distal end of the socket and the line that passes through the GT and the centre of the knee.
- Position of the clamp (knee-foot joint). In the proximal side of C shape Runner Ottobock foot there is a buttonhole for fixing the knee-foot pyramidal joint, so that can be placed in different positions. This prosthesis part is also curved in the sagittal plane; the centre of this arc of circumference is in the sole of the foot in a position representing the metatarsal joint (indicated by an adhesive): this is called zero point. When the alignment is completed, the zero point must be in the sagittal plane under the GT because it must be the projection of the GT on the ground. Between the two extremities of the buttonhole there are 8° of rotation.
- Foot rotation in the sagittal plane: the rotation could be the result of different adjustment, for example changing the position of the clamp and adjusting screws of the pyramidal joint. This last one induces a forward or backward translation of the foot because the rotation happens around the joint and not around the zero point. To compensate this secondary effect the O.T. can translate the foot to restore the static alignment.
- Position of the tip of the foot / foot advancement: if the zero point is forward the GT-K line the tip of the foot is in an advanced position, vice versa if it is backward.
- Prosthesis height.
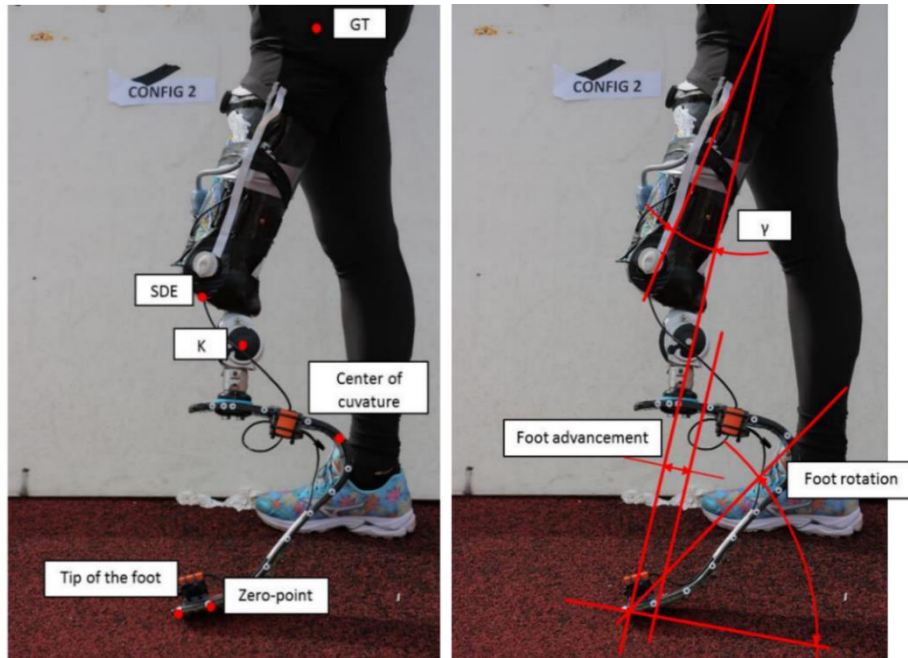
Figure 2.1: Alignment parameters [15]

Instead, for a transtibial athlete, the parameters that must be considered to improve performance in sprint running are known from manuals indications (Figure 2.2) and practical technicians experience. Depending on the type of foot there is a recommended alignment. The most important parameters are the following:

- Median socket axis (red segment in Figure 2.2).
- Socket Tilt (S): angle between the socket axis the perpendicular to the ground.
- TAP (Foot Tip Anterior Posterior): distance between the tip of the prosthesis and the perpendicular to the ground. If, as advised by the technicians, the socket tilt is set equal to 0°, then TAP is the distance between the tip of the prosthesis and the socket axis. TAP can be set changing the position of the clamp and adjusting screws of the pyramidal joint.
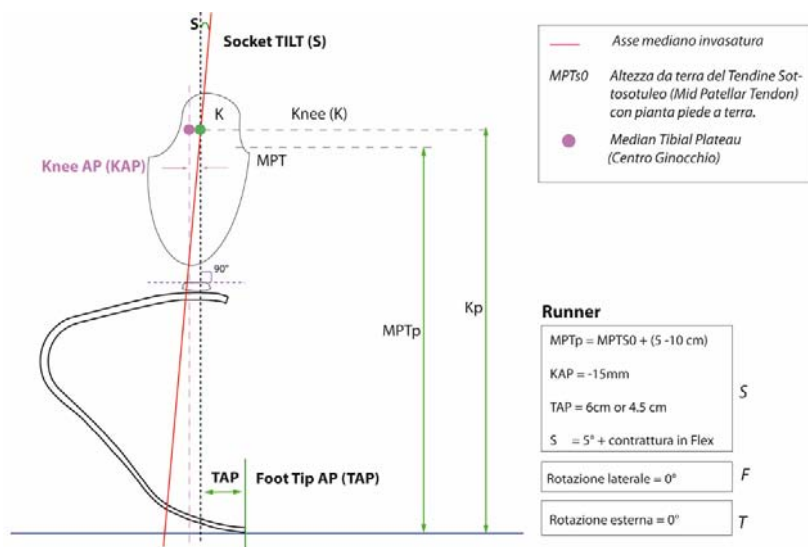
Figure 2.2: Mounting general instructions for transtibial athletes that use C shape Ottobock Runner prosthesis [26]

During the experimental bench tests, clamp adjustment was analysed, considering three different positions (-4°, 0°, +4°) shown in Figure 2.3. The clamp position was chosen because, between the parameters listed before, it is the easiest to modify in field before the run. The clamp allows to connect the prosthesis to the mechanical knee. The position of the clamp modifies the inclination of the foot, but also changes the stiffness of the foot itself.

Figure 2.3: Clamp positions

Therefore, the goal of the experimental tests consisted in evaluating the effect of the clamp position on the stiffness of the prostheses, considering four different instants that occur during the foot contact phase. The four moments considered are outlined in the following Figure 2.4, which will be recreated on the bench by setting the right relative orientation between the socket and the ground.
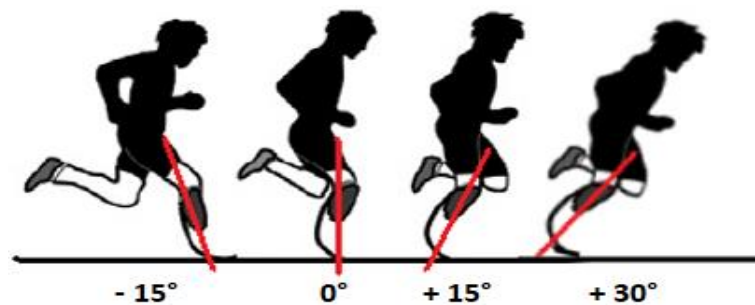
Figure 2.4: Sketch of four different instants during the running stance phase

Simultaneously with the experimental tests, a FEM model of the prosthesis, subject of study of this thesis, was developed. The aim was to reproduce, using the ANSYS Workbench software, the experimental results acquired and then to predict the mechanical structural behaviour of the prosthesis, even for different load conditions with respect to those performed during the tests.

As regards the prosthesis, it is made by overlapping several carbon fibres sheets. Each foil must be considered orthotropic: both strength and stiffness change according to the direction considered. However, the internal layout of the prosthesis is unknown because the manufacturer can not provide this information. In fact, materials, orientation of the sheets, lay-up and number of sheets are unknown.

For this reason, before starting any simulations with composite materials, we asked ourselves if it was possible to simplify the overall mechanical behaviour of the prosthesis by modelling it using an equivalent isotropic material. Therefore, the aim is to determine a single equivalent elastic modulus value by which it is possible to find numerically the forces and/or deformations obtained in the various experimental tests.

2.2 Materials, instrumentation and methods

2.2.1 Bench test for running specific prostheses

The experimental tests were performed using the "Colossus" bench test designed and built in the Laboratory of Mechanical Engineering of the University of Padua [16]. The bench test is shown in Figure 2.5.
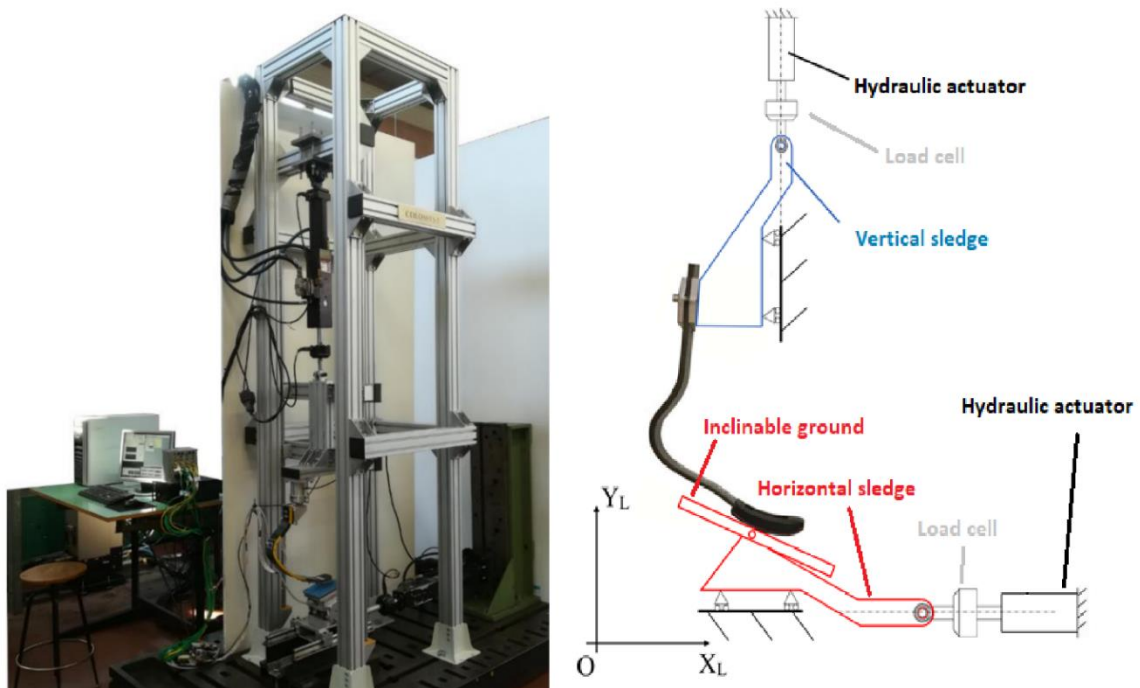
Figure 2.5: Photograph (left) and sketch (right) of the "Colossus" bench test [16]

The bench test has three degrees of freedom: it is equipped with a vertical sledge moved by a hydraulic actuator on which the prosthesis is hooked using the titanium pyramidal joint; the foot is flattened on a platform that can move horizontally thanks to a second slide operated by another hydraulic cylinder. On the top of the platform was put an aluminium plate covered with tartan material, which allows to simulate the real track contact conditions between the ground and RSF. In addition, on the horizontal slide there is a mechanical system with a hinge (Figure 2.6). In this way it is possible to rotate the platform, define the relative orientation between the prosthesis and the ground and to be able to recreate the various instants of the running stance phase (mentioned in the previous section 2.1).

Figure 2.6: Horizontal system of inclination [17]

Two load cells are collocated on the vertical and horizontal cylinders to control forces values and two potentiometers give information about actuators stroke. Also, the bench machine was provide itself by two load cells: a triaxial load cell measured reaction ground forces and it was situated under the contact plate while a 6-axes load cell, placed between the clamp and the vertical sledge, measured forces and torques.

Therefore, using this system it is possible to determine the mechanical stiffness of RSFs, applying a known vertical force (and simultaneously a known horizontal force) and measuring the corresponding reaction forces and cylinders strokes.

2.2.2 Reference Systems and ϑ_{Ground} definition

In literature no standard reference systems were already adopted so it is necessary to present the reference system established in order to evaluate forces, angles and displacements.

The test bench was designed to ideally reproduce the socket of a transtibial athlete. This means that the forces of the hydraulic cylinders are applied in the vertical and horizontal direction in the socket reference frame (X_S, Y_S, Z_S).

During static tests, the socket tilt (as suggested by the technicians, in case of transtibial athlete) and the socket flexion angle (in the case of transfemoral athlete) were not considered. In addition, the foot was simply mounted vertically using the pyramidal joint. During this operation, the screws were not adjusted: therefore, the rotation of the clamp and the rotation of the prosthesis in the sagittal plane, were not changed. For this reason, during tests, the socket reference system coincided with the clamp reference system, which we introduced here. It is a moving frame positioned in the centre of the clamp area in which the vertical axis Y_C is the clamp axis and horizontal axis X_C is tangent to the prosthesis surfaces hooked by the clamp (Figure 2.7).
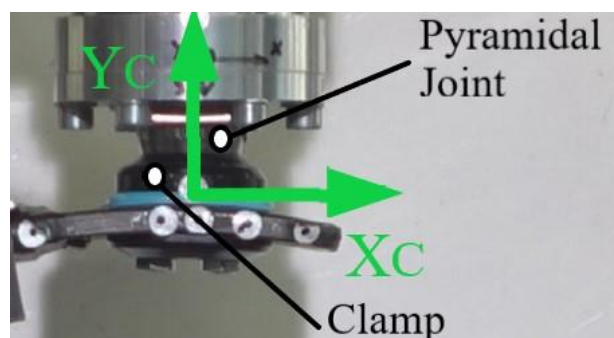
Figure 2.7: Clamp reference system centred in the middle of the clamp

This reference system is very important: all the graphs that will be plotted later will refer to the quantities in the clamp reference system because, during the numerical simulations, the constraints and loads will be read at the clamping area.

However, for the tests, the reference systems adopted [17] are the following ones (Figure 2.8):

- Absolute Lab Reference System (X_L, Y_L, Z_L): inertial reference system fixed outside Colossus bench.
- 6-axes Clamp Reference System (X_C, Y_C, Z_C) or Socket reference frame (X_S, Y_S, Z_S): moving frame centred in the middle of the clamp and translating along the Y_C clamp axis. Here, because the screws were not adjusted, X_C axis is parallel respect to the X_L Lab axis and Y_C is parallel respect to the Y_L Lab axis.
- Ground Reference System (X_G, Y_G, Z_G): moving frame having the Y_G axis orthogonal to the platform and the X_G axis parallel respect to the impact surface.
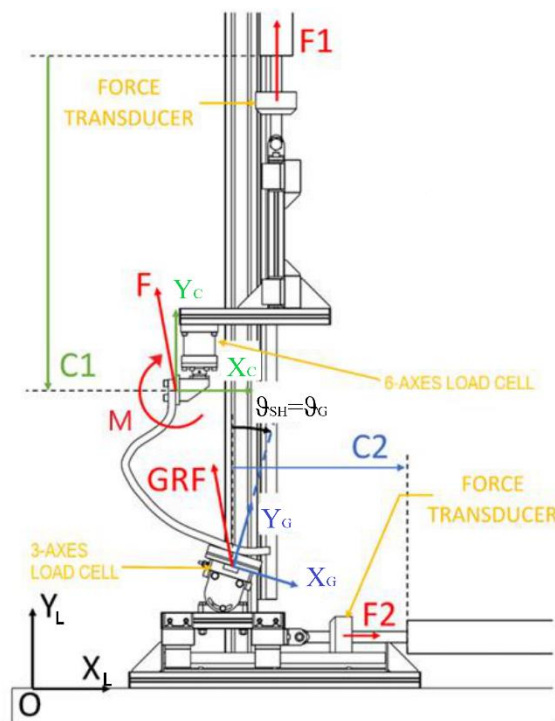
Figure 2.8: Reference systems used in bench tests

Another important definition is the absolute leg angle ϑ_{SH} (Figure 2.8): it is defined as the angle between the socket axis Y_S and the normal to the ground. Obviously, this angle during the step is not constant, but varies during the contact time.

Setting the relative orientation on the sagittal plane between the clamp reference system and the ground one means replicating this relative orientation ϑ_{SH}. This is the principle on which benching tests were executed: if the socket frame is considered fixed in the space, so becoming coincident with the clamp reference system, ϑ_{SH} is recreated by rotating the ground frame. This is the reason why the impact ground surface is rotated during experiments, in order to recreate different contact instants.

This angle will often be called ϑ_{Ground} because the platform was the rotating element of the bench system.

Finally, to describe the RSF behaviour, convention for relative angles ϑ_{Ground} between the clamp reference system and the ground reference system was established: negative angles were used to indicate the braking initial stance phase while positive angles were typical of the propulsive phase after mid-stance (Figure 2.9).

Figure 2.9: Platform inclination angle convention

2.2.3 Prostheses

Two prostheses (Figure 2.10), used by a transfemoral female athlete, were considered during tests:
- RS3, Ottobock Runner Standard C-shaped category 3
- RS4, Ottobock Runner Standard C-shaped category 4

Figure 2.10: RSF Ottobock Runner Standard Category 3 (left) and Category 4 (right)

As previously said, the prostheses were hooked to the vertical system using a pyramid adapter in titanium produced by Ottobock: it ensures to change quickly the foot or to adjust the foot angles orientations with respect to the ground in the frontal and in the sagittal plane acting on 4 screws.

The two prosthetic feet had the spiked plate under their sole, which is important for traction (Figure 2.11). Thanks to spikes and the tartan on the platform it is possible to recreate the same contact conditions that there are on field.

Figure 2.11: Spiked sole of the prosthesis

2.2.4 Static tests description

During all the experimental tests carried out the prostheses were kept vertical while the inclination angle was changed for the lower platform, in order to simulate different instants of the contact phase of the prosthesis with the ground. The bench tests were performed considering various configurations, which were obtained by the combination of:

- 3 different clamp positions: -4°, 0°, + 4°
- 4 different angles ϑ_G of the platform: -15°, 0°, +15°, +30°
- 3 different load ratios applied $\rho = F_{XC}/F_{YC}$: -0.2, 0, 0.2. The sign of ρ depends on the direction of the horizontal force: force F_{XC} is negative or positive in accordance with the X axis of the Lab reference system (oriented as the X_C clamp axis).

All static tests were carried out in force control varying the vertical load F_{YC} using three load steps (500N/1000N/1500N), giving enough time for the stabilization of values, and applying a horizontal force with the second actuator in order to guarantee the desired ratio ρ. It was decided to not exceed these vertical load values because in this way the prosthesis was not stressed excessively (load applied for several seconds). Moreover, at higher loads and for some ground inclination configurations, the tartan was heavily damaged due to the presence of spikes under the prosthesis.

Initial position of the vertical actuator d_{YC}=0 was considered when the prosthesis tip was in contact with the surface without loading it. Displacement d_{YC} was defined, for each load step, as the difference between the final and the initial stroke of the vertical hydraulic cylinder: d_{YC} is the displacement from the first contact condition. Forces were measured using the test bench load cells.

2.3 Creation of prostheses CAD Models using SolidWorks

First, the CAD models of the two prostheses were made using SolidWorks software since these were not provided by the manufacturer. In particular, the two models were created using two different approaches:

- RS3: made by importing the photograph of the prosthesis profile in the sagittal plane, with the correct dimensional scale, and taking care to consider the correct thickness and depth of the prosthesis (Figure 2.12).
- RS4: created by 3D scanning of the prosthesis, then imported the acquired file into SolidWorks to correct it. The corrections were made due to the fact that carbon fibres are a reflective material, not optimal for laser scanning, so the starting model had slightly uneven surfaces.

Figure 2.12: Prosthesis Ottobock Standard Category 3 CAD model

Both CAD models were created for without modelling the sole and spikes. In addition, the buttonhole in proximal part of prostheses was modelled as a circumference arc in the sagittal plane, with the centre coincident with the zero point (Figure 2.13) as described in section 2.1.
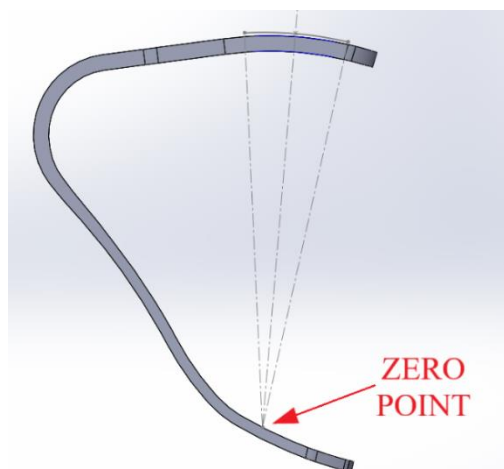

Figure 2.13: Zero Point in the CAD model

For the prosthesis Ottobock standard Category 3, a parametric sketch of the external profile of the prosthesis in the sagittal plane is shown below (Figure 2.14); in this way the reader has the opportunity to replicate the CAD drawing. The sketch was obtained by dividing it into 6 segments "S" (lines or circumference arcs) and in 7 remarkable points "P" (end points of the segments). All segments were drawn tangent to each other at the connection points. In Tables 2.1 and 2.2 the following informations were reported:

- The coordinates of the points P (Table 2.1) and the coordinates of the centres C of the circumference arcs (Table 2.2) with respect to the Clamp reference frame (X_C, Y_C) placed in the centre of the clamp when it is positioned at the buttonhole centre (clamp 0°). Note also in Figure 2.14 that the centre C1 coincides to the zero point and the radius of the segment S1 has its own centre in C1. The coordinates are reported in millimeters.
- Radius (R) of the circumference arcs and the length (L) of the straight section using the blue color (Figure 2.14 and Table 2.2). Dimensions are reported in millimeters.
- Angular dimension $(\Delta\gamma)$ of the circumference arcs or inclination of the straight section with respect to the horizontal axis of the clamp using the red color (Figure 2.14 and Table 2.2).
- Thickness (in millimeters) of the prosthesis in the sagittal plane, at the points P, using the black color (Figure 2.14 and Table 2.1). Thicknesses between the various points vary linearly with the curvilinear abscissa.

It is always necessary to remember that the CAD model and these coordinates were obtained by importing the photograph of the prosthesis, so the final geometry may be subject to some inaccuracies. However it can be considered a good starting model for subsequent simulations.
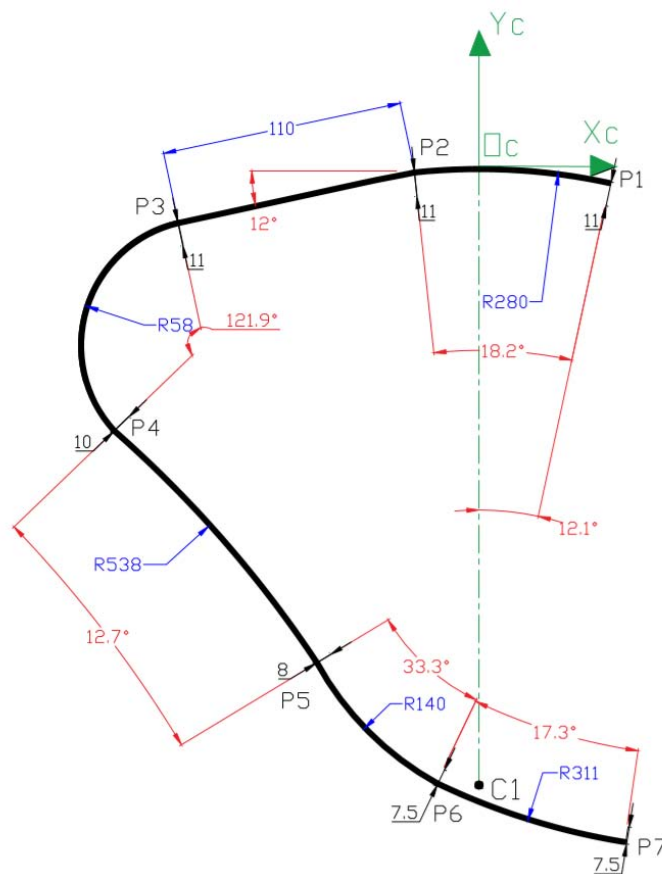

*Figure 2.14: Parametric sketch of the external profile of the prosthesis
Ottobock standard Category 3 in the sagittal plane*

Points P	Coordinates [mm]	Thickness [mm]
P1	(+59.5 ; -7)	11
P2	(-29 ; -2)	11
P3	(-136.5 ; -25)	11
P4	(-166 ; -120.5)	10
P5	(-74 ; -225.5)	8
P6	(-19.5 ; -280.5)	7.5
P7	(+66 ; -307.5)	7.5

Table 2.1: Coordinates of the points P and thicknesses of the prosthesis in the sagittal plane (in millimeters)

Segment	End points	L [mm]	R [mm]	$\Delta\gamma$ [deg]	C Coordinates [mm]
S1	P1-P2	/	280	18.2	C1 (0 ; -280)
S2	P2-P3	110	∞	12	/
S3	P3-P4	/	58	121.9	C3 (-123.5 ; -81.5)
S4	P4-P5	/	538	12.7	C4 (-517 ; -520)
S5	P5-P6	/	140	33.3	C5 (+48.5 ; -158.4)
S6	P6-P7	/	311	17.3	C6 (+115 ; +1.5)

Table 2.2: Length L, radius R , angular dimension $\Delta\gamma$ of the segments and coordinates of the centre of circumference arc segments

In addition, three different configurations in the upper part of the prosthesis were created, each having an area that represents one of the clamp positions considered during the experimental bench tests. These three clamp positions are shown below in Figure 2.15.
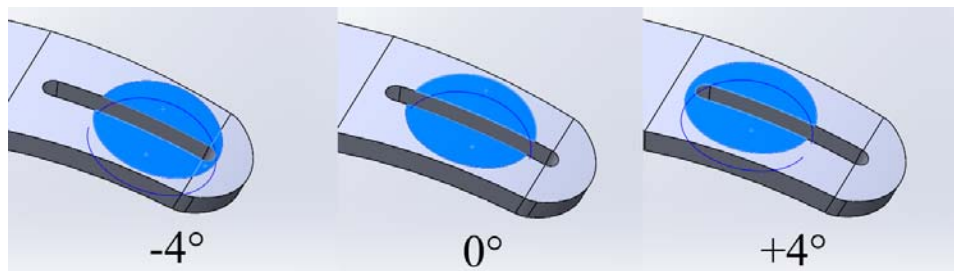
Figure 2.15: CAD Clamp configurations (-4°/0°/+4°)

Finally, a parallelepiped (300x150x20mm) was created and used as horizontal platform. With SolidWorks the assemblies, with the prosthesis and the platform, were made to reproduce the different ground configurations of the experimental tests (Figure 2.16), imposing the correct orientation (-15°, 0°, +15°, +30°) between the axis of the clamp Y_C and the perpendicular axis Y_G to the platform.
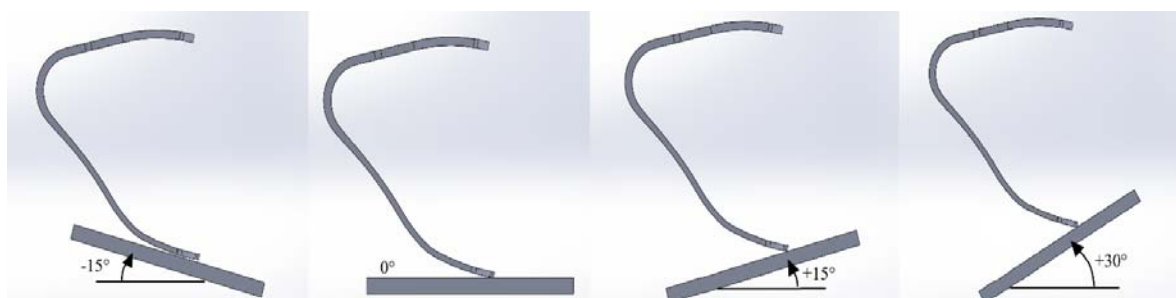
Figure 2.16: Four Ground configurations (-15°/0°/+15°/+30°) for each clamp positions

2.4 Numerical validation in ANSYS Workbench

In this validation phase, only the prosthesis Ottobock Category 3 was considered.
The software ANSYS Workbench was used. The type of analysis performed is the static structural. Therefore, the "Static Structural" toolbox was chosen from the left menu of the project screen (Figure 2.17). The box presents the different subfields [18] ordered according to the logical sequence that is used to perform a finite element analysis:

- Engineering Data (materials definition)
- Geometry (geometries definition)
- Model (creation of FEM model and mesh)
- Setup (settings, constraints and loads)
- Solution (setting the FEM solver)
- Results (processing of results)
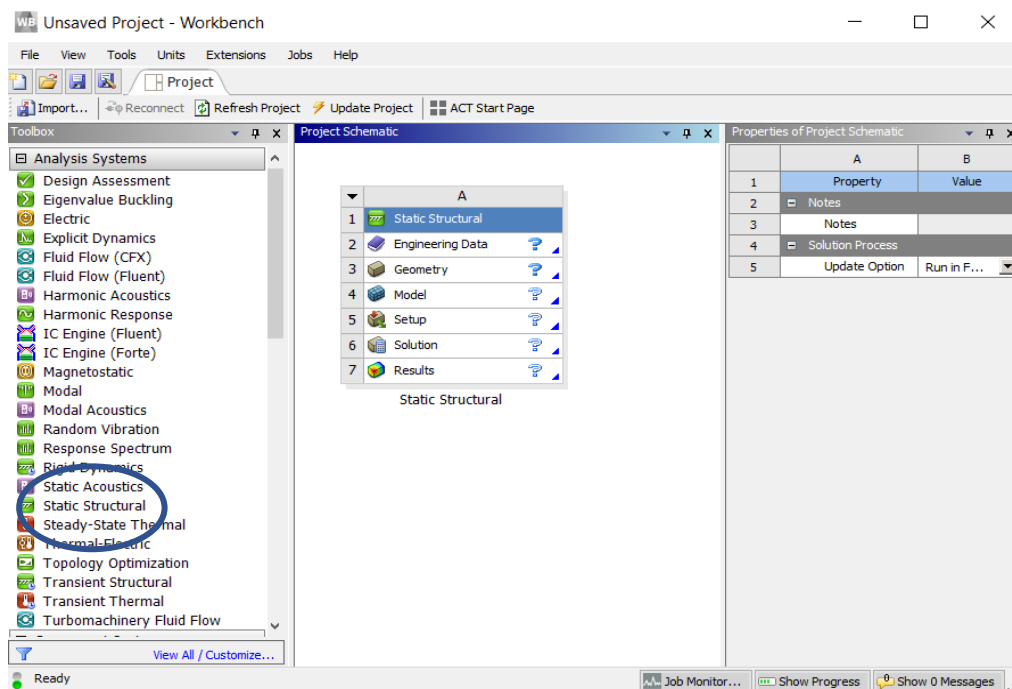
Figure 2.17: ANSYS Workbench project screen. The static structural toolbox is highlighted

2.4.1 Creation of the materials library

ANSYS Workbench has an ample library of materials inside. It is also possible to manually create the materials to be added to the project and it is also possible to realize a customised library. Since during these computer tests it will be necessary to perform more simulations by modifying the unknown equivalent material of the prosthesis, a material library was created for this purpose.
To create a new library was selected Engineering Data → Engineering Data Sources → "Click here to add a new library".

To create a new material to add to the library:
- Activate "Edit Library"
- In "Outline" click on "Click here to add a new material" and write the name for the new material
- On the left list click on "Linear Elastic" and drag the "Isotropic Elasticity" box to "Property"
- Define the properties of Young elastic modulus and the Poisson's ratio for the material
- Follow the previous steps for all added materials
- Save the library

The lower platform it is made using Tartan material (polyurethane). Properties are shown in Figure 2.18.
- Young's elastic modulus E = 600 MPa
- Poisson's ratio ν = 0.38
- Density ρ = 746 kg/m^3

		A	B	C	D	E
		Property	Value	Unit		
1		Property	Value	Unit		
2		Material Field Variables	Table			
3		Density	746	kg m^-3		
4		Isotropic Elasticity				
5		Derive from	Young's Modulus and Poisson...			
6		Young's Modulus	600	MPa		
7		Poisson's Ratio	0,38			
8		Bulk Modulus	833,33	MPa		
9		Shear Modulus	217,39	MPa		

Figure 2.18: Proprieties of Tartan material

For the prosthesis, as already explained in the paragraph 2.1, the properties of the material are not known. Therefore, many equivalent isotropic materials were created and for each of them a different value of Young's modulus of elasticity were chosen. Numerical validation consists in finding a single equivalent elastic modulus value which allows to estimate the real mechanical behaviour of the prosthesis.

2.4.2 Importing the geometry

In ANSYS Workbench it is possible to create geometries using the internal modeler or it is possible to import the geometries developed in an external CAD environment. In this case, therefore, by right clicking on "Geometry" of the project box, the CAD geometry previously saved as ".IGS" file was imported.
Then, the CAD model was divided in half using the internal modeler "DesignModeler" of ANSYS Workbench (Figure 2.19). In order to obtain this, it is necessary to create a division plane and use the "Slice" tool to slice all the bodies for that plane. Then one of the two halves was suppressed. In this way, it was possible to reduce the number of nodes used and the calculation time.
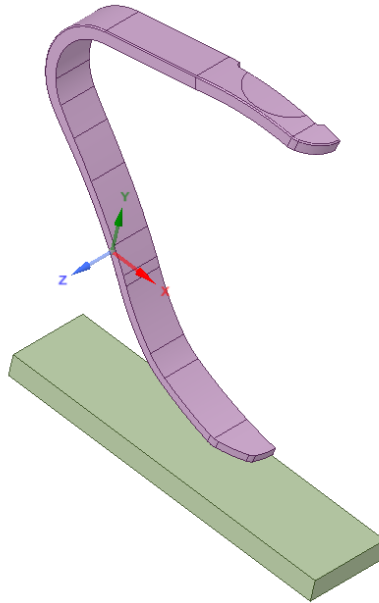
Figure 2.19: Half prosthesis CAD model

In addition, a 1 mm fillet surface was created along the entire profile of the prosthesis to help the convergence. In fact in this way, for many configurations, the initial contact between the ground and the prosthesis tip will take place along this surface, desirable condition, and not on an edge (Figure 2.20).
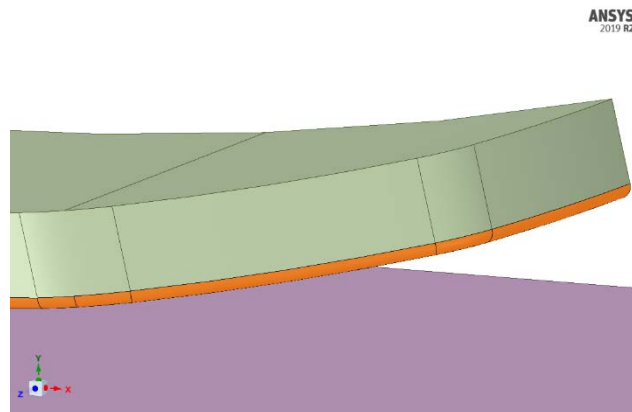
Figure 2.202.19: 1mm fillet surface along the whole profile of the prosthesis

2.4.3 FEM Preprocessing

In order to start the pre-processing phase, the "Model" field in the "Static Structural" box of the project was opened. In this way, the previously imported geometry was recreated in the FEM environment.

By selecting and opening "Geometry", the two solid components appear on the left (the prosthesis and the platform). By clicking on the two elements, the possibility of attributing material properties to each of them appears at the bottom left. Tartan material was assigned to the platform while one of the equivalent materials previously created was assigned to the prosthesis.

Then the model discretization was performed by creating the mesh. During a contact analysis, it is necessary to carry out a good discretization near the area of interest if you want to know in detail the status of the contact during the simulation. However, since we have focused only on how the prosthesis is globally deformed and how the reaction forces changed, it is not essential to create a fine mesh in the contact area.

A possible example of mesh (Figure 2.21) could be the following:

- Mesh mapped on the surface of the fillet and on the contact faces using the "Face Meshing" command.
- A size control ("Sizing") on the prosthesis and on the platform. It was assigned the size 2mm to the fillet, 6mm to the prosthesis and 8mm to the platform, with the "soft" option. In this way the mesher will try to create elements of that size but with a certain adaptability in the management of the size.
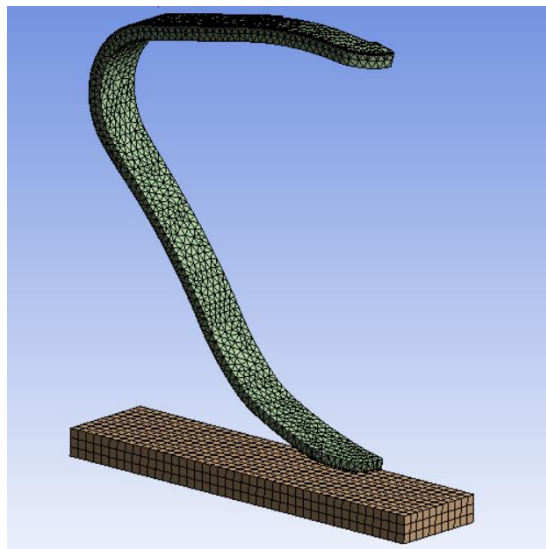
Figure 2.20: Mesh of the prosthesis model

Therefore, the contact between prosthesis and platform was defined. ANSYS Workbench automatically recognizes the surfaces in contact if the CAD model has multiple bodies "close" to each other. Clearly it is necessary to verify that the assumption made by ANSYS is correct. Optionally, it is possible to modify it or it is possible to manually define the contact surfaces using, always from the tree on the left, the "Connections" branch: Connections → Contacts → Insert → Contact manual region.

Afterwards, the following contact properties [19] were set in the lower left window (Figure 2.23):

- First the contact's behaviour was defined. An "asymmetric" type contact was set: contact having all the contact elements on one surface and all the target elements on the other surface. This is usually the most efficient way to model surface-to-surface contact. The "contact geometry", highlighted by FEM with the red colour, was matched to the lower surfaces of the prosthesis while the "target geometry" was assigned to the contact surface of the platform (blue colour). However, it was observed that, by inverting the contact and target surfaces, the outputs of interest that will be analysed do not undergo appreciable changes. The selected surfaces are shown in the Figure 2.22.

Figure 2.21: Contact prosthesis surfaces (red colour) and
Target ground surface (blue colour)

- A "Frictional" contact type was defined. In this way the two bodies can separate to each other (just as happens experimentally at the tip of the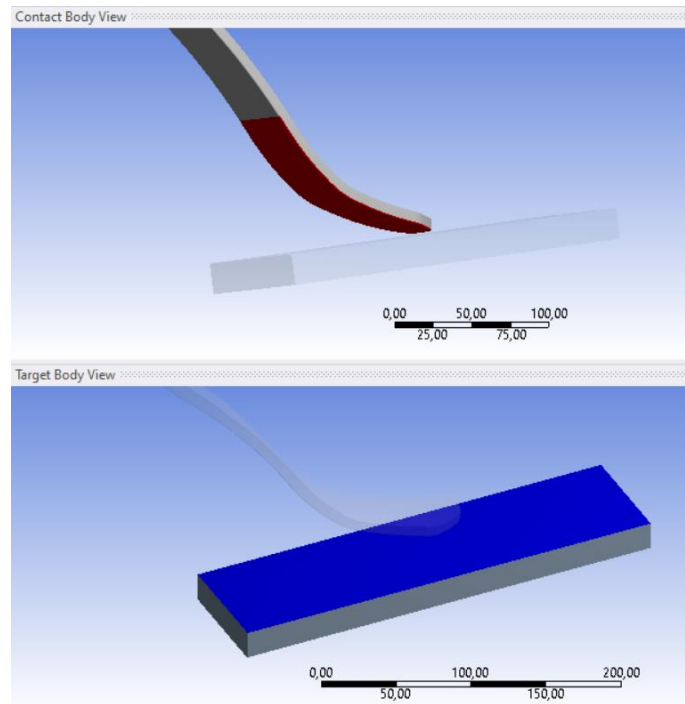 prosthesis respect to the tartan) and they can carry shear stresses up to a certain amplitude through their interface before starting to slide the one respect the other. Once the shear stress is exceeded, the two geometries will slide together.

  Since the two bodies can separated in the normal direction, the frictional contact turns out to be a nonlinear contact. A model with nonlinear contact requires that the matrix inversion be repeated until the convergence tolerance is satisfied. The use of these types of contact usually involves longer solution times and may have possible convergence problems due to the non-linearity of the contact. If there are convergence problems, consider using a finer mesh on the faces or edges of the contact.

  To simulate the presence of spikes between prosthesis and tartan, a high friction coefficient equal to μ=1 was assumed. This prevents sliding between the contact surfaces.

- ANSYS has several algorithms for contact management. It is set to Advanced → Formulation: "Augmented Lagrange". This formulation is recommended in problems with friction where penetration can be important and in large deformations problems.

- Normal stiffness factor is a parameter that influences both accuracy and convergence. Smaller is this factor, greater is the penetration (lower is the contact stiffness) and faster is the convergence. A large stiffness value provides greater precision, but the convergence can become more difficult to achieve. In fact, if the contact stiffness is too large, the model could oscillate.

  The default normal stiffness is automatically defined by the simulation, but the user can manually enter a value. "1.0" is the default value from ANSYS. For bending problems, it is recommended to manually enter a "Normal stiffness factor" from "0.01" to "0.1". So, "0.1"

24

was used as "Factor". Moreover, with the "Update Stiffness" command, it is also possible allow to ANSYS to update the stiffness of the contact between each iteration.

- The contact status is monitored in an area identified by the "Pinball Region". It is a spherical region surrounding each contact identification point (node). A 20 mm radius is set for the pinball region.

Details of "Frictional - Cat3_0°_0°_sez\RSP Ottobock CAT3 To Cat3_0°_0°_sez\Ground"	
Scope	
Scoping Method	Geometry Selection
Contact	14 Faces
Target	1 Face
Contact Bodies	Cat3_0°_0°_sez\RSP Ottobock CAT3
Target Bodies	Cat3_0°_0°_sez\Ground
Protected	No
Definition	
Type	Frictional
Friction Coefficient	1,
Scope Mode	Manual
Behavior	Asymmetric
Trim Contact	Program Controlled
Suppressed	No
Advanced	
Formulation	Augmented Lagrange
Small Sliding	Program Controlled
Detection Method	Program Controlled
Penetration Tolerance	Program Controlled
Elastic Slip Tolerance	Program Controlled
Normal Stiffness	Factor
Normal Stiffness Factor	0,1
Update Stiffness	Each Iteration
Stabilization Damping Factor	0,
Pinball Region	Radius
Pinball Radius	20, mm
Time Step Controls	None
Geometric Modification	
Interface Treatment	Add Offset, No Ramping
Offset	0, mm
Contact Geometry Correction	None
Target Geometry Correction	None

Figure 2.22: Settings of the contact between prosthesis and platform

2.4.4 Loads, constraints and analysis settings

Before explaining how to set the loads and constraints in ANSYS Workbench, it is necessary to present the idea behind these simulations.

As mentioned before, the experimental tests were carried out by lowering the vertical hydraulic cylinder, to which the prosthesis was attached, while the horizontal cylinder was connected to the mobile platform. The tests were carried out in force control in order to obtain the various load configurations desired. From the experimental tests the forces involved in the X_C and Y_C direction (thanks to the 6 axis load cell for example) are known, as well as the displacement d_{YC} of the vertical cylinder.

As the experimental tests, during FEM simulations the prosthesis was kept vertical while the inclination of the ground was changed. All loads and constraints are applied in the clamp reference system (X_C, Y_C): on ANSYS, a displacement in the Y_C direction equal to d_{YC} of the vertical actuator

is applied to the prosthesis clamp area. Additionally, the platform was constrained from moving in the Y_C direction but is left free to move in the X_C direction. The platform can also slide without any F_{XC} force that is opposed to the motion direction. In this way it was possible to simulate all load tests at $\rho = F_{XC}/F_{YC} = 0$.

Instead, for tests at ρ≠0 with the presence of a force $F_{XC} \neq 0$, the idea was to carry out the simulations using two load steps:
1st step: the prosthesis was lowered in Y_C direction by a few millimeters so that the tip was in contact with the platform, which is left free to slide;
2nd step: while the clamp area is constrained to move by a displacement equal to d_{YC}, the force F_{XC} in the X_C direction is applied on one of the side faces of the platform.

Then the simulations were carried out, imposing the displacement of the prosthesis d_{YC} (and F_{XC} for ρ≠0 test), by iterating the value of the equivalent elastic modulus of the prosthesis until finding a satisfying match between the experimental known force F_{YC} and the numerical reaction force read as FEM output. Correspondence is reached when the relative error on the vertical force $err_{F_{YC}}$, calculated using the Equation (2.1), is lower than a certain value chosen by the user (typically 5-10%).

$$err_{F_{YC}}(d_{YC}) = \left| \frac{F_{YC,FEM}(d_{YC}) - F_{YC,exp}(d_{YC})}{F_{YC,exp}(d_{YC})} \right| \, (\%) \qquad (2.1)$$

The flow chart used during numerical tests is shown in the following Figure 2.24.
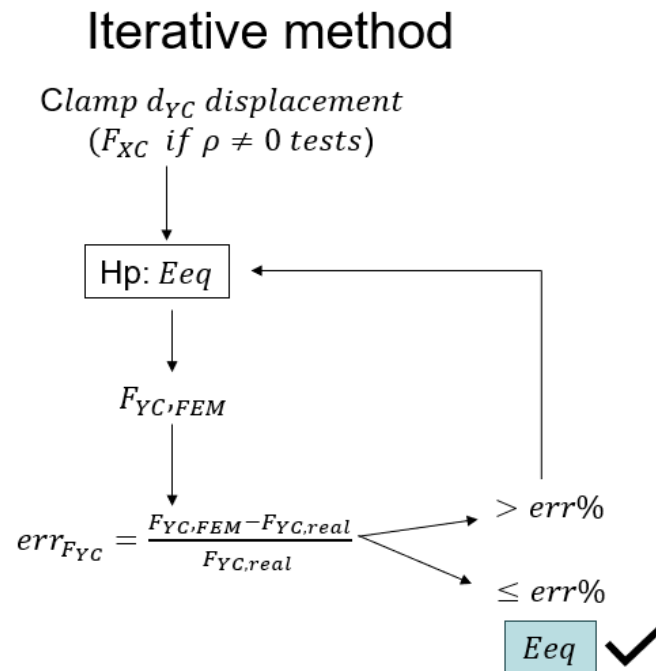

Figure 2.23: Iterative method followed during the calibration tests

These conditions just described were recreated in ANSYS Workbench. In the features tree in correspondence with the "Static Structural" branch there is the "Analysis Settings" sub-field that allows to define to the solver controls.

First on "Step Controls", in "Number of Steps", "2" was put; in this way two load steps were created. The presence of contact makes this problem non-linear. To solve problems of this type, the software applies the load gradually, verifying the convergence step by step. The following controls [18] are set to manage and govern convergence (Figure 2.25):

- The "Auto Time Stepping" option was chosen in "On" mode. This informs the software that you want to control the load application split.
- Set "Define by" to "Substeps": the software will gradually apply the load by providing several equal increments between them.
- "Initial Substep": the software is told that it is desired to apply the load on a certain number of steps (ex 100 substeps).
- Minimum "Minimum Substeps": the software wants to split the application of the load in no less than n-steps (ex: 100).
- "Maximum Substeps": if there are difficulties in numerical convergence, the software can automatically slow down the application of the load by dividing it to, for example, 1500 substeps.

These controls are set for both the two load steps. For the second load step it is possible to reduce the number of substeps with which the load is divided.

In addition, on "Solver Controls", the "Large Deflection" option was put in "On" mode. This setting introduces another non-linearity into the system.

Details of "Analysis Settings"	
Step Controls	
Number Of Steps	2,
Current Step Number	1,
Step End Time	1, s
Auto Time Stepping	On
Define By	Substeps
Initial Substeps	100,
Minimum Substeps	100,
Maximum Substeps	1500,
Solver Controls	
Solver Type	Program Controlled
Weak Springs	Off
Solver Pivot Checking	Program Controlled
Large Deflection	On
Inertia Relief	Off
Rotordynamics Controls	
Restart Controls	
Nonlinear Controls	
Output Controls	
Analysis Data Management	
Visibility	

Figure 2.24: Details of Analysis Settings

On ANSYS Workbench loads and constraints are always inserted in the features tree in correspondence with the "Static Structural" branch (Figure 2.26). Once the branch is selected, simply click with the right mouse button to access to all the available functions.
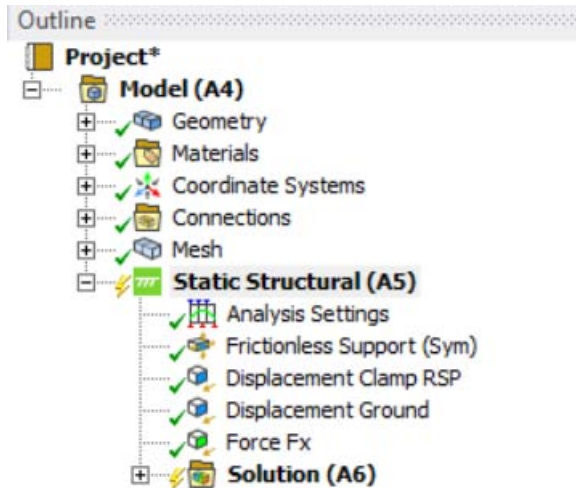
Figure 2.25: Summary of loads and constraints applied

Loads and constraints [20] used are the following (in the following figures a configuration with 0° of platform inclinations and 0° clamp position will be shown):

- If a half prosthesis model is considered, it is necessary to introduce the symmetry constraint (Figure 2.27). To do this, one of the possibilities offered by ANSYS Workbench is to use the "Frictionless Support" constraint. This constraint must be applied on the sectioned faces of the prosthesis and the platform.

Figure 2.26: Symmetry constrain applied on the sectioned faces of the model (blue colour)

- The movement in Y_C direction of the prosthesis was applied by using the "Displacement" command and applying it to the clamp areas on the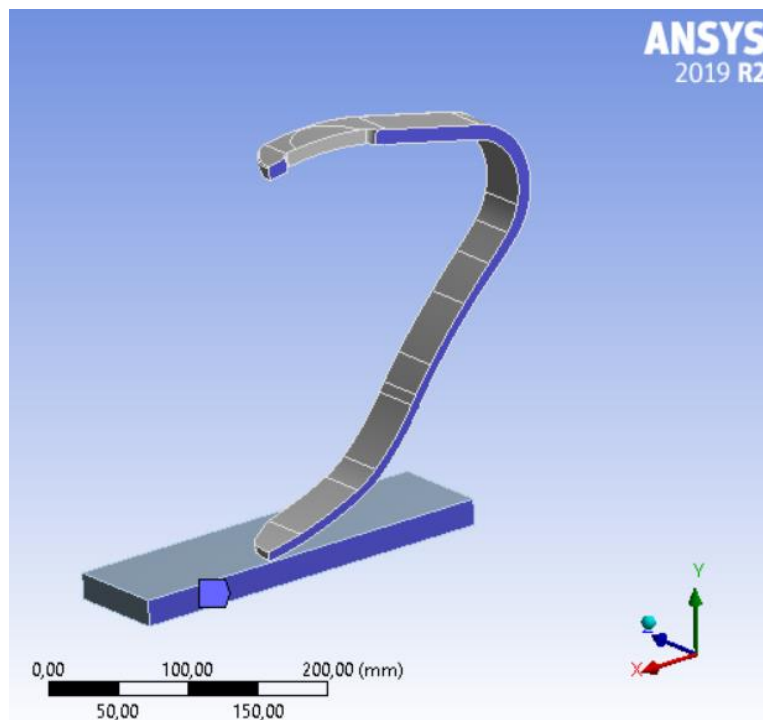 upper part of the prosthesis (Figure 2.28). In "Displacement" options it is better to choose "Components" and assign the value "0" in the X_C direction, assign the known displacement value d_{YC} in the Y_C direction and leave the displacement in the Z_C direction free because it is still constrained by the presence of symmetry. In this way, the vertical clamp displacement was applied linearly between 0 and the set value.
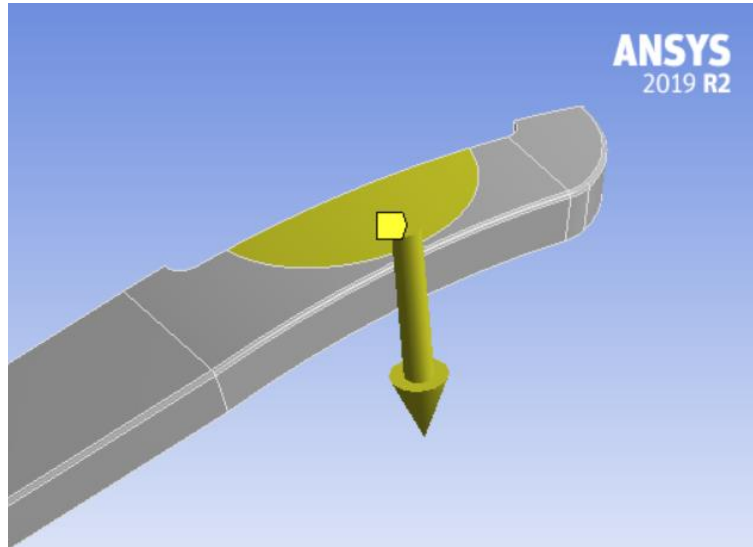
Figure 2.27: d_{YC} vertical displacement applied to the clamp areas (yellow colour)

- Another "Displacement" was applied on the lower face of the platform. The platform is prevented from moving in the Y_C direction by setting "0" as the value, but is left free to move in the X_C and Z_C direction using the "Free" command.

- Finally, on one of the 2 lateral faces of the platform, a horizontal force (Figure 2.29) was applied with component only in the X_C direction, the modulus and sign of which is known from the experimental data.

Figure 2.28: Example of F_{XC} force applied on the lateral face (green colour) of the platform. In this figure the horizontal force applied is negative/breaking.

For the assignment of the F_{XC} force, attention must be paid to the following things:
- If you are considering an half sectioned model, the force applied on the face of the platform must be, in module, divided by two with respect to the experimental value.
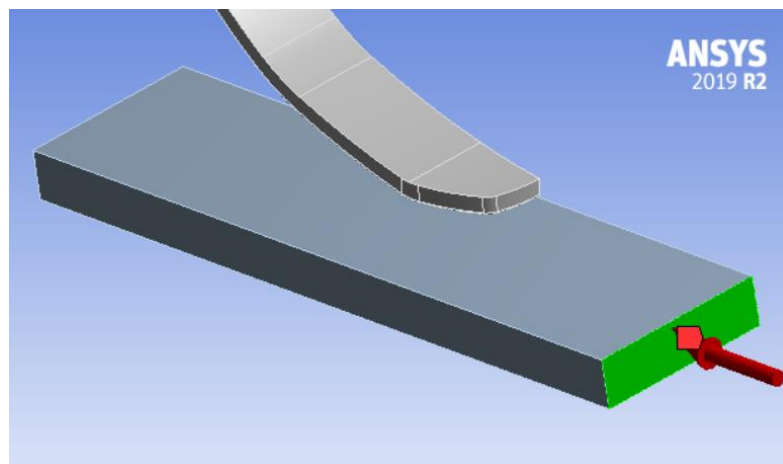- The force must be applied only in the second load step. In fact, if the force were applied already in the first step, the system would be labile. This is because a platform would be loaded in the horizontal direction which however can free move without friction.

- Therefore, when defining the force, it's necessary to deactivate it, by clicking with the right button, for step 1 (the line of the "Tabular Data" will turn grey) and make it active for step 2 (white line). An example is shown in the following Figure 2.30. Also in this case the horizontal force was applied linearly between 0 and the set value.

	Steps	Time [s]	✔ X [N]	✔ Y [N]	✔ Z [N]
1	1	0,	0,	= 0,	= 0,
2	1	1,	0,	0,	0,
3	2	2,	100,	= 0,	= 0,

Figure 2.29: Tabular Data of the horizontal force. F_{XC} is activated in the second step (white line) while is deactivated in the first step (grey line)

2.4.5 Selection of the desired outputs

In the branch of the tree that is located under "Solution", it is possible to choose the output of interest by clicking on it with the right button. The plotted results are the following:

- The global deformation of the system ("Total Deformation") to see and measure if the numerical prosthesis graphically deforms in a similar way to the real one.
- The clamp reaction forces ("Probe" → "Force Reaction") (Figure 2.31). Take care if only a half prosthesis is used: the forces plotted will have a half value. Remember to multiply the forces read by 2 and then compare them with the real one.
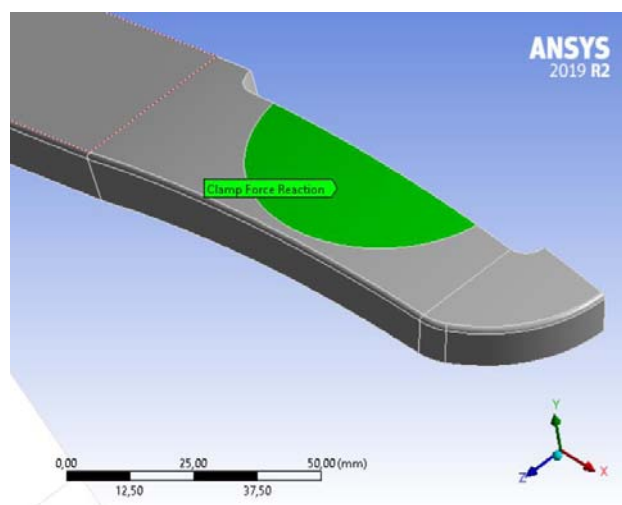

Figure 2.30: Reaction Forces plotted to the clamp areas (green colour)

After having applied all the previous settings, the solution is launched with the "Solve" command (right button above "Solutions"). It's possible to control what is happening by viewing the "Solution Information" (for example "Force Convergence") (Figure 2.32).
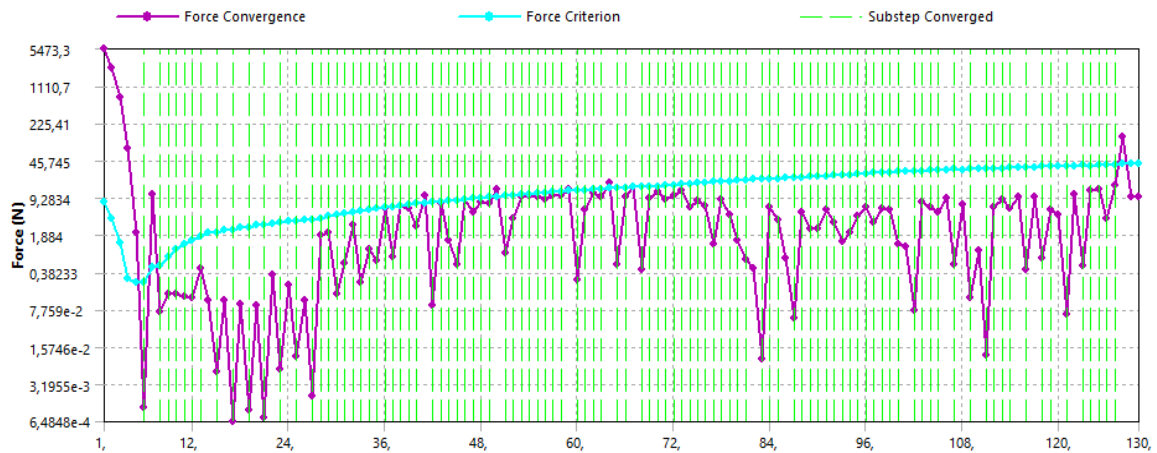
Figure 2.31: Force Convergence diagram

2.4.6 Postprocessing of the results

To perform the calibration of the numerical model, three different configurations were chosen, in terms of position of the clamp and inclination of the platform:
- Clamp 0°, Ground 0°
- Clamp -4°, Ground 30°
- Clamp + 4°, Ground 15°

For each configuration, several load tests, previously carried out experimentally, were simulated with the aim of finding a single equivalent isotropic elastic modulus using the flow chart shown in Figure 2.24. The results found are the following:

- The prosthesis total deformation observed during the numerical simulations is comparable to the real deformation obtained in the respective experimental test. However, the tip of the numerical prosthesis tends to lift more than the real one. The reasons were identified in the fact that the CAD model does not have the sole and spikes, which tend to locally stiffen the prosthesis. Furthermore, the interaction between the spikes and the tartan hold the tip of the prosthesis, but this condition can not be realized in ANSYS. In Figure 2.33 two examples are shown.
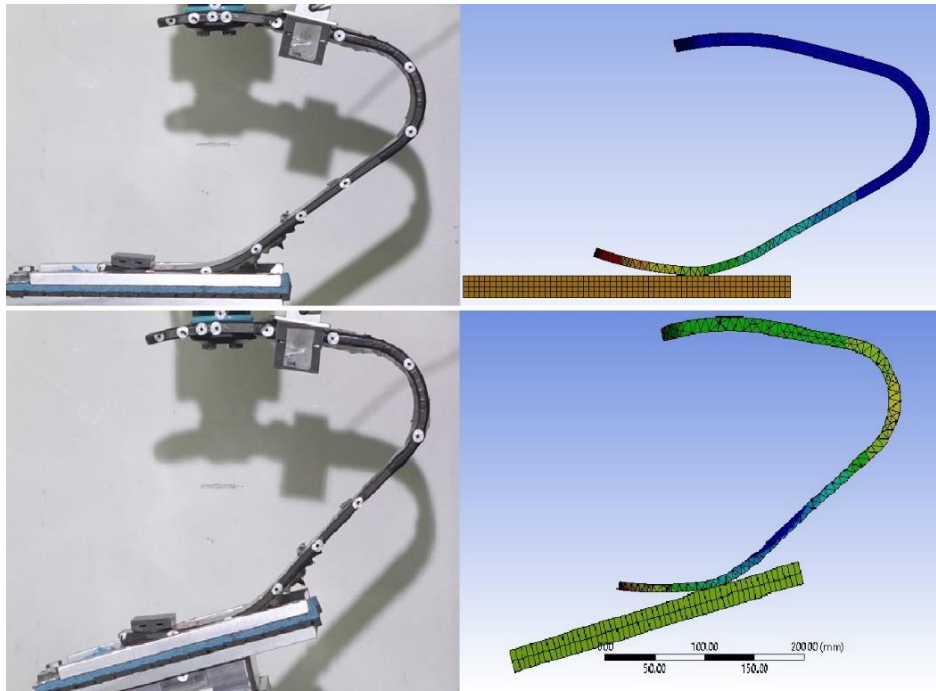
Figure 2.32: Examples of comparison between real and numerical global deformation of the Prosthesis Ottobock Standard Runner CAT3. Up the configuration with clamp 0°, ground 0°, F_{YC}=1000N, F_{XC}=0N. Down the configuration with clamp +4°,ground -15°, F_{YC}=1500N, F_{XC}=-300N.

- The fundamental result is the following: although, as what has just been said, the deformation is not perfectly equal to the real one, it is noticed that for a single isotropic elastic modulus value it is possible to find, for a given configuration, forces F_{YC} equal (with an $err_{F_{YC}}$<5%) to those evaluated experimentally.

  Furthermore, among the three configurations considered, the elastic modules found are very similar. In these cases:

- Clamp 0°, Ground 0°: E=33000 MPa

d_{YC} [mm]	F_{XC} [N]	$F_{YC,exp}$ [N]	$F_{YC,FEM}$ [N]	$err_{F_{YC}}$ [%]
38,8	-100	505	500	1
44	-4	501	198	0.6
48,7	103	499	499	0
62	-179	1016	969	4.6
69,1	6	1020	1003	1.7
76,2	205	1024	1046	2.1
79,5	-309	1520	1545	1.6
89	-6	1517	1536	1.3
97,5	311	1514	1519	0.3
			$err_{F_{YC},mean}$ [%]	1.5

- Clamp -4°, Ground +30°: E=34000 MPa

d_{YC} [mm]	F_{XC} [N]	$F_{YC,exp}$ [N]	$F_{YC,FEM}$ [N]	$err_{F_{YC}}$ [%]
44,8	-92	464	458	1.3
54,3	5	480	475	1
62,1	90	470	490	4.3
109,2	-188	944	945	0.1
118,6	-4	948	959	1.2
128,6	203	948	998	5.2
			$err_{F_{YC},mean}$ [%]	2.2

- Clamp +4°, Ground -15°: E=32000 MPa

d_{YC} [mm]	F_{XC} [N]	$F_{YC,exp}$ [N]	$F_{YC,FEM}$ [N]	$err_{F_{YC}}$ [%]
20,9	-102	516	536	3.9
24,7	-1	526	530	0.8
28	109	529	520	1.7
33,7	-195	1027	1065	3.7
41,3	-12	1032	1065	3.2
47	205	1024	1034	1
48,5	-296	1523	1588	3.6
58,9	-22	1536	1561	1.6
64,6	306	1504	1478	1.7
			$err_{F_{YC},mean}$ [%]	2.4

Therefore, observed these results, an equivalent static elastic modulus, average of the three values found, equal to $E_{eq,s}$ = *33000 MPa* has been assumed for successive simulations.

- Observation on the friction coefficient μ: among the variables not exactly known there is also the friction coefficient that had been assumed equal to 1. Other tests were subsequently performed, maintaining the same configuration and the same mesh, changing the value of μ: 0.3, 0.5 and μ = ∞ (using the "Rough" command). After carrying out these simulations, no appreciable changes were observed in terms of the value of the reaction forces and deformation. The reason is:
- During the first load step in which the prosthesis goes down and the platform is free to slide, due to the frictional contact the two components move together and there is no relative motion between the two bodies.
- During the second load step the clamp is forced to remain fixed and the horizontal force in X_C direction is applied. However, all tests are performed with forces F_{XC} less than $μF_{YC}$: this is because ρ is equal to -0.2, 0 or 0.2, while μ is always greater than 0.2. So, the platform can not slide under the prosthesis and it moves together with it (there is no relative motion between the two bodies).
Therefore, for values of μ> 0.2, the results do not change. This means that there is not a problem to unknown the friction coefficient for this type of test which, due to the presence of spikes, is certainly greater than 0.2.

CHAPTER 3: STATIC-NUMERICAL STIFFNESS CURVES

3.1 Introduction

Once the calibration of the numerical model, described in paragraph 2.4, was performed, it was possible to predict the mechanical behaviour of the prosthesis for different load conditions than those performed during laboratory tests. In this phase the stiffness of the prosthesis was evaluated, even for vertical loads higher than 1500N of the experimental tests, analysing the behaviour up to 3500 N. It is necessary to specify that an athlete, who uses this type of prosthesis considered, hardly reaches similar loads: for example, during run there are load peaks around 2500N, which are exceeded only during the last step before a long jump test (3000-3500N). The advantage of having a calibrated numerical model allows to study load limit conditions without risk of breaking the prosthetic foot.

Numerical stiffness curves were determined in the clamp reference frame considering F_{YC}, measured via ANSYS, and the vertical displacement of the clamp d_{YC}. Since these curves were plotted for each configuration, these necessarily depend on the load ratio ρ and the inclination of the platform ϑ_G.
Therefore, many curves will be shown below, and some of these will be compared with the results found during the experimental static tests. For this reason, it was decided to use:

- a continuous line to represent the curves found numerically, where the indicators will be squares (curves with ρ=-0.2), circles (curves with ρ=0) or triangles (curves with ρ=+0.2)
- a dashed line to represent the curves found experimentally, where the indicators will be stars.

In addition, the following color code, summarizes in Table 3.1, was used for the graphs in paragraph 3.

Parameter	Colour
Ground -15°, Clamp 0°	
Ground 0°, Clamp 0°	
Ground +15°, Clamp 0°	
Ground +30°, Clamp 0°	
Clamp -4°	
Clamp +4°	

Table 3.1: Color code for the following figures

3.2 Definitions for stiffness evaluation

In order to evaluate the prosthesis stiffness obtained during static test, in literature there is no clear reference standard. To characterize the results obtained during the different numerical tests, in this thesis the following definitions were used to define and measure stiffness:

- $K_L^{Y_C}(\rho, \vartheta_G)$ [N/mm]: first term coefficient of the approximated trend line (blue line in Figure 3.1) which minimizes the root mean square error, passing through the origin of the graph and considering all the curves with the same vertical force peak value of 3500 N. The subscript L means "linear" because this stiffness value depends of the trend line, while the superscript Y_C reminds that the stiffness curves are obtained by considering two quantities (F_{YC} and d_{YC}) in the clamp reference system.

- $K_{L1}^{Y_C}(\rho, \vartheta_G)$ [N/mm]: first term coefficient of the approximated trend line (red line in Figure 3.1) which minimizes the root mean square error, passing through the origin of the graph and considering the first part of the stiffness curve up to 1500 N.

- $K_{L2}^{Y_C}(\rho, \vartheta_G)$ [N/mm]: first term coefficient of the approximated trend line (green line in Figure 3.1), which minimizes the root mean square error, which interpolates the second part of the stiffness curve (from 1500 N to 3500 N).
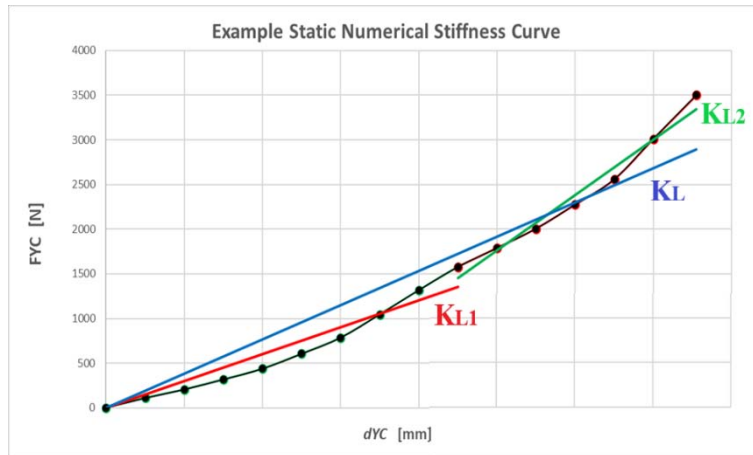

Figure 3.1: Three different trend lines used for the evaluation of K_L (blue line), K_{L1} (red line), K_{L2} (green line). The black curve is a generic static stiffness curve (force/displacement plot)

- $K_{eq}^{Y_C}(\rho, \vartheta_G)$ [N/mm]: this approach is perhaps the simplest and easiest to justify, since the prosthesis is considered to be a spring capable of absorbing energy when compressed and returning it later. This equivalent stiffness value is determined by applying the following energetic approach:

$$\frac{1}{2} * K_{eq} * d_{YC,max}^2 = A \tag{3.1}$$

Where A is the area below the stiffness curve and $d_{YC,max}$ is the maximum vertical displacement of the clamp when the vertical force is equal to 3500 N (Figure 3.2). It is possible to evaluate the area calculating the integral using, for example, the trapezoid rule.
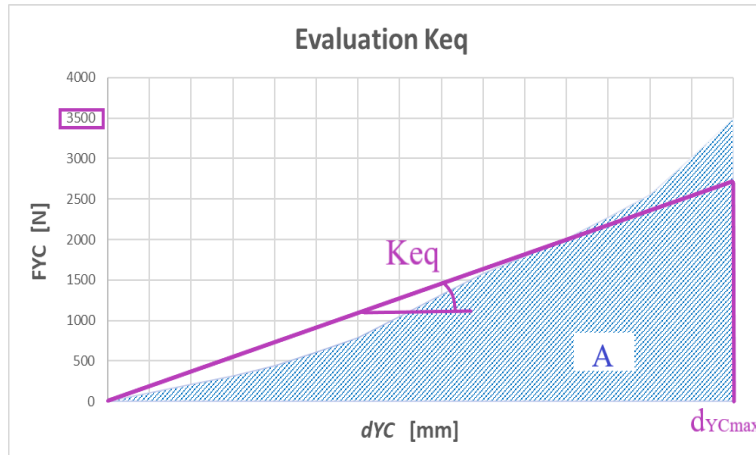
Figure 3.2: Sketch for the K_{eq} evaluation

An important note must be made for K_{L1} and K_{L2}. The choice to try to define these two stiffnesses is linked to what was seen in an experimental thesis, previously made in the laboratory of the University of Padua, by L. Mazzanti [17]. During the static tests carried out by the latter, two long jump prostheses (C shaped Ottobock Custom category 3 and J shaped Ossur Cheetah Xtreme category) were vertically loaded on the test bench up to 3500 N, but with the horizontal cylinder released from the platform. The analysis of the results shows, for both prostheses, a stiffness curve with a non-linear trend that could be approximated as bilinear, with a stiffening in correspondence of 1500 N.

Therefore, in order to use the definitions of K_{L1} and K_{L2}, also for the prosthesis considered in this thesis, the hypothesis of bilinearity of the stiffness curves must be verified, with change of slope at 1500 N of vertical load. Therefore, it was decided to evaluate the second derivative of the stiffness curve using the central difference method on the numeric ANSYS data collected in Excel [21]. The estimate for the first derivative and the second derivative on the discrete data were made using the following generic equations:

$$\frac{\Delta y}{\Delta x} = \frac{y_{+1} - y_{-1}}{2h} \tag{3.2}$$

$$\frac{\Delta^2 y}{\Delta x^2} = \frac{y_1 - 2y_0 + y_{-1}}{h^2} \tag{3.3}$$

Where h is the increment of the generic independent variable x.

If the previous hypothesis is verified, we expect a clear variation of the second derivative where there is a change of slope, as is shown in the following Figure 3.3.
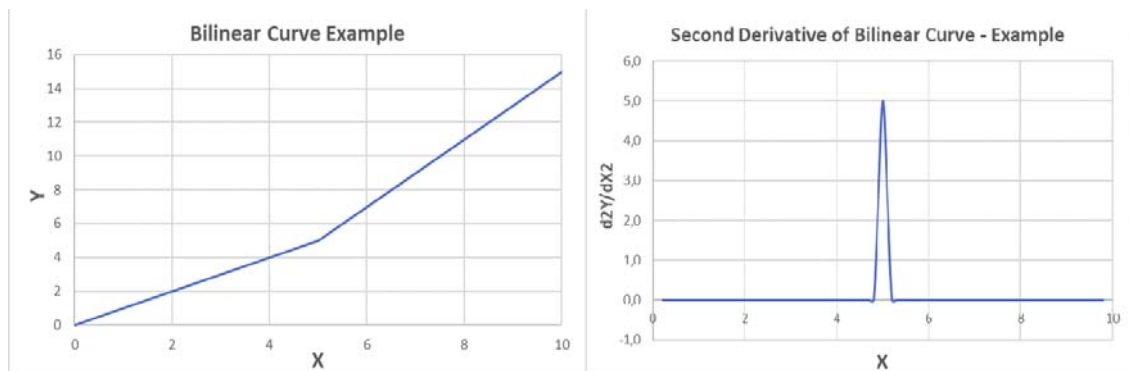

Figure 3.3: Example of bilinear curve and its second derivative.
The second derivative change at the X value where the slope

37

3.3 Bilinearity hypothesis check and analysis of the centre of pressure

In order to verify bilinearity hypotheses was initially considered the Ottobock Category 3 prosthesis configuration with the platform at 0° ("midstance" phase of the run), the clamp in the central position (0°) and simulations were performed with null horizontal force F_{XC} (ρ=0 case).
Therefore, new tests were carried out on ANSYS Workbench in which:

- Tartan material was assigned to the platform (E = 600 MPa).
- The value previously found in paragraph 2.4.6, equal to E=33000 MPa, is taken as the equivalent isotropic elastic modulus for the prosthesis.
- The platform is free to move in the X_C direction (ρ = 0 test).
- A certain displacement d_{YC} is applied to the clamp in the direction Y_C (negative).
- The vertical forces, in the Y_C direction, are read at the clamp area.

Once the simulation was performed, the numerical results found were plotted in a $F_{YC} - d_{YC}$ graph (Figure 3.4). Remember that, during simulations carried out using half prostheses, the reaction forces found were half: these values were multiplied by a factor of 2.
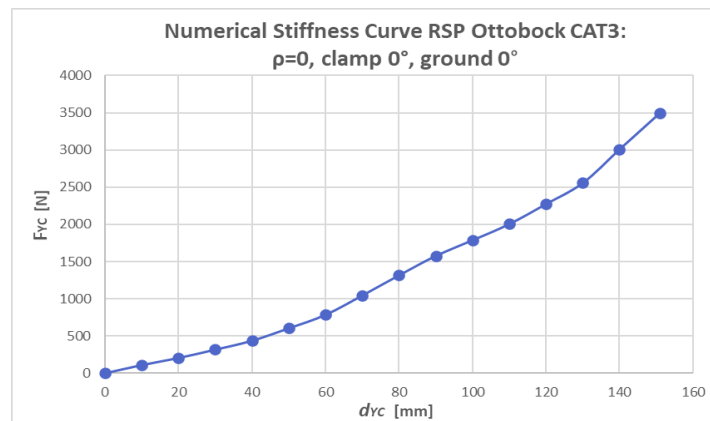

Figure 3.4: RSP Ottobock Category 3 stiffness curve ($F_y - d_{YC}$) obtained in static test in conditions of clamp 0°, ground 0°, ρ = 0

Figure 3.4 allows to analyse how the stiffness curve of the prosthesis changes as the load increases. It can be observed that the stiffness tends to increase changing the vertical loads from 0 to 3500 N. This means that the stiffness curve has a non-linear trend. However, it was observed that the curve was not always increasing, but it shown an clear oscillation at 1500 N.
Therefore, it was evaluate the second derivative of the stiffness curve using the central difference method described in section 3.2. The trend of the second derivative is plotted in the following Figure 3.4, where the vertical force value F_{YC} was placed on the abscissa axis.
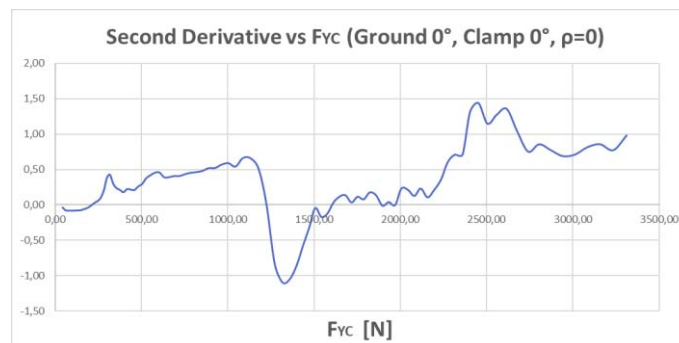

Figure 3.5: Plot of the second derivative as a function of the vertical load F_{YC} (ground 0°, clamp 0°, ρ=0)

As it is shown in this last Figure 3.5, the second derivative diagram does not present a single clear peak, as we hoped in order to confirm the bilinearity hypothesis, but here there are two main peaks. Instead, it was noted that, where the second derivative is equal to zero, the stiffness curve has its inflection points, i.e. the points where there is a convexity variation of the curve. In fact, It can be observed that the stiffness curve (Figure 3.4) has a convex shape (positive curvature) up to 1200-1300N, from 1300N to 1900N it presents a concave shape (negative curvature) and then again a convex shape.

Similar considerations can also be made by analyzing the results plotted in Appendix A.1, found considering configurations with the clamp placed at 0° and load ratio ρ=0, changing the inclination of the ground (-15°, +15°, +30°). In all of these cases, neither an evident peak for the second derivative nor a maximum peak for the same vertical force F_{YC} value were observed.

Therefore, it can be concluded that, since the hypothesis of bilinearity can not be confirmed, the definitions of K_{L1} and K_{L2} inevitably lose value.

For this reason only the K_L and K_{eq} stiffnesses were calculated in the following sections.

The last thing to do was to try to understand the reason why the behaviour of the prosthesis is not linear. In order to achieve that it was decided to evaluate how the position of the centre of pressure changes when the load increases. The centre of pressure (COP) can be defined as the centre of the contact area between the prosthesis and the platform, where the ground reaction force vector can be visualized.

As it is shown in Figure 3.6, the centre of pressure position X_{COP}^C was defined as the distance, in the *clamp reference system*, between the pressure centre and the centre of the clamp (X_{clamp}).
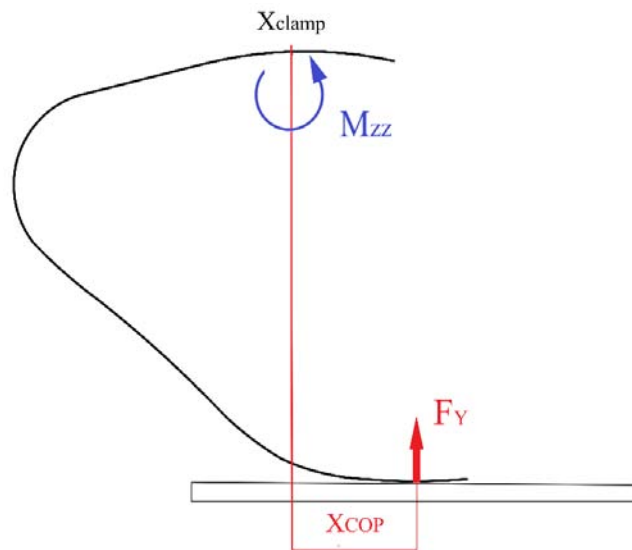

Figure 3.6: Sketch of the centre of pressure position X_{COP} (distance between the pressure centre and the centre of the clamp). It is also highlighted the reaction force applied in the COP and the bending moment Mzz due to F_Y.

Here it is considered for simplicity the configuration with ϑ_G=0, clamp 0° and ρ=0. Looking at the total deformation during the simulation (Figure 3.7), as the load increases, the prosthesis changes considerably its shape compared to the undeformed initial position and significantly increases the contact area due to the rolling of the surface of the prosthetic foot on the platform.
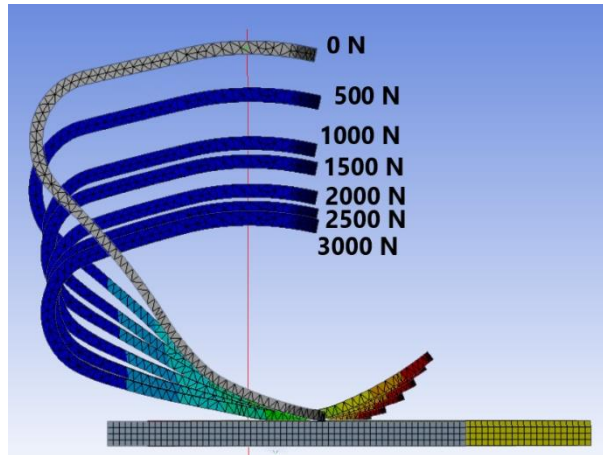
Figure 3.7: Sequence of different deformation instants of the prosthesis obtained via ANSYS Workbench (0 N/ 500 N/ 1000 N/ 1500 N/ 2000 N/ 2500 N/ 3000 N)

The stiffness change previously described is probably due to the fact that, while the vertical force tends to increase, the position of the centre of pressure (X_{COP}) tends to approach the centre of the clamp (X_{clamp}). Because of this, the arm of the reaction force F_Y (i.e. X_{COP}, Figure 3.3) tends to decrease as the load increases and the bending moment, due to the reaction force F_Y, increases gradually less. If bending moment decreases also curvature decreases and stiffness increases consequently.

Therefore, to verify this hypothesis, the position of the centre of pressure X_{COP} was plotted respect to the vertical reaction force F_Y (equal in modulus to the F_{YC}). FEM analysis is always used to evaluate it. The clamp reaction moment in the Z direction was chosen as another output of the simulation ($M_{C,zz}$). It was possible to easily find how X_{COP} changed as the load increased using the following equation.

$$M_{C,zz} = F_Y * X_{COP} \rightarrow X_{COP} = \frac{M_{C,zz}}{F_Y} \qquad (3.4)$$

That equation was used because, in this ρ=0 test, there is no horizontal force that gives any additional component to $M_{C,zz}$. The results found are reported in Table 3.2 and plotted in Figure 3.8.
Furthermore, Figure 3.9 shows the trend of the moment $M_{C,zz}$ when the reaction force F_Y changes.
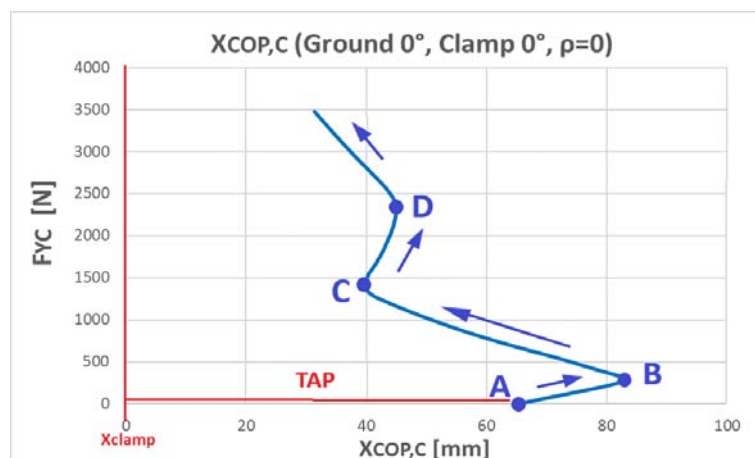

Figure 3.8: COP trend during static tests loading with clamp 0°, ground 0°, ρ=0. The lever arm of ground reaction forces tends to decrease as the vertical load increases. Clamp axis and points A, B, C, D, are highlighted

d_{YC}[mm]	F_Y [N]	$M_{C,zz}$ [Nmm]	X_{COP} [mm]
0	0	0	/
10	111	8046	72,8
20	206	16350	79,5
30	318	26318	82,8
40	438	33650	76,9
50	605	41576	68,8
60	785	46908	59,8
70	1045	51284	49,1
80	1316	53342	40,5
90	1577	64180	40,7
100	1788	75992	42,5
110	2006	88158	43,9
120	2275	102242	44,9
130	2558	110768	43,3
140	3011	111904	37,2
150	3474	108960	31,4

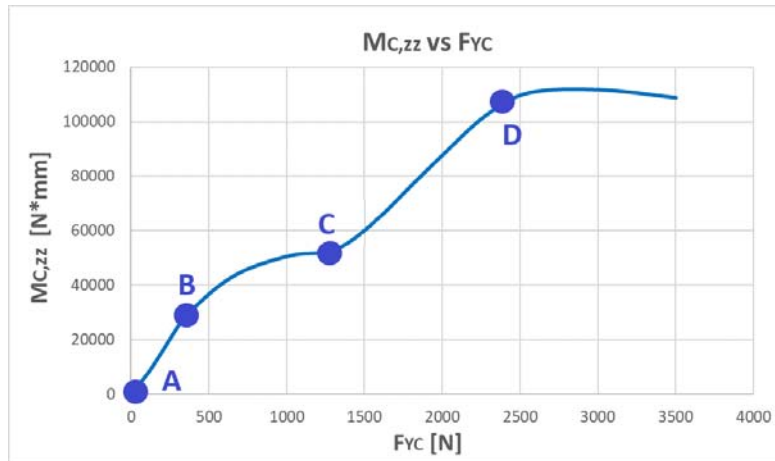*Table 3.2: F_Y, $M_{C,zz}$, X_{COP} collected every 10 mm of displacement d_{YC}*

Figure 3.9: Curve $M_{C,zz} - F_{YC}$ obtained in static test in conditions of clamp 0°, ground 0°, ρ = 0

From the COP analysis of Figure 3.8, four reference points were defined (A, B, C, D) which correspond to the instants in which the centre of pressure changes its rolling direction. Moreover, it was observed that, in the first phases of load application (up to 1300 ÷ 1400 N, point C), the centre of pressure is located far from the centre of the clamp and tends to approach it quickly due to the prosthesis rolling on the platform. From 1400 N onwards, X_{COP} tends to grow slightly (≈ 5 mm) and then decrease again when the force is around 2400 N (point D). It is interesting to note that these two points (around 1300 N and 2400 N) coincide with the force values at which the 2 major peaks occur in the plot of the second derivative (Figure 3.5).

In addition, this is reflected in the trend of the previously plotted stiffness curve. When the stiffness curve is convex, as the load increases, the X_{COP} arm tends to decrease, the moment M_{zz} tends to reduce its growth until it stabilizes and the stiffness increases. On the other hand, when the curve is concave, the arm tends to increase and with it the bending moment, while stiffness decreases. Similar considerations can also be made by analysing Figures plotted in Appendix A.1.

Finally the following important note was made concerning the stiffness and COP curves plotted in this paragraph and in Appendix A.1 (curves obtained at clamp 0°, ρ=0 and changing the inclination angle of the platform):

- The trend of the centre of pressure and of the stiffness curve is due the combination of the applied load and the portion of the prosthetic foot which is in contact with the platform. Although the CAD model was made by importing the photograph of the prosthesis, so the final geometry may be subject to some inaccuracies, the shape of the prosthesis studied by the manufacturer plays a fundamental role in the results found
- All the diagrams that describe the trend of the centre of pressure (shown in the Figure 3.10) are *conventional* (ρ=0, ϑ_G fixed). These curves depend exclusively on the type of static test that was carried out on the test bench, in which the prosthesis was flattened increasing the vertical load and keeping the angle of inclination of the ground fixed. Therefore these curves do not concern the real trend of the COP during the whole running step, where the angles of the ground change during the contact time.

However, these results are of interest because, thanks to the analysis of the position of the COP, it was possible to explain the non-linearity of the prosthesis stiffness obtained during these types of static tests.
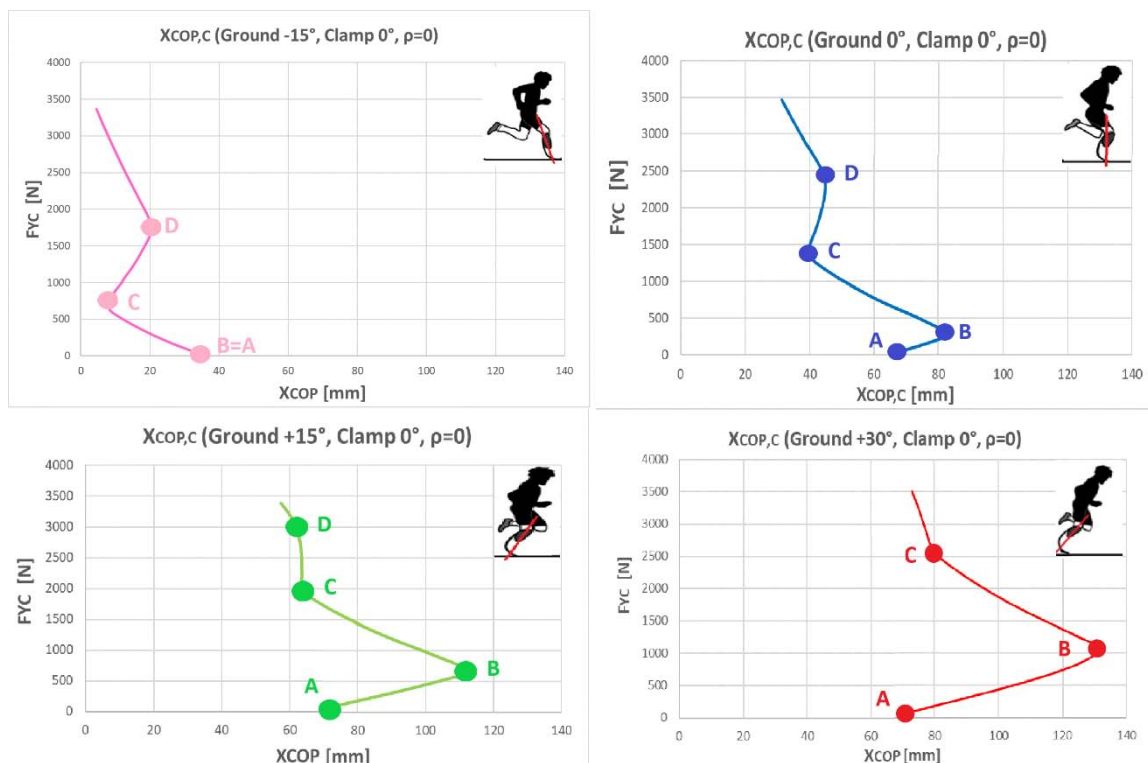

Figure 3.10: X_{COP} during static tests loading with clamp 0°, ρ = 0 and changing the platform inclination angle (-15°, 0°, +15°, +30°)

3.4 Effect of the load ratio ρ on the prosthesis stiffness for a given ground inclination angle (clamp 0°)

Considering the same prosthesis, the stiffness was evaluated in conditions of platform placed at 0° and clamp in the central position, when the load ratio $\rho = F_{XC}/F_{YC}$ was varied. Values of ρ used are: -0.2, 0, +0.2.
The results are plotted in the following Figure 3.11. For each curve, K_L and K_{eq} values were calculated using the definition of paragraph 3.2.
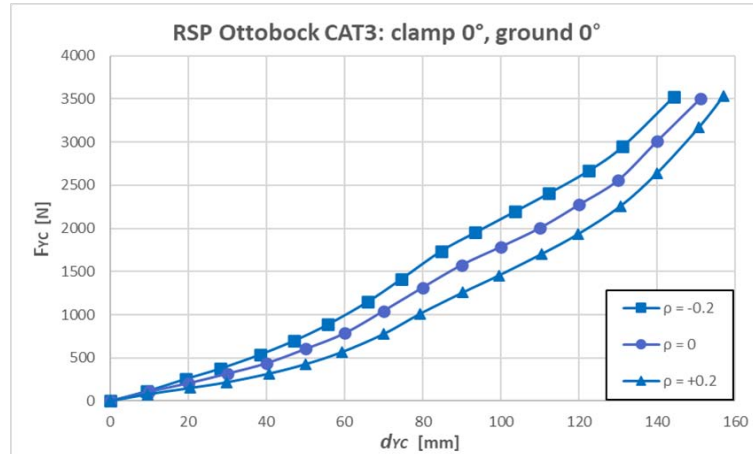

Figure 3.11: RSP Ottobock Category 3 numerical stiffness curves ($F_{YC} - d_{YC}$)
obtained in static test in conditions of clamp 0° and ground 0° when the load ratio ρ
changes. Note that the prosthesis stiffness decreases from ρ=-0.2 to ρ=+0.2

It was observed that, by increasing the ratio ρ from a negative value (-0.2) to a positive value (+0.2), the stiffness of the prosthetic foot decreases. The prosthesis is stiffer when ρ is negative because in this condition the horizontal force F_{XC} is a braking force. This means that, while the prosthesis is flattened vertically of a certain amount, the horizontal force acts on the tip of the same tending to compress it further.

Stiffness value obviously depends on the curve considered and therefore on the load ratio ρ. Furthermore, both for K_L and K_{eq}, the percentage differences Δ, respect to the stiffness obtained in the case ρ = 0, were calculated using the general following equation.

$$\Delta_i = \frac{K_i(\rho) - K_i(\rho=0)}{K_i(\rho=0)} \%$$

(3.5)

Where i depends on if you are considering K_L ($i = L$) or K_{eq} ($i = eq$).

The results are shown in the Table 3.3.

ϑ_G =0°, Clamp 0°	$\rho = -0.2$	$\rho = 0$	$\rho = +0.2$
K_L [N/mm]	21.31 (R^2=0.987)	19.19 (R^2=0.975)	17.38 (R^2=0.952)
Δ_L [%]	+10.9	/	-9.4
K_{eq} [N/mm]	18.18	17.4	14.05
Δ_{eq} [%]	+4.5	/	-19.2

Table 3.3: K_L and K_{eq} values obtained in numerical static test in conditions of clamp 0° and ground 0° when the load ratio ρ changes. Δ values were calculated respect to the stiffness obtained in the case ρ=0

Similar considerations can be made by studying the stiffness curves and tables, reported in Appendix A.2, for the remaining angle of inclination of the platform (-15°, +15°, +30°) as the load ratio ρ varies.

Looking at the tables it is possible to see how K_{eq} is always lower than K_L. However, K_{eq} changes similarly to K_L. So both definitions of stiffness can be used to characterize all different curves.

3.5 Effect of the clamp position on the prosthesis stiffness (ρ=0)

The effect of the clamp position on the stiffness of the prosthesis was initially evaluated, considering the initial configuration in which there is no horizontal force (ρ=0) and in conditions of ϑ_G = 0°. Using ANSYS and loading the prosthesis up to 3500 N, it is observed that, during this type of static test, the position of the clamp does not present any significant variation on the stiffness of the prosthetic foot.
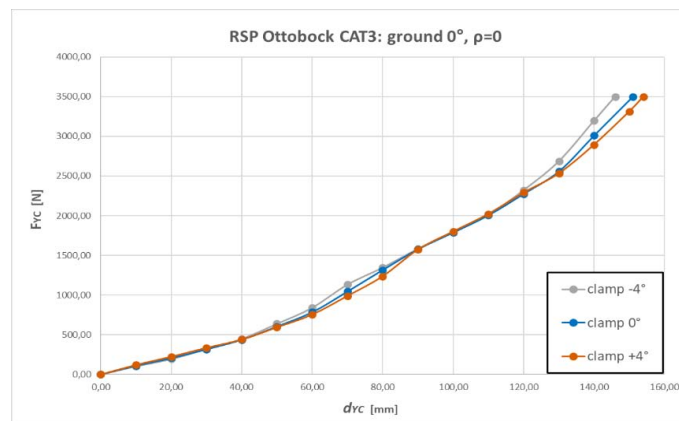The numerical results are shown in the following Figure 3.12.

Figure 3.12: RSP Ottobock Category 3 numerical stiffness curves (F_{YC} - d_{YC}) obtained in numerical static test in conditions of ρ=0 and ground 0° when the clamp position changes.

It can be noticed that up to 2000-2500 N the three curves tend to overlap to each other; some differences were observed for higher loads. This is confirmed also by the experimental tests (Figure 3.13), where up to 1500 N the curves were almost coincident.
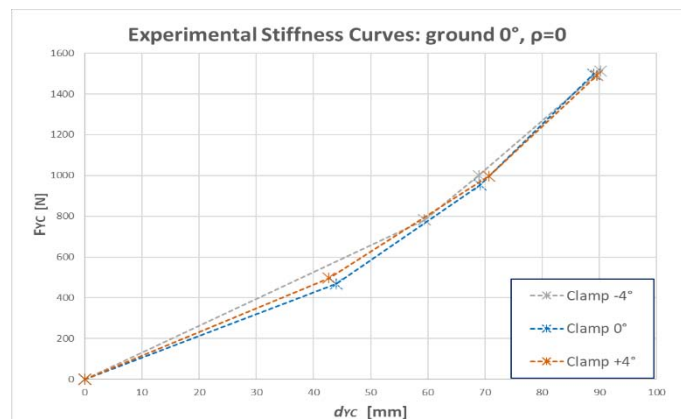

Figure 3.13: RSP Ottobock Category 3 experimental stiffness curves (F_{YC} - d_{YC}) obtained during static test in conditions of ρ=0 and ground 0° when the clamp position changes.

44

Also in this case the numerical stiffness were evaluated using the two definitions previously provided. These stiffnesses clearly depend on the position of the clamp and therefore on the curve considered. The results are shown in the following Table 3.4. Moreover, the percentage differences Δ, respect to the stiffness obtained in the case of clamp 0°, were calculated. As it was supposed looking at the plotted curves, the values in the table are not characterized by appreciable differences.

$\vartheta_G = 0°$	$clamp + 4°$	$clamp\ 0°$	$clamp - 4°$
K_L [N/mm]	19.4 (R²=0.978)	19.19 (R²=0.975)	19.79 (R²=0.974)
Δ_L[%]	+1.1	/	+3.1
K_{eq} [N/mm]	17.56	17.4	17.84
Δ_{eq}[%]	+0.9	/	+2.5

Table 3.4: K_L and K_{eq} values obtained in numerical static test in conditions of ρ=0 and ground 0° when the clamp position changes. Δ values were calculated respect to the stiffness obtained in clamp 0° case

Similar considerations can be made by studying the stiffness curves and tables, reported in Appendix A.3, for the remaining angle of inclination of the platform (-15°, +15°, +30°). It was observed how the small differences between the stiffness curves, for platform angles of -15° and 0°, tend to decrease further for ϑ_G angles of +15° and +30°, with the curves that are almost overlapped up to 3500 N.

The results found during these tests are in disagreement with what was learned from field experience with athletes. In fact, typically athletes, during the race, perceive stiffer configurations with the clamp positioned at +4°. However, these static tests are not able to recreate the conditions that occur during a running step, as the tests are carried out by loading the prosthesis while the inclination of the ground is kept fixed.

3.6 Variation of prosthesis stiffness during the running stance changing the ϑ_G angle

It was evaluated how the stiffness of the prosthesis changes during the contact phase (Figure 3.14), from the initial instant of the running stance ("Heel strike"), represented for simplicity by the configuration with the ground at -15°, to the final one ("Toe off"), defined instead by the configuration with the platform at +30°.
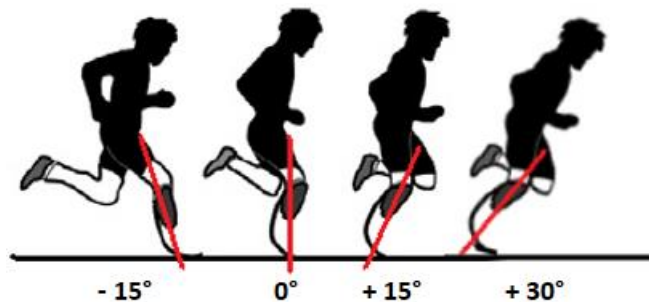

Figure 3.14: Sketch of the running stance phase

Considering the situation in which no horizontal force is applied (ρ=0) and the clamp is placed at 0°, it is observed that the stiffness of the foot tends to decrease during the running stance. The results are shown in Figure 3.15.
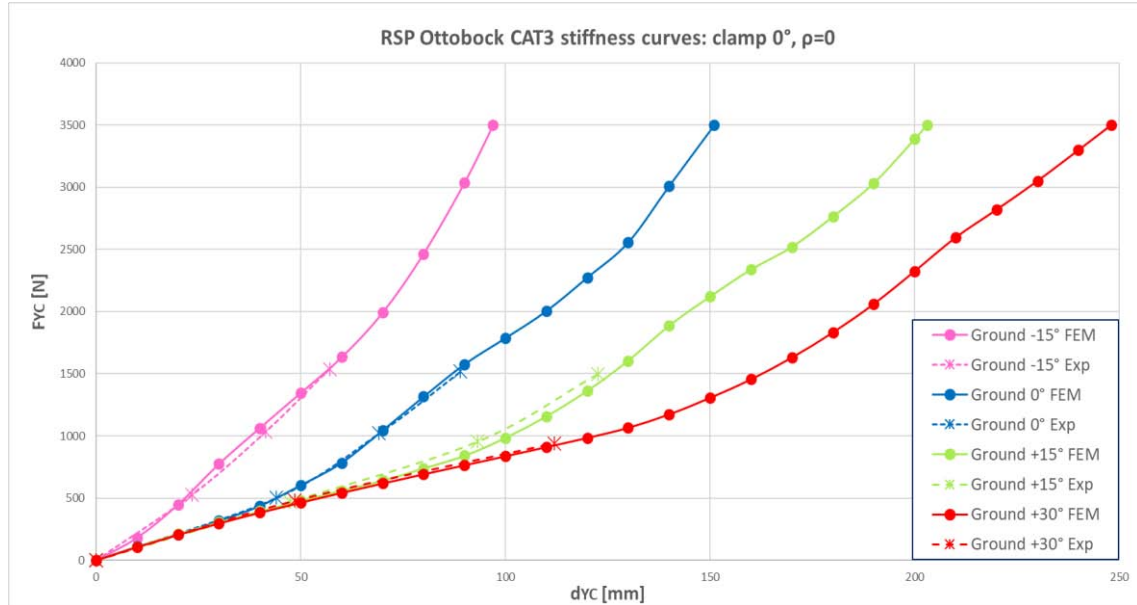

Figure 3.15: Map of numerical stiffness curves ($F_{YC} - d_{YC}$) obtained in static test in conditions of clamp 0° and ρ=0 when the ground inclination changes. Both the numerical curves (continuos line) and the experimental curves (dashed line) are reported

In this case, however, since this figure is a summary graph of several configurations, in addition to the results of this numerical model ("FEM"), the results of the stiffness curves obtained from the experimental tests ("Exp") are reported. It can be observed how the experimental curves, obtained from the tests with vertical loads F_{YC} up to 1500 N, and those found with ANSYS are practically coincident. In fact, to evaluate the model validity, the percentage error on the vertical force $err_{F_{YC}}$ was calculated for each configuration and for each displacement imposed on the clamp d_{YC} using equation (2.1). The results are shown in the following Table 3.5.

ϑ_G [deg]	d_{YC} [mm]	$F_{YC,exp}$ [N]	$F_{YC,FEM}$ [N]	$err_{F_{YC}}$ [%]
-15	23.5	526	570	8.37
-15	41.5	1032	1105	7.07
-15	57.1	1536	1547	0.72
0	44	501	491	2.00
0	69.1	1020	1037	1.67
0	89	1517	1522	0.33
+15	47.4	469	468	0.21
+15	93.2	953	882	7.45
+15	122.7	1497	1447	3.34
+30	48.6	479	463	3.34
+30	112	941	911	3.19

Table 3.5: Summary table of $err_{F_{YC}}$ calculated considering numerical and experimental values of F_{YC} for a given clamp displacement d_{YC} (clamp 0°, ρ=0)

The average percentage error was also calculated considering all the N $err_{F_{YC}}$ previously reported in the Table 3.5. It was used the following equation:

$$\overline{err_{F_{YC}}} = \frac{\Sigma_i^N err_{F_{YC,i}}}{N} \qquad (3.6)$$

In this case $\overline{err_{F_{YC}}}$ was a small value and equal to 3.4%.

These results allow us to have further proof regarding the method used to calibrate the elastic modulus of the prosthesis.

In Appendix A.4 was reported the maps of the stiffness curves found also in cases of load ratios different than zero (ρ=-0.2 and ρ=+0.2). Comparisons with the experimental static curves were made and the average percentage errors were calculated: also in these cases a satisfying correspondence between experimental data and numerical results was observed.

In addition, maps of the stiffness curves are shown in Appendix A.4 obtained when the load ratio is zero, but the clamp position changes (clamp -4° and +4°). By analysing figures and tables, it is possible to make similar considerations to the previous ones.

The advantage of having a calibrated numerical model allows also to evaluate the static behavior of the prosthesis under load conditions with a platform inclined differently from what was done during the experimental tests. Therefore, stiffness curves were obtained with ANSYS changing the angle of the platform between -20° and +30° considering intervals of 5°. The stiffness map is shown below in Figure 3.16, with clamp 0° and ρ=0. Moreover, since the position of the clamp does not cause any significant variation on the stiffness of the prosthetic foot during these static tests, Figure 3.16 can also be used for configurations with clamp +4° or -4° and ρ=0.
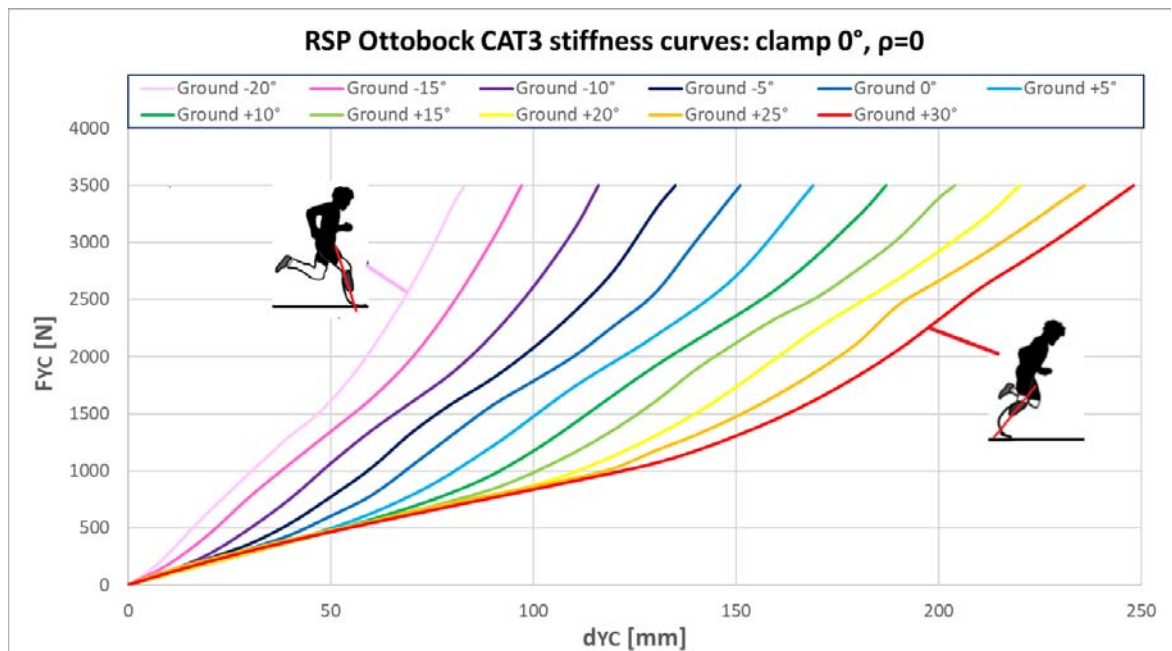

Figure 3.16: Map of numerical stiffness curves ($F_{YC} - d_{YC}$) obtained in static test in conditions of clamp 0° and ρ=0 when platform orientation varies between -20° and +30° considering intervals of 5°.

Finally, all these static tests results were summarized by calculating, for each curve of clamp 0° case (function of the load ratio ρ and the inclination of the platform ϑ_G), the stiffness values K_L and K_{eq}.

The values of K_L were listed in the following Table 3.6.

K_L^{Yc} [N/mm]		ρ		
		-0.2	0	+0.2
ϑ_G	-15°	35.69	31.42	27.15
	0°	21.31	19.19	17.38
	15°	15.3	14.35	12.9
	30°	12.35	11.68	10.76

Table 3.6: K_L values of each stiffness curve function of the load ratio ρ and the inclination of the platform ϑ_G (case clamp 0°)

The results of Table 3.6 were reported in the following final summary Figures 3.17 and 3.18.
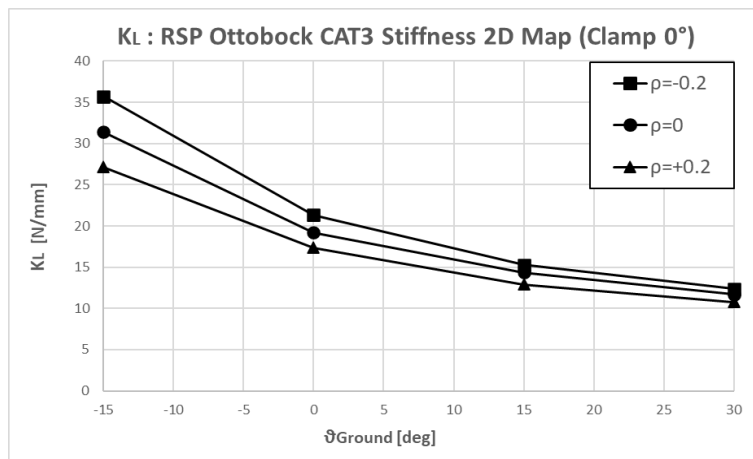

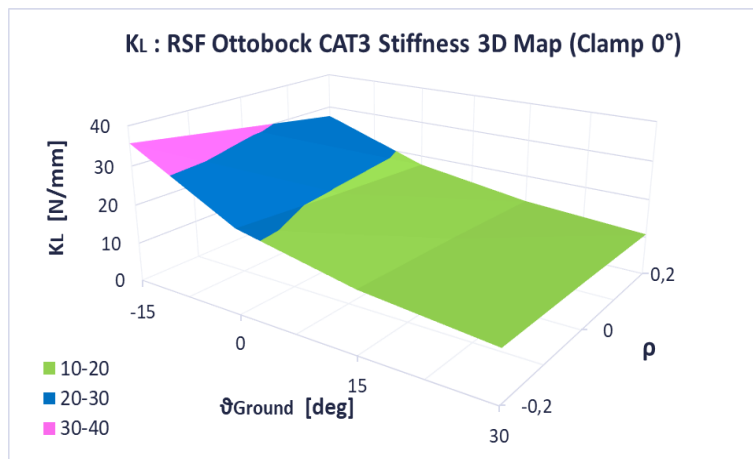Figure 3.18: K_L stiffness values 2D Map (Clamp 0°)

Figure 3.17: K_L stiffness values 3D Map (Clamp 0°)

From the analysis of the Table 3.6 and the Figures 3.17 and 3.18, the same observations explained above can be made:

- The stiffness of the foot tends to decrease during the running stance (from -15° to +30°)
- Changing the ratio ρ from the negative value (-0.2) to the positive value (+0.2), the stiffness of the prosthetic foot decreases.

K_{eq} values are also shown below in Table 3.7 and Figure 3.19 and Figure 3.20.

$K_{eq}^{Y_C}$ [N/mm]		ρ		
		-0,2	0	+0,2
ϑ_G	-15°	35.53	29.23	24.27
	0°	18.18	17.4	14.05
	15°	14.29	13.04	11.45
	30°	11.62	10.42	9.14

Table 3.3.7: K_L values of each stiffness curve function of the load ratio ρ and the inclination of the platform ϑ_G (case clamp 0°)
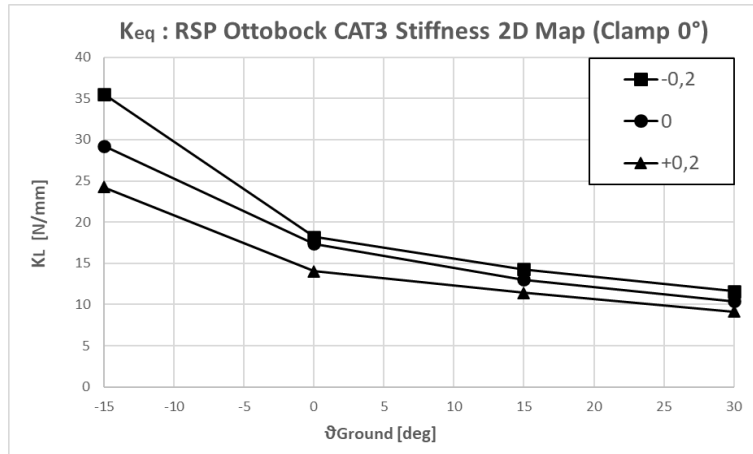

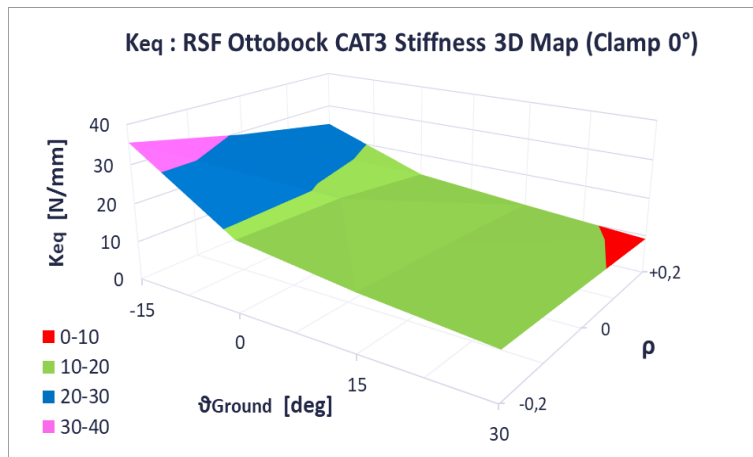*Figure 3.20: : K_{eq} stiffness values 2D Map (Clamp 0°)*

Figure 3.19: K_{eq} stiffness values 3D Map (Clamp 0°)

3.7 Evaluation of limit conditions of prosthesis use

In this paragraph some observations were presented which must be debated as *conventional*. The reason was related to the fact that these considerations were made using the following data that had different origins:

- Force values measured experimentally during a whole running step of a elite paralympic athlete in field;
- Numerical stiffness curves, and therefore the displacements of the clamp (for a given angle of the ground), obtained from the static FEM tests previously described.

As already mentioned in paragraph 3.3, these stiffness curves depend exclusively on the type of static tests that were carried out on the bench test, who are unable to reproduce the complete step but only an instant of it keeping the angle of inclination of the ground fixed.

For this reason it would not be optimal to use static curves and to compare them with forces obtained dynamically during the real step. However, this study has still been reported because it allows to make useful considerations that can be used for future static tests on the bench test.

In this paragraph the outdoor test session n°8 was considered: these was carried on in Budrio (19-04-2019), at the athlete's track, by the elite paralympic athlete Martina Caironi. [15]

During this session several runs were recorded, and for each of them it was possible to measure the ground reaction forces (GRFs) one of the following methods:

- Via Kistler force platform 9281EA (600x400 mm): multicomponent force plate with wide range for measuring ground reaction forces, moments and the centre of pressure. [15]
- Via instrumented Running Prosthetic Foot (iRPF) [22]. In some previous theses, carried out at the University of Padua and in collaboration with INAIL, it was designed an instrumented Running Prosthetic Foot: using it can be possible to directly measure loads on the foot and indirectly the GRFs. [15] [16] [23]

  Between the instrumented prostheses that were calibrated and validated there is also the prosthesis studied in this thesis (Ottobock Runner Standard C-shaped category 3).

  In order to instrument the prosthesis it was decided to apply three half strain gauge bridges for measure bending moment: the first two bending bridges are attached on the straight segment of the prosthesis near the clamp bottomhole and the third bridge is positioned orthogonally with respect to the curved tract, along the arch of curvature. The half bridges are composed by two strain gauges each, that are positioned symmetrically one on the external surface and one on the internal surface of the foot. [15] [23]

  Thanks to the calibration it is possible to know loads on the prosthesis in the Foot Reference System (X_F, Y_F in Figure 3.21): is the reference frame of the prosthetic foot. The origin is located at medial straight section of the foot, near the clamp (this point coincides with the position BRG1). The X_F axis is parallel to medial straight section of the foot with a posterior-to-anterior direction (this axis joins the first with the second strain gauge bridge). The Y_F axis is orthogonal to the medial straight section of the foot and directed upwards. The transversal axis Z_F axis is obtained with the right-hand rule. [15]
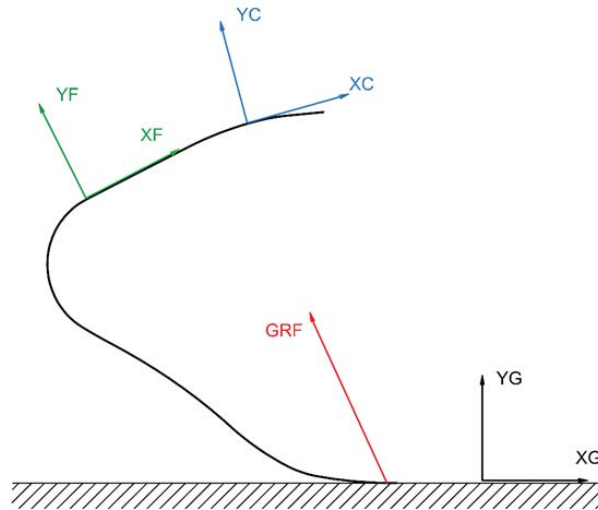
*Figure 3.21: Frame systems sketch. The positions of the Foot (green colour),
Clamp (blue colour) and Ground (black colour) reference system are shown*

Finally, knowing the orientation of the Foot reference frame respect to the Ground reference frame (X_G, Y_G in Figure 3.21), it is possible to measure indirectly the GRFs.
Ground reference frame has the origin located at a fixed point of the ground. The X_G axis is parallel to the ground in the sagittal plane with a posterior-to-anterior direction. The Y_G axis is orthogonal to longitudinal axis and directed upwards. The Z_G axis is the transversal axis obtained using the right-hand rule.

Ground reaction forces measured during three different RUNs of session n°8 were taken into account, summarized in the following Table 3.8.

RUN number	Test type	Clamp positions	GRFs
9	Run on track	+4°	by iRPF
12	Run on track	+4°	by iRPF
14	Run on force platform	-4°	by force platform

Table 3.8: Runs considered of test session n°8 (Budrio 8th April 2019)

The ground reaction forces ($GRFx$ and $GRFy$) taken by each RUN were plotted, using trigonometric equations, in the clamp reference system (F_{XC} and F_{YC}) because, as said, all the static-numerical stiffness curves, that were used for the following observations, refer to this reference frame (X_C, Y_C in Figure 3.21).
In addition, the following color code, summarizes in Table 3.9, was used for the following figures.

Parameter	Colour
$GRFx$ (Ground reference frame)	
$GRFy$ (Ground reference frame)	
F_{XC} (Clamp reference frame)	
F_{YC} (Clamp reference frame)	

Table 3.9: Color code for the following figures of forces

Furthermore, as it was done before, it was used continuous lines to represent the curves found numerically and dashed lines to represent the curves found experimentally.

3.7.1 RUN 9: Run on track (Martina Caironi, 19-04-2019 Budrio, RSF Ottobock Standard CAT3, Configuration 2 (Clamp +4°))

Right now, the stiffness of the prosthesis was numerically evaluated, changing the angle of the platform ϑ_G, up to vertical loads of 3500N. However, the athlete does not stress the prosthesis at maximum load in every instant of the run. In fact, forces vary during the step, with the vertical load peak near the "midstance" instant.

An example of a graph of the components of the ground reaction forces, as a function of the contact time, is shown below in Figure 3.22; it was obtained by analysing the data measured by the iRPF during step n°8 of the RUN9 performed by the elite athlete Martina Caironi.
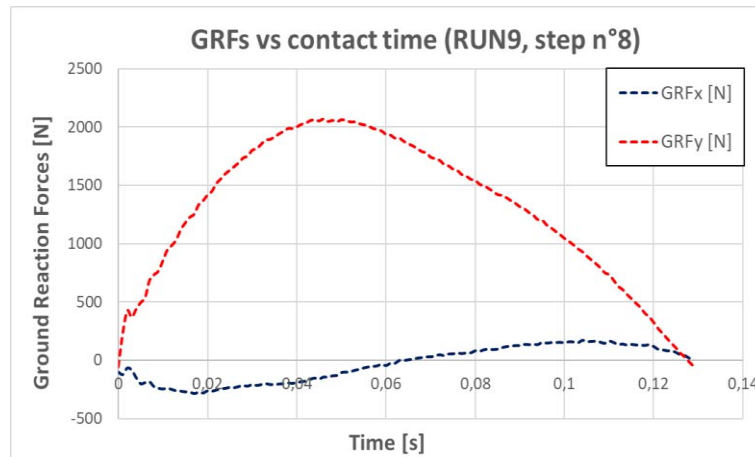

Figure 3.22: Ground reaction forces in the Ground reference frame (step n°8, RUN9)

Therefore, in this Paragraph 3.7, it was studied what are the limit conditions of use of the prosthesis, beyond which it is not practical to analyse using the test bench how the prosthetic foot behaves.

As said before, thanks to the instrumented prosthesis, it was possible to know the reaction forces in the ground reference system (Figure 3.22 is an example) once they were measured in the Foot reference system. However, during the numerical analyses previously done, the forces and stiffness curves were evaluated in the clamp reference frame (X_C, Y_C). It is therefore necessary to plot the reaction forces of the ground in this reference system.

In section 2.2.2 it was asserted that the relative position between the two reference systems X_C, Y_C and X_G, Y_G allowed to define at any time the angle of the ground ϑ_G (Figure 3.23): ϑ_G is the angle between the Y_C axis and Y_G axis (or X_C and X_G), positive if anticlockwise for the convention adopted.
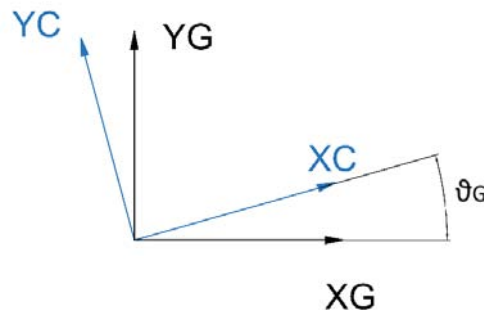

Figure 3.23: Sketch of the ground angle ϑ_G

Furthermore, it should be noted that, considering a general treatise, the reference system of the clamp is not unique: it is possible to define a greater numbers based on the number of positions in which the clamp can be locked (e.g.: -4°, 0°, +4°).

Before explaining how to calculate the reaction forces in the clamp reference system, the first thing to do is to plot these forces no longer as a function of the contact time but as a function of the angle of the platform ϑ_G, which varies during the running stance. In this way it is possible to know the value of the reaction forces for each value of the angle of the ground.

During the field trials of 19-4-2019,all the tests were performed by Martina while wearing the Xsens suits. The Xsens MVN is an inertial motion capture system for full-body human motion capture; the system is based on inertial sensors and wireless communication combined with algorithms, using assumptions of biomechanical models. The Xsens MVN is a portable system usable both indoor and outdoor. The Xsens suit was used to capture the absolute orientation of the foot ϑ_{Foot}, necessary for indirect evaluation of GRFs from iRPF, but the use by an amputee runner required some adaptations: with a transfemoral athlete, like Martina, the Lower LEG (shank) sensor is applied on the RPF proximal end and the FOOT sensor is applied on RPF distal End (Figure 3.24). [15] [23]
This mean the Lower LEG sensor described not the tibia/shank orientation but the orientation of the iRPF: this angle coincides with the absolute angle of the prosthetic foot ϑ_{Foot} with respect to the horizontal and it was determined as the angle between the X_F and X_G axes, positive if anticlockwise (Figure 3.25).
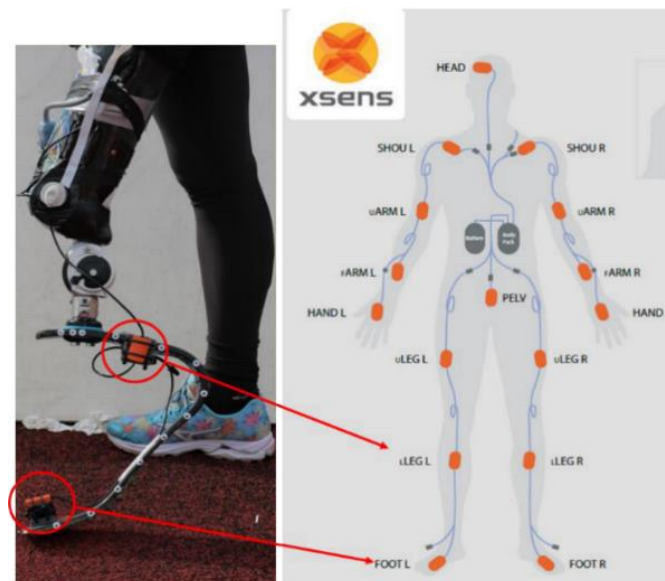

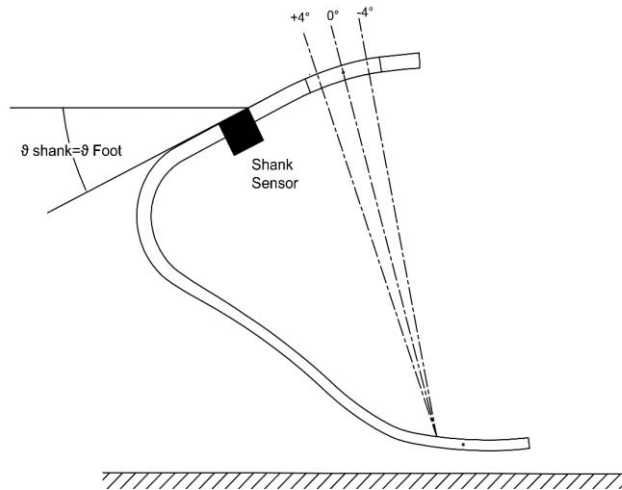*Figure 3.24: Sensors position on the iRPF*

Figure 3.25: Sketch of the position of the Xsens sensor on the prosthesis and the angle ϑ_{Foot}.
The axis of the clamp for the three configurations is also shown (clamp +4°, 0°, -4°)

Experimentally, there was a variation of this angle practically linear over time. In this particular example, shown in Figure 3.25, ϑ_{Foot} varied between -28.5° and +12°.

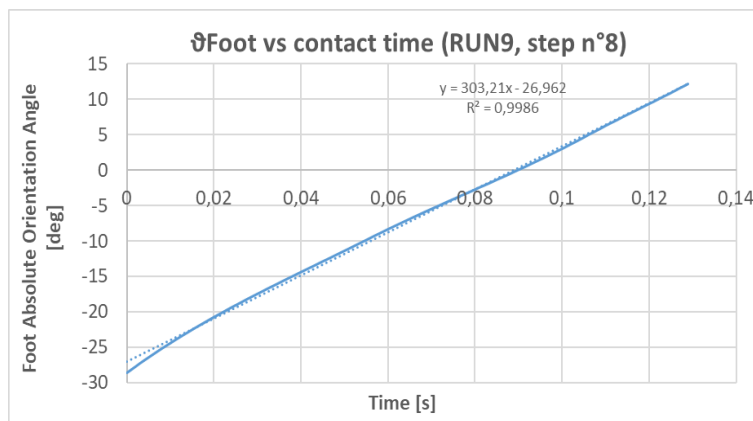*Figure 3.25: Foot absolute orientation angle (RUN9, step n°8)*

The knowledge of this angle is necessary to determine how the angle ϑ_G changes during the step. Using the CAD drawing of the prosthesis, an angle α can be defined between the X_C axis of the clamp reference system and the straight part of the foot (X_F axis), where the sensor is placed. α angle clearly can change according to the position of the clamp considered (Table 3.10 and Figure 3.26). However, for a given position of the clamp, when the prosthesis is undeformed (for example in the previous instant before contact), α is constant.

Clamp position	α
+4°	8
0°	12
-4°	16

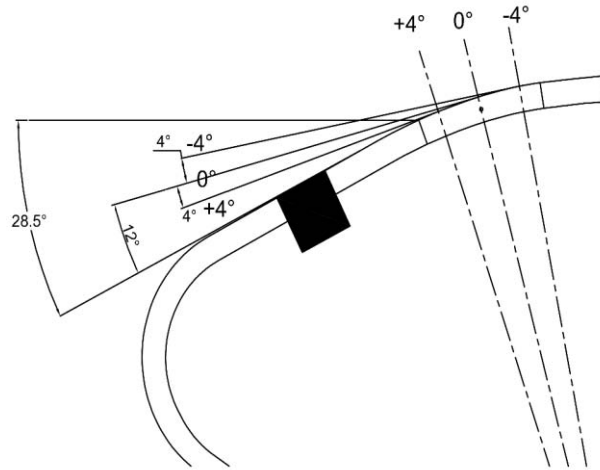*Table 3.10: α values changing the clam position*

Figure 3.26: Sketch used for α evaluation

Now, considering the initial instant of contact ("Heel Strike") when the prosthesis has not begin to deform, the following general equation can be used to calculate the angle of the ground ϑ_G at the t = 0s instant of contact:

$$\vartheta_{G,h-s} = \vartheta_{Foot,t=0} + \alpha \tag{3.7}$$

where $\vartheta_{Foot,t=0}$ is the foot angle measured at the initial contact instant and α is the angle between the X_C and X_F axis (Figure 3.27). So, in this clamp +4° case of RUN9 (α = 8°), being ϑ_{Foot} = -28.5° when t = 0s, the angle of the ground $\vartheta_{G,h-s}$ is equal to -20.5°.
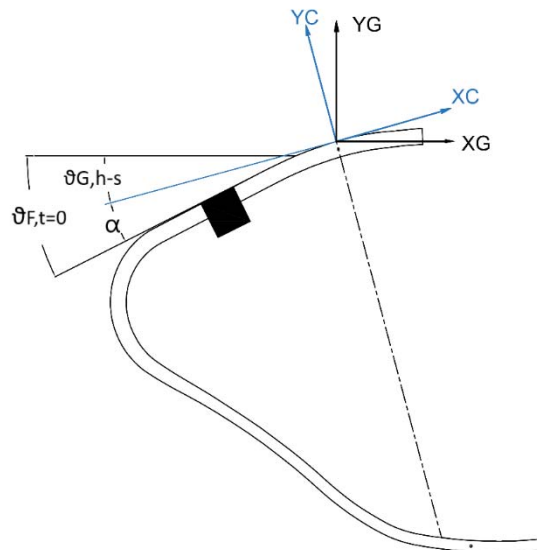
Figure 3.27: Sketch used for $\vartheta_{G,h-s}$ evaluation

Therefore, for a given position of the clamp, the value of the angle ϑ_G at the initial instant t=0 is known. It is also considered the hypothesis that ϑ_G varies linearly over time as ϑ_{Foot} (according to a straight line of angular coefficient "m" equal to the angular coefficient of ϑ_{Foot}), it is possible to plot ϑ_G as a function of the step contact time (Figure 3.28). The straight line equation of ϑ_G is the following:

$$\vartheta_G = m * t + \vartheta_{G,h-s} \tag{3.8}$$

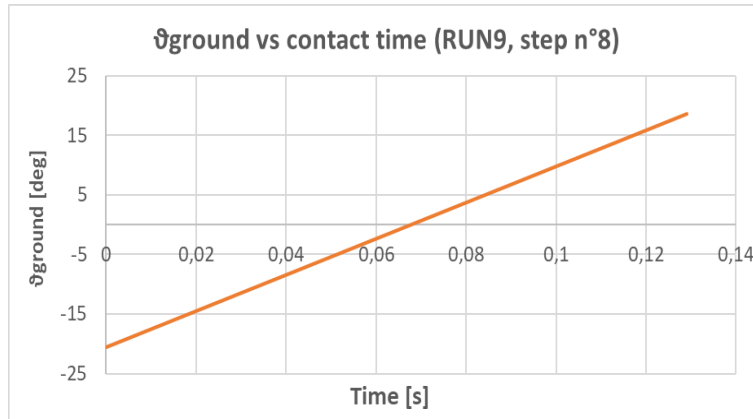*Figure 3.28: Plot of ϑ_G as a function of the step contact time (RUN9, step n°8)*

Therefore, an inclination of the ground is assigned at every instant. So, it is possible to plot the reaction forces, in the ground reference system, as a function of ϑg, as shown in Figure 3.29.
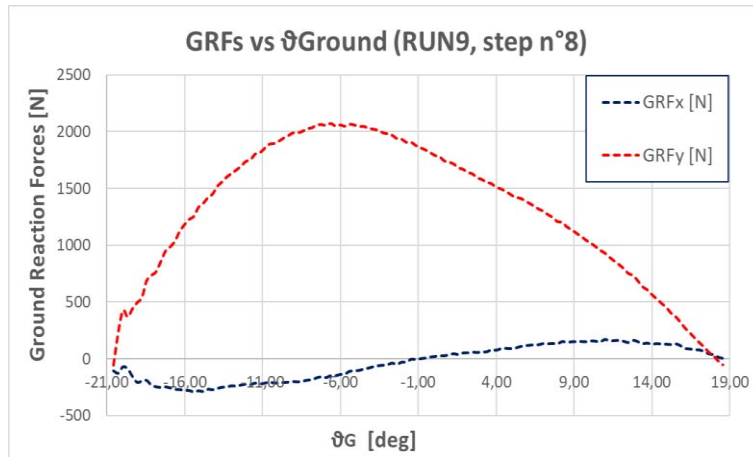

Figure 3.29: Ground reaction forces as a function of ϑ_G in the Ground reference frame (step n°8, RUN9)

These forces are known in the ground reference system (X_G, Y_G) but, as mentioned before, during FEM analyses the clamp forces were evaluated. Therefore, the GRFs must be plotted in the clamp reference frame (X_C, Y_C). In order to obtain this, the following trigonometric equations were used, which consider the signs of the forces and ground angle:

$$F_{XC} = GRFx * \cos(\vartheta_g) - GRFy * \sin(\vartheta_g) \tag{3.9}$$

$$F_{YC} = GRFx * \sin(\vartheta_g) + GRFy * \cos(\vartheta_g) \tag{3.10}$$

$$\rho = \frac{F_{XC}}{F_{YC}} \tag{3.11}$$

In Appendix B is shown a summary table of the loads involved, for the +4° clamp configuration of the RUN9. In Figure 3.30 these reaction forces are represented in the clamp reference system as a function of ϑ_G.
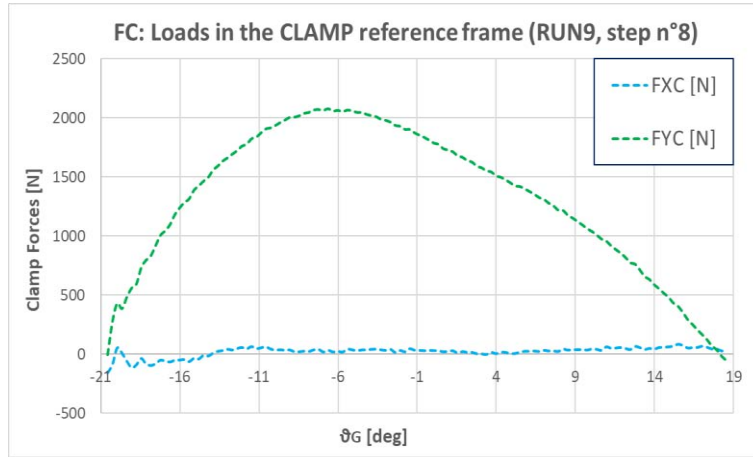
Figure 3.30: Reaction forces as a function of ϑ_G in the Clamp reference frame (step n°8, RUN9)

Thanks to this last graph, it is possible to have an idea of the loads acting on the prosthesis in the clamp reference system during the whole stance phase. Furthermore, in this case the following aspect is observed: although the force F_{YC} does not have appreciable variations in the reference system of the clamp, the same can not be said for F_{XC}. The trend of this horizontal force clearly depends on the position of the clamp, and this influences the load ratio $\rho = F_{XC}/F_{YC}$ in the clamp reference frame. In this case, for example, the average load ratio ρ is almost null during the step contact time.

These forces of Figure 3.30, evaluated in the clamp reference system, coincide with the loads that were considered below to evaluate the limit conditions of use of the prosthetic foot. As mentioned at the beginning of paragraph 3.7, in addition to considering the forces measured experimentally during an entire stance phase, the numerical stiffness curves obtained from static FEM tests were used. In particular, the stiffness curves of Figure 3.16 obtained in clamp conditions 0° and ρ=0 were considered. However, since the position of the clamp does not cause any significant variation on the stiffness of the prosthetic foot during these static tests, Figure 3.16 can be also used for the configuration of RUN9 with clamp +4° and load ratio ρ=0 in the clamp reference frame.
In addition, for subsequent evaluations it was considered load conditions higher than those measured during the field tests by increasing F_{YC}. A vertical force value increased by 20% was evaluated.

$$F_{YC,max} = 1.2 * F_{YC} \tag{3.12}$$

The following procedure were used below: from the experimental load curve (Figure 3.30) it is known, for every inclination of the ground, the value of the force F_{YC} in the clamp reference frame. Known the angle ϑ_G, the corresponding static stiffness curve, among those plotted in Figure 3.16, is chosen. Considering this curve, it is found the value of the clamp displacement d_{YC} to which that real load value F_{YC} matches. The same is done for the 20% increased vertical load.

Since, for this particular step, the angle of the ground varied between -20.5° and +18.5°, the data of the following Table 3.11 were considered.

ϑ_G [deg]	$F_{YC,Exp}$ [N]	$d_{YC,FEM}$ [mm]	$F_{YC,max} = 1.2 * F_{YC,Exp}$ [N]	$d_{YC,max}$ [mm]
-20°	430	14.2	515	16.5
-15°	1390	51.6	1668	61.0
-10°	1938	82.0	2326	93.5
-5°	2062	98.8	2474	112.9
0°	1789	99.2	2147	115.1
+5°	1453	98.8	1744	112.8
+10°	1041	93.7	1249	103.7
+15°	484	51.7	581	62.1

Table 3.11: $F_{YC,Exp}$ and $d_{YC,FEM}$ values changing the angle of the ground

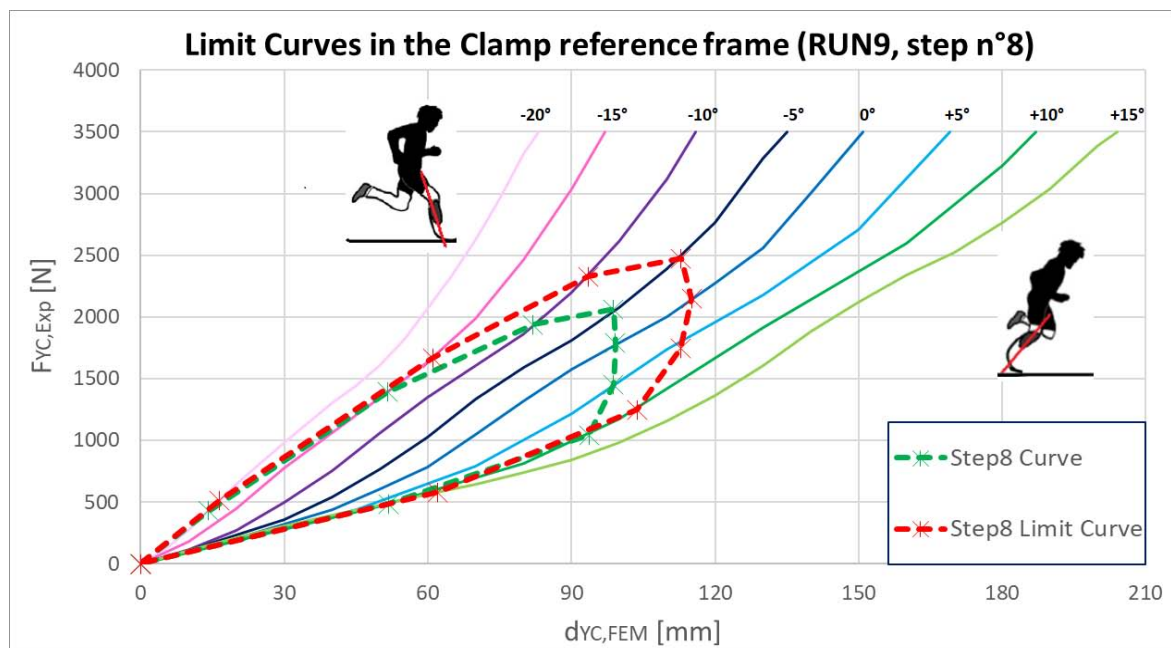The results found, shown below in Figure 3.31, were plotted in the $F_{YC} - d_{YC}$ map.

Figure 3.31: Curve of use (green color) and limit curve of use of the
RSP Ottobock Standard Category 3 (RUN9, step n°8)

Although this is a conventional treatise because experimentally measured forces were compared with numerical static stiffness curves, it allows to estimate the curve of use of the prosthesis (green curve in Figure 3.31) during the generic step performed by the paralympic athlete Martina Caironi. The red curve, on the other hand, has a much more interesting meaning: it represents the limit (forces increased by 20%) beyond which there is not practical sense to study the behavior of the prosthesis because, during the run, the athlete will not reach greater loads.

3.7.2 RUN 12: Run on track (Martina Caironi, 19-04-2019 Budrio, RSF Ottobock Standard CAT3, Configuration 4 (Clamp +4°)). Evaluation of three different steps.

In the previous paragraph 3.7.1, considerations were made by evaluating only one generic step. However, during the run, the athlete can not take steps that are all the same.

Therefore, three different steps (step n ° 9-10-12) performed in another run (RUN 12) by Martina were analyzed. These steps present ground reaction forces with very similar trends and load peaks. Instead, the angle of the prosthetic foot ϑ_{Foot} measured during the contact phase varies between the three steps, and therefore also the angle of the ground ϑ_G.

Using the method defined in the previous paragraph, known experimentally ϑ_{Foot} angles for the three steps, the variations of ϑ_G were evaluated. Table 3.12 shows the values of the angles ϑ_{Foot} and ϑ_G at the start ("heel strike") and at the end ("toe off") of each step.

	$\vartheta_{Foot,h-s}$[deg]	$\vartheta_{Foot,t-0}$[deg]	$\vartheta_{G,h-s}$[deg]	$\vartheta_{G,t-o}$ [deg]
Step 9	-27.5	+12	-20	+21.5
Step 10	-18	+20	-10	+31
Step 12	-15.5	+25	-7.5	+32

Table 3.12: ϑ_{Foot} and ϑ_G values at the start ("heel strike") and at the end ("toe off") of each step

As done before, known experimentally the reaction forces of the ground, these forces were evaluated in the clamp reference system, using equations (3.9) and (3.10), and they were plotted as a function of ϑ_G (Figure 3.32):
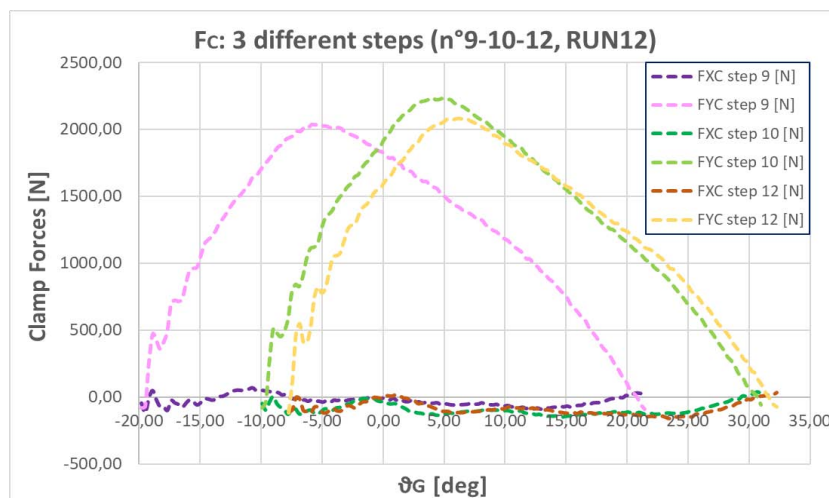

Figure 3.32: Reaction forces as a function of ϑ_G in the Clamp reference frame (step n°9-10-12, RUN12)

Also in this case, for clamp +4° position, the load situation in the clamp reference frame was very close to the load configuration ρ=0: the numerical stiffness curves of Figure 3.16 are therefore considered again. Here, for simplicity, only $F_{YC,max}$ forces increased by 20% compared to their real value were used. The following values (Table 3.13) were found for each step. Also these values were plotted in Figure 3.33: it shows the limit load curves of the three steps in the graph $F_{YC} - d_{YC}$.

ϑ_G [deg]	STEP 9		STEP 10		STEP 12	
	$F_{YC,max}$ [N]	$d_{YC,max}$ [mm]	$F_{YC,max}$ [N]	$d_{YC,max}$ [mm]	$F_{YC,max}$ [N]	$d_{YC,max}$ [mm]
-20	306	10.8	/	/	/	/
-15	1265	47.1	/	/	/	/
-10	2032	85.0	336	23.3	/	/
-5	2436	111.8	1504	77.2	934	56.3
0	2200	117.4	2310	121.9	1880	103.4
+5	1798	112.7	2678	149.2	2472	142.2
+10	1422	110.6	2324	148.0	2269	145.5
+15	892	91.3	1868	141.4	1894	142.4
+20	134	13.4	1378	135.7	1496	141.9
+25	/	/	842	96.8	1000	114.0
+30	/	/	72	5.1	314	30.8

Table 3.13: $F_{YC,max}$ and $d_{YC,max}$ values changing the angle of the ground (RUN12, step n°9-10-12)
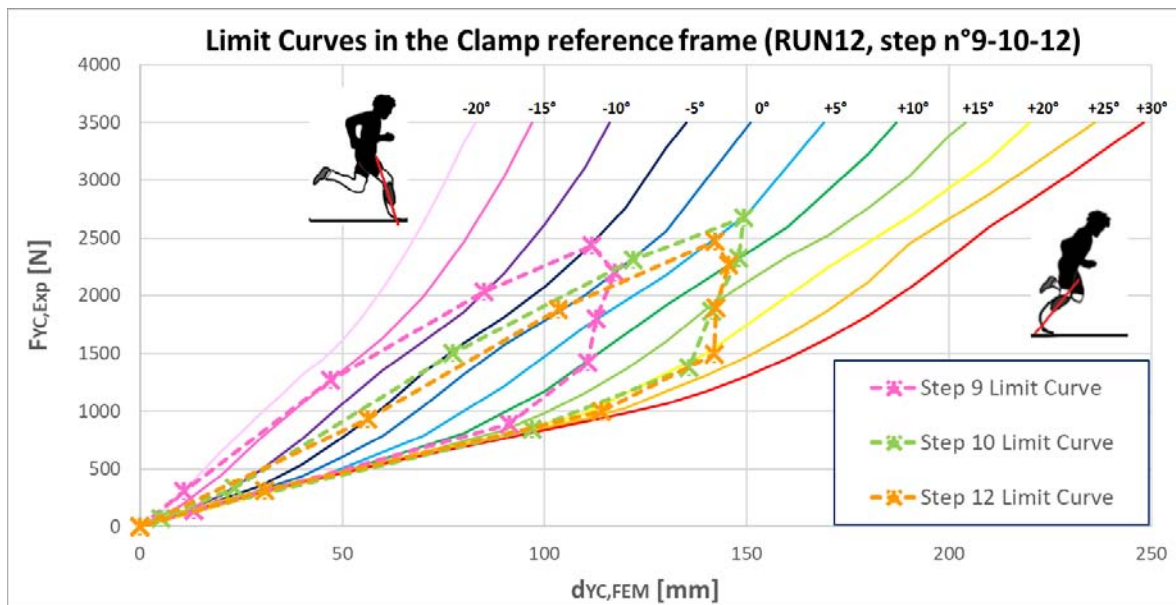

Figure 3.33: Limit curves of use of the RSP Ottobock Standard Category 3 (RUN12, step n°9-10-12)

From the analysis of this Figure 3.33, the following observations were made:
- The vertical force peak may not occur when the ground angle is 0°.
- Since the curves of the various steps are not overlapping to each other, in order to determine the limit conditions of use of the prosthetic foot during the "stance" phase, it is not correct to consider a single step (as done in section 3.7.1). Taking into account several curves, concerning to a greater number of steps, it is possible to obtain a single final summary map, by envelope of curves, shown in Figure 3.34. This graph can be particularly useful in future experimental laboratory tests on the same prosthesis. In fact, from the analysis of Figure 3.34 it can be understood, for example, how it can be interesting to study the behavior of the prosthetic foot beyond 2000 N for ground angles ϑ_G between -10° and +10°. Vice versa, it is not practical to perform bench tests with vertical forces equal or greater than 1500 N for example for ground angles of -20°, -15°, +25°, +30°. This is because the athlete, with this prosthesis, will never reach similar loads on the track during the initial and final part of the stance phase. These considerations on the loads to be considered in the various static tests can be made for each angle of the ground ϑ_G.
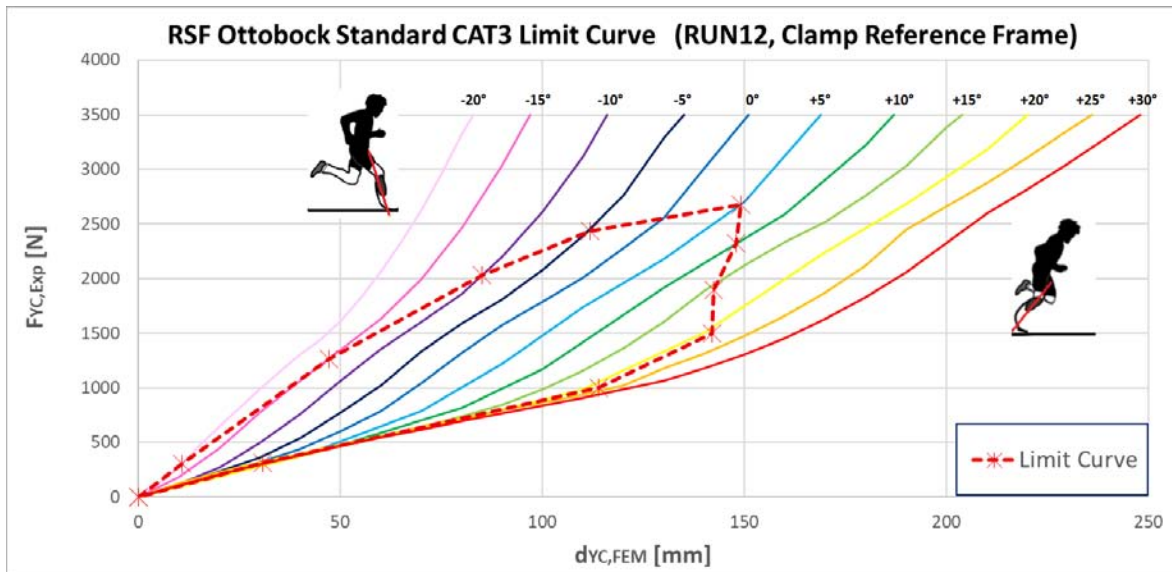
Figure 3.34: Final limit curve of the RSP Ottobock Standard Category 3 (RUN12)

3.7.3 Comparison between a step with clamp +4° (RUN9) and a step with clamp -4° (RUN14) (Martina Caironi, 19-04-2019 Budrio, RSF Ottobock Standard CAT3)

All the steps considered in the two previous sections referred to configurations in which the clamp was positioned at +4°. What it was done here is to evaluate the behavior of the prosthesis during a step in which the clamp were placed at -4° and compare this result with that found for a clamp + 4° configuration.

RUN14 of 19/04/2019 were considered for this purpose: ground reaction forces measured by a force platform placed along the track were used as reference forces. The load values found and the step contact time were very similar to those measured in the previous runs (Figure 3.35).
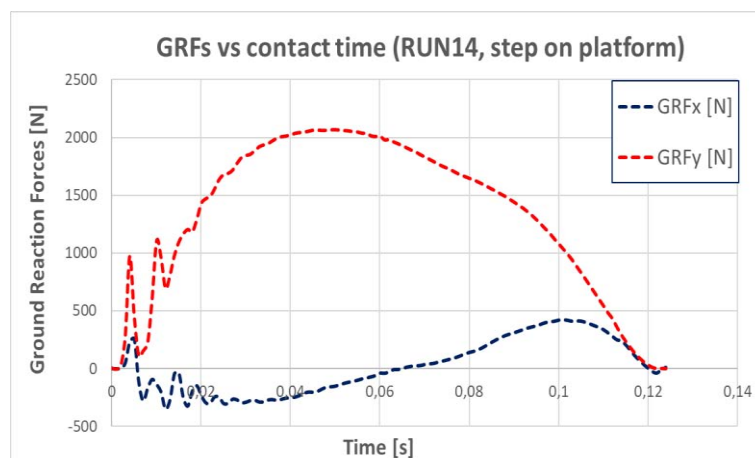

Figure 3.35: Ground reaction forces in the Ground reference frame (step on platform, RUN14)

Also in this case the absolute angle of the foot is known, which varied from the initial instant ("heel strike", equal to $\vartheta_{Foot,h-s}$ = -34°) to the final contact one ("toe off", equal to $\vartheta_{Foot,t-o}$ = +22°). Using the method defined in paragraph 3.7.1, known ϑ_{Foot} angles during the step, the variation of the ground angle ϑ_G (evaluated considering the position of the clamp -4 °, α = 16 °) were determined: in this case $\vartheta_{G,h-s}$ = -18° and $\vartheta_{G,t-o}$ = +38°.

By defining the following range:

$$\Delta\vartheta = \vartheta_{Foot,h-s} - \vartheta_{Foot,t-o} = \vartheta_{ground,h-s} - \vartheta_{ground,t-o} \qquad (3.13)$$

It is possible to make the following observation: this range is greater in the case of clamp -4° ($\Delta\vartheta_{-4°} \approx 55°$) than in the case of clamp +4° ($\Delta\vartheta_{+4°} \approx 40°$, look at the step of RUN9 or RUN12). Therefore two steps, obtained with the clamp positioned differently, are more differentiated by this range value and not by the loads involved or the step contact time itself.

Using equations seen in paragraph 3.7.1, it was possible to calculate the reaction forces from the ground reference system (X_G, Y_G) to that of the clamp (X_C, Y_C). F_{XC} and F_{YC} were plotted as a function of ϑ_G in Figure 3.36.
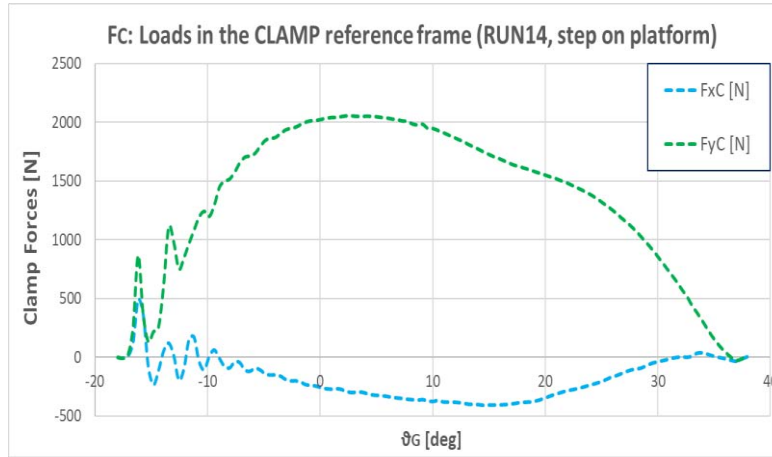

Figure 3.36: Reaction forces as a function of ϑ_G in the Clamp reference frame (step on platform, RUN14)

From this figure it can be seen that the horizontal force plotted in the clamp reference system, in the case of clamp -4°, was negative for almost the entire duration of the step, unlike what happened during RUN9, where the clamp were placed at +4°.

The trends of the limit curves in the graph $F_{YC} - d_{YC}$ are shown below in Figure 3.37. In order to make a comparison, the RUN9 limit curve (clamp +4°) were plotted in the same graph.
It was noted that the area below the limit curve relating to the RUN14 step is greater than that relating to the RUN9: the reason is due to the fact that, as mentioned before, the forces involved are similar for the two steps , but the range $\Delta\vartheta$ is larger during RUN14.
However, these observations may depend on the fact that the forces of the RUN14 were measured by a force plate, and it was seen in a previous thesis ([15]) that when the athlete run over a platform, it changes its usual running technique to catch it and what the plate collect is a false step.
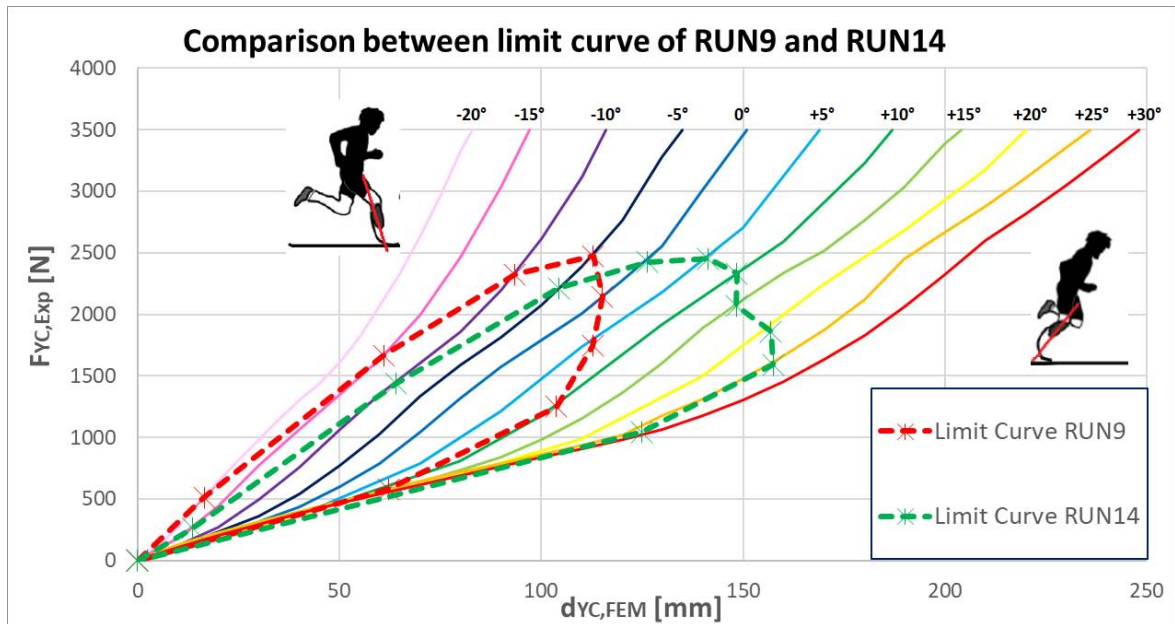
Figure 3.36: Comparison between limit curves of RUN9 (red colour) and RUN14 (green colour) of the RSF Ottobock Standard Category 3

3.8 Cyclic Tests

During the experimental thesis developed by L. Mazzanti [17], in-vitro cyclic tests were carried out according to what was read in literature [9]. It was called cyclic test the loading and unloading test for different configurations of ground orientation.

The adopted method consisted in inclining the platform at 0° and then at +15° and putting an aluminium 10mm plate over due aluminium rollers (Figure 3.37). Ottobock Standard Category 3 RSF was tested: the foot contact was between the sole and tartan placed over the aluminium plate.

Figure 3.37: Roller system as contact surface [17]

The maximum vertical force F_{YC} reached for every load-unload cycle was about 2500 N and pre-established from vertical cylinder control: the experiments were all made in displacement control setting (4.5 mm/s vertical actuator displacement).

RS3 was hooked with the clamp placed at +4° and with the tip advanced 50 mm (TAP) with respect the centre of the 6-axes load cell.

Thanks to the use of the two rollers, the aluminum plate was free to slide horizontally X_G in the ground reference system. For this reason tangential force F_{XG} was almost zero (its maximum value was about 2% maximum F_{YG}) and it increased increasing the normal force because it depended on friction between the two rollers and the sledge. Therefore, F_{XG} was considered negligible and F_{YG} was the total resultant force.

As a further validation of the FEM model and the value of the equivalent elastic modulus found (33000 MPa), it was decided to recreate these conditions also in the Static environment of ANSYS Workbench, using however only the load part of the cyclic test.

Preprocessing steps (import the geometry ensuring the correct TAP=50 mm, define the material proprieties and the surfaces of symmetry, select the contact surfaces, create the mesh) are the same as explained in Chapter 2. The only difference lies in the constraint applied to the ground. In fact, during the static tests described in paragraph 2.2, the platform was moved by the horizontal cylinder in the X_C direction of the clamp reference system. However, during these cyclic tests, as just mentioned, thanks to the presence of the two aluminium rollers, the plate is free to slide in the X_G direction of the ground, which coincides with X_C only when ϑ_G=0°.

Therefore, another reference system representative of the ground reference frame was created within ANSYS, placed on the upper surface of the platform (Figure 3.38). Hence, when the platform constraint is set, it is left free to slide no longer in the X_C direction but in the X_G direction of the new reference system (Figure 3.39).
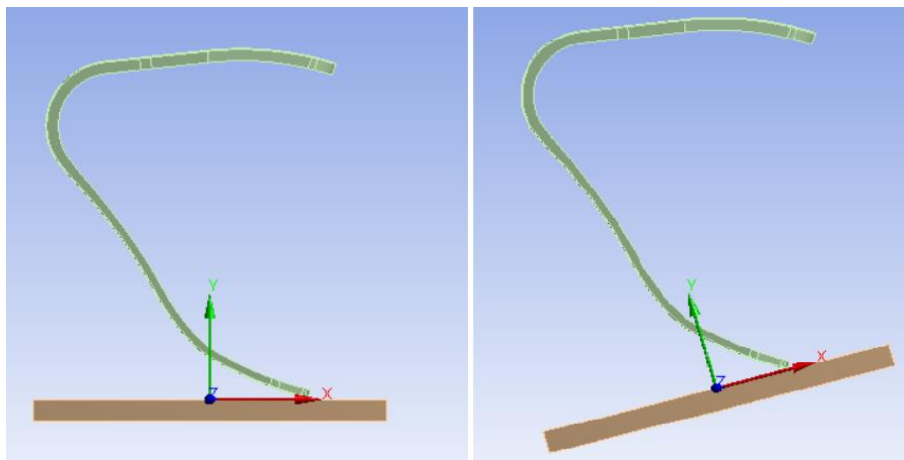

Figure 3.38: Ground reference frame created on the upper surface of the platform

Figure 3.39: Ground free to slide in the X_G direction

Instead, the vertical displacement d_{YC} imposed on the clamp area is known from experimental tests (here 125 mm for the ground 0° case and 130 mm for the ground +15° case).

Once simulations were performed for the two ground orientations, the results found were plotted in a $F_{YC} - d_{YC}$ graph (Figure 3.38), where numerical curves were compared with the experimental ones.
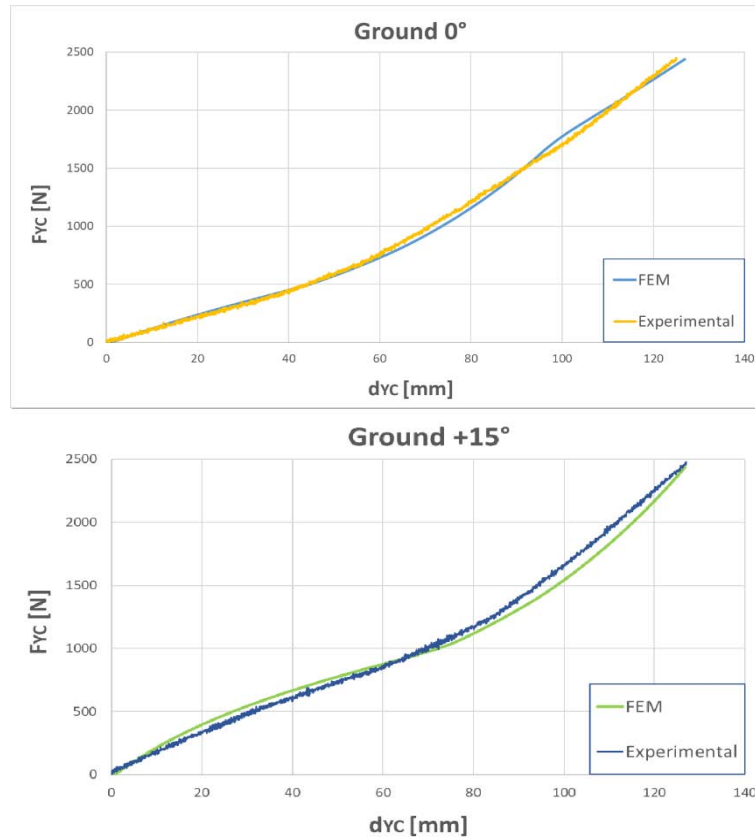

Figure 3.38: Comparison between FEM and experimental stiffness curves. Up curves for ϑ_G=0°, down curves for ϑ_G=+15°

Also in this case, stiffness is not linear during the test. Looking to the concavity, there is a sort of softening for +15° configuration till about 1000 N, while the 0° curve is always hardening till the peak.

In order to compare the numerical and experimental results, K_L stiffness was calculated for each curve, evaluated by linear interpolation up to the peak force of 2500N. Moreover, the percentage differences Δ, respect to the stiffness obtained in experimental test, were calculated for each ground configuration. Results are shown in Table 3.14.

	$K_{L,FEM}$ [N/mm]	$K_{L,Exp}$ [N/mm]	Δ [%]
Ground 0°	16.56 (R^2=0.976)	16.47 (R^2=0.979)	+0.54
Ground +15°	16.13 (R^2=0.989)	16.69 (R^2=0.989)	-3.35

Table 3.13.4: K_L numerical and experimental values obtained when the inclination of the ground changes. Δ values were calculated respect to the stiffness obtained in the case ρ=0

The graphic analysis of the stiffness curves of Figure 3.38 and the data shown in the Table 3.14 are a further confirmation of the proper functioning of this FEM model also for this different type of bench test.

CHAPTER 4: NUMERICAL SIMULATION OF A RUNNING STEP

4.1 Introduction

In Chapter 2 the calibration of the RSF numerical model was performed using experimental static tests as reference. Assuming the material behaviour as isotropic linear elastic, it was possible to determine an equivalent static elastic modulus for the FEM prosthesis, equal to:

$$E_{eq,s} = 33000 \, MPa$$

The goal of this Chapter consists in reproducing numerically, using ANSYS Workbench, a whole step during the running stance phase. In order to succeed in doing that, the real trajectories of at least two points of the system have to be known; doing that, it is possible to describe the displacement and rotation constraints of the RSP in the sagittal plane.

Once the FEM simulations were performed, the numerical reaction forces of the ground (GRFs) were evaluated. Then these forces were compared with the real reaction forces measured by a force platform during the athlete's run. From this comparison it is easily understandable how the numerical model reproduces the real prosthesis behaviour during the whole step.

Then the potentiality of the FEM simulations was used to obtain other information such as the trend of the centre of pressure (COP) and to compare it with the real one measured by the force platform.

In the following paragraphs many graphs concerning the reaction forces in the ground reference system will be presented. In particular it was decided to use continuous lines to represent the curves found numerically and dashed lines to represent the curves found experimentally.

Moreover, the following color code, summarizes in Table 4.1, was used for the following GRFs figures.

Parameter	Colour
$GRFx$ (Ground reference frame)	
$GRFy$ (Ground reference frame)	

Table 4.1: Color code for the following Chapter 4 GRFs figures

4.2 Evaluation of trajectories by Kinovea

The purpose of this first part consists in evaluating the equations, functions of time, that describe the displacement and rotation of at least one point of the RSP in the sagittal plane. These equations are necessary because they will later be used as constraints for the numerical simulations.

One of the videos recorded during an outdoor test session was used to evaluate these trajectories. In this case, it was used a video recorded during the RUN14 of test session n°8: these was carried on 19-04-2019 in Budrio at the athlete's track. For this run the configuration of the prosthetic structure used the clamp placed at -4°. The track was equipped with a Kistler force platform (600x400 mm) and to capture the kinematic of the run it was used two high-speed cameras. [15]

Watching the video, the movement of the prosthesis are observable, but also the movement of the athlete's mechanical knee; this is connected to the prosthesis via clamp joint. This structure that connects the mechanical knee to the prosthesis can be assumed rigid during the step (Figure 4.1). A rigid body in the plane has three degrees of freedom since it can translate along two perpendicular directions and rotate. So, in order to reproduce numerically the step, it is necessary to know the trajectory of two points. Doing that, it is possible to describe the movement in the vertical and horizontal direction of the body, but also the rotation.

For this reason, it was decided to measure the trajectory of the mechanical knee's centre and the trajectory of the clamp, that are the extreme points of the knee-foot joint.
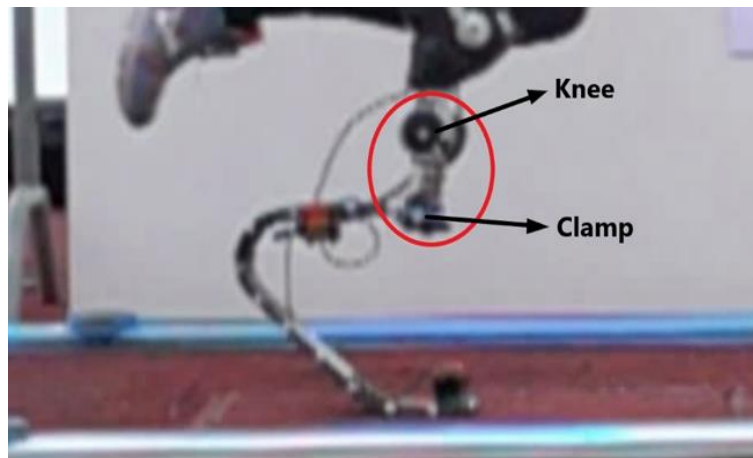

Figure 4.1: Midstance phase of the run: the mechanical knee-clamp structure is highlighted.

These motions were evaluated using an optical motion capture software called Kinovea, importing into it the acquired video of outdoor athlete's run over the force platform.
The procedure which was followed is here explained:
- Open the file video in Kinovea.
- Insert the fixed reference system of the ground $X_G - Y_G$ in the motion plane. The ground reference frame has X_G axis in the gait direction, Y_G axis in the vertical direction, Z_G axis is directed out of the plane by the right-hand rule.
- Define a dimensional scale on an object of known size: as reference length is selected the distance between the tip's marker and the superior part of the prosthesis. The length, equal to 29.5 cm, is shown in green in Figure 4.2.
- Identification of the marker position of the clamp and the mechanical knee centre position (black and white circle in Figure 4.2).

- Tracking of marker motion: reconstruction of the trajectories of the clamp and knee (red curves in Figure 4.2) between the "heel strike" instant and the "toe off" event.
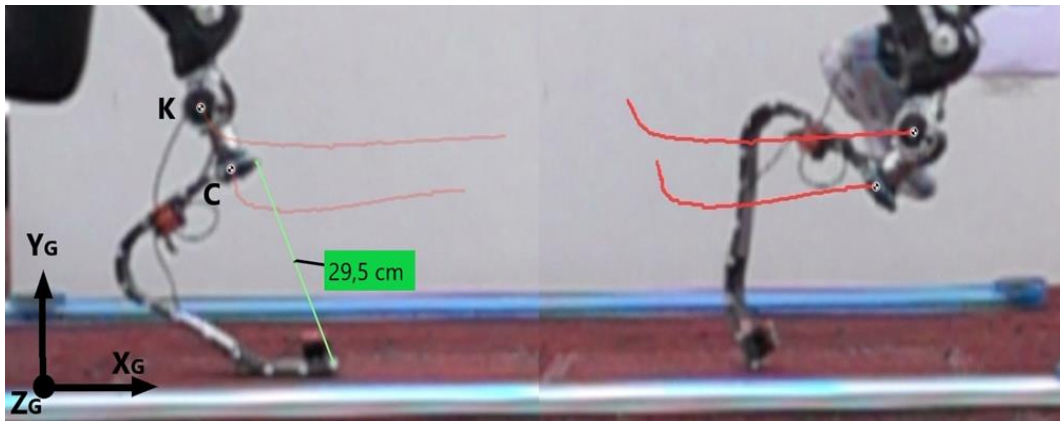

Figure 4.2: "Heel strike" and "toe off" instants photographed with Kinovea

Since the quality of the video was unsatisfactory, it was decided to evaluate the trajectories, both for the clamp and the knee, three times and average them instant by instant, obtaining two average trajectories. For example, the knee trend is shown in the following Figure 4.3.

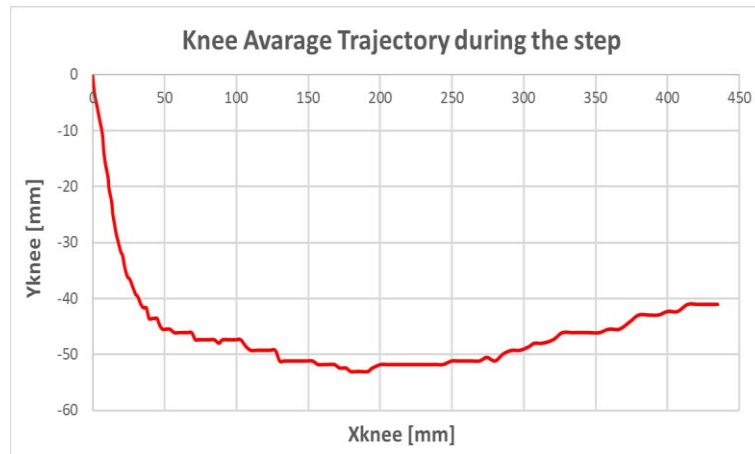
Figure 4.3: Trajectory of the mechanical knee centre in the sagittal plane.

Also, the graph of the knee movement in horizontal direction X_G and vertical direction Y_G is plotted, in Figure 4, as a function of the step contact time (in this case equal to t_c = 120 ms).
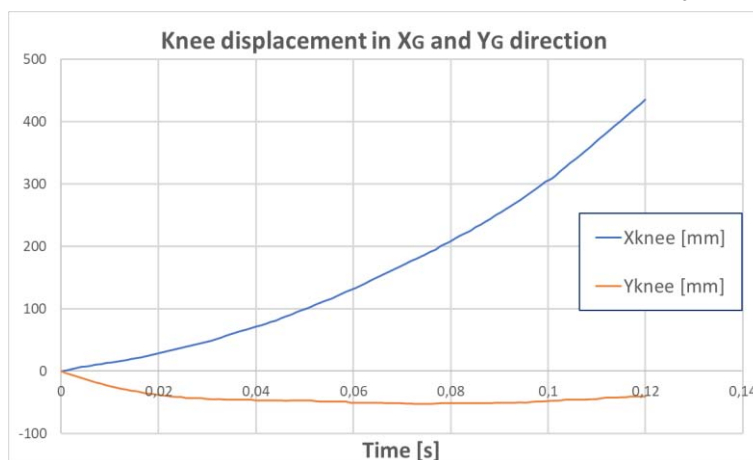

Figure 4.4: Trajectory of the mechanical knee centre in horizontal and vertical direction as a function of t_c

These two curves are extremely important for the subsequent FEM simulations. In fact, by calculating the polynomial regression curves that minimize the least squares, the equations of the knee displacement in the X_G and Y_G direction as a function of time can be evaluated.

$$X_{G,knee} = f(time) \tag{4.1}$$

$$Y_{G,knee} = f(time) \tag{4.2}$$

$$0 \leq time \leq t_c \tag{4.3}$$

Then (4.1) and (4.2) equations will be used in ANSYS, as it will be analysed in section 4.3.1, as displacement constraint to be applied to the mechanical knee centre.

Finally, the rotation around the Z axis was analyzed using both the trajectory of the mechanical knee and the trajectory of the clamp, as shown in Figure 4.5.
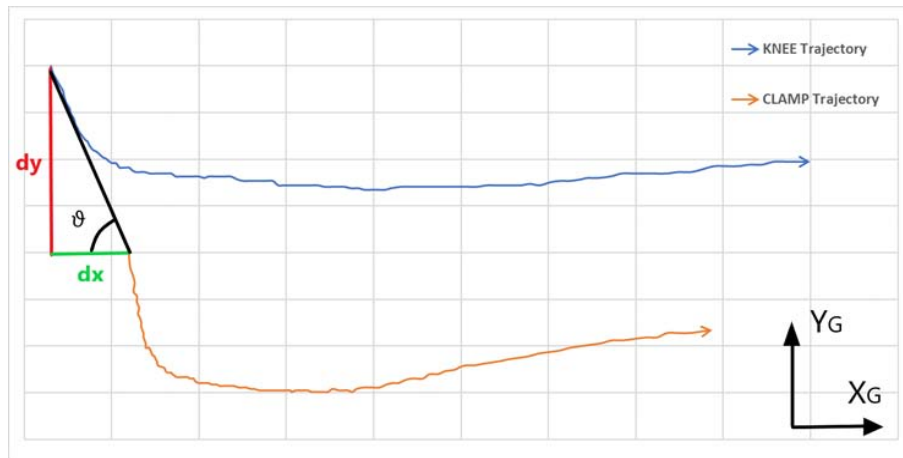

Figure 4.5: Schematization used for calculating the knee-clamp system orientation at heel-strike instant

In order to determine the orientation ϑ of the knee-clamp system, it was considered the initial instant of contact (t_c=0). The orientation was calculated with the arc tangent, using the following equation.

$$\vartheta|_{tc=0} = \arctan \frac{dx}{dy}\Big|_{tc=0} \tag{4.4}$$

Where dx and dy are easily measurable if the two trajectories are known (Figure 4.5). The same method was used for all the pairs of points of each instant of the step, obtaining the system's orientation $\vartheta(time)$ as a function of the contact time.

However, in ANSYS there is the need to introduce not the absolute orientation, but an equation that describes the range of rotation $\Delta\vartheta$ that the mechanical knee-clamp structure undergoes from the initial instant of contact to the detachment from the ground. Since the system performs a clockwise rotation and the Z_G axis is positive if it is out of the sagittal plane (Figure 4.2), the range measured with the following expression will be negative.

$$rotZ_{G,knee}(time) = \Delta\vartheta(time) = \vartheta(time) - \vartheta|_{tc=0} \tag{4.5}$$

In Figure 4.6 the graph of range is plotted as a function of the step contact time.
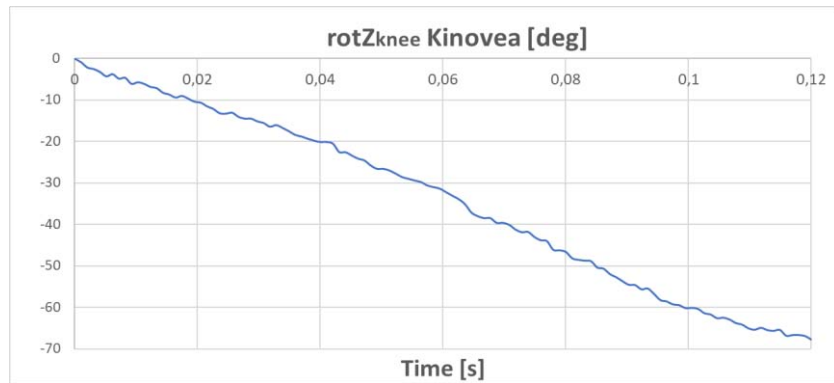
Figure 4.6: Rotation of knee-clamp system in the sagittal plane as a function of the step contact time

By calculating the polynomial regression curve that minimize the least squares, the rotation equation $rotZ_{knee}(time)$ as function of time can be evaluated.

So, using these three polynomial equations as constraint equations, it will be possible to describe the RSP movement during the whole step between the "heel strike" and the "toe off" instant.

4.3 Numerical Analyses in ANSYS Workbench

Before carrying on with numerical simulations, the initial working *hypothesis* needs to be explained. Although the step is a dynamic action, it was decided to run the simulations in a *static* environment. It is supposed that the knowledge and introduction of the time function equations, which describes the displacement that the prosthetic system undergoes due to the load (by inertia and weight of the athlete), may allow to describe the dynamics of the step itself.
Therefore, it was performed a "Static Structural" simulation in ANSYS Workbench using the same equivalent elastic modulus that it was found for the previous static tests.

4.3.1 Preprocessing

Since the simulation will be started from the initial contact moment, the FEM model must be oriented respect to the ground as the real prosthesis is at the heel strike instant. To guarantee this condition Kinovea can be used. At the initial instant of contact, it was measured how a part of the prosthesis is oriented, for example the upper straight section (Figure 4.7). Doing that, the same initial condition for the FEM model was recreated.
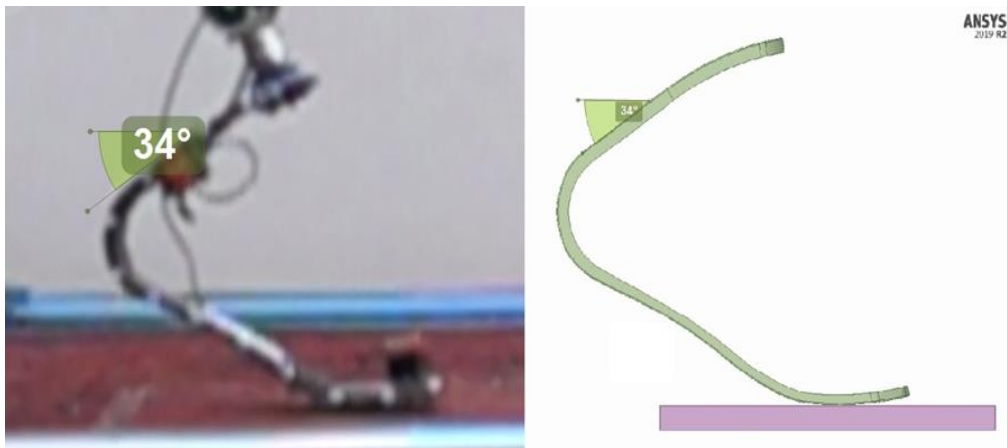
Figure 4.8: Initial contact condition recreated in ANSYS Workbench

Since during the RUN14 the clamp was locked in -4° position, a prosthesis model that has the same clamp position is imported (Figure 4.8). In addition, as done in section 2.4.2, a half prosthesis model is used, in order to reduce the number of nodes used and the calculation time. A 1 mm fillet surface is also created along the entire profile of the prosthesis to help the convergence in the final part of the step. In this way the final contact will take place along a surface, desirable condition, and not on an edge.
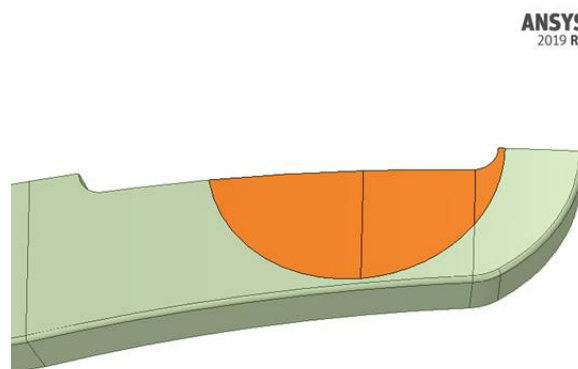

Figure 4.7: -4° Clamp area of the CAD model

In addition to the usual work steps (import the geometry, define the material proprieties and the surfaces of symmetry, select the contact surfaces, create the mesh) the following settings, constraints and displacements are entered:

- In general, in static analyses, time does not affect the results. However, in this case, since the constraints are based on those time function equations which were discussed earlier, it is necessary to enter the contact time in order to apply the correct constrain. So, in "Analysis Settings", it was created one "Load Step" with "Step End Time" equal to the contact time t_c=0,120 s.
- The ground is fixed, so it can not move in any directions.
- A remote point representative of the mechanical knee center is created, as is shown in Figure 4.9. The initial position of the knee compared to the centre of the clamp can be easily measured with Kinovea. This point is then connected by rigid beams to the upper clamp area on the prosthesis.
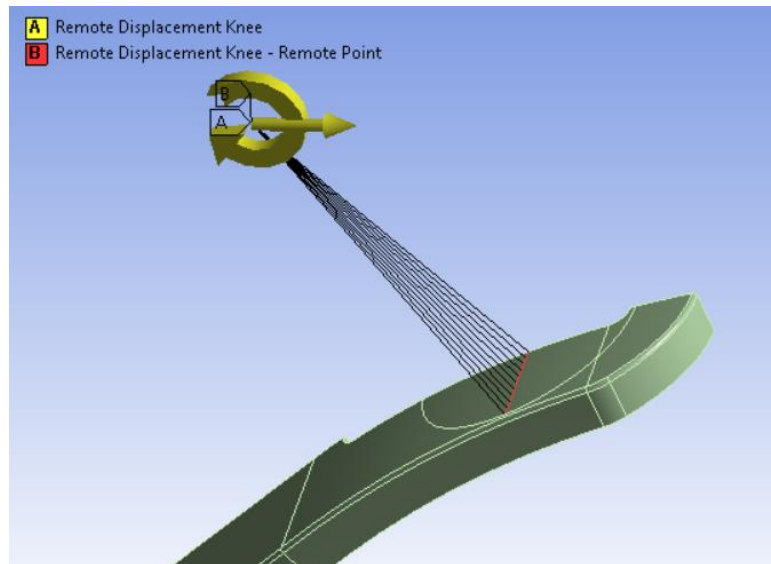
Figure 4.10: Knee remote point connected by rigid beams to the upper clamp area on the prosthesis

- A "Remote Displacement" is assigned to the knee remote point (Figure 4.9). In this way, it is possible to constrain, in the desired way, both the translations and the rotations of the knee. The translations in the X_G and Y_G directions are described by the equations previously found during the analysis of clamp trajectory (section 4.2), while the translation in the Z_G direction is set to "Free" (because the model is symmetrical). The rotation in X_G and Y_G direction are fixed while in Z_G direction the rotation is described by the equation $rotZ_{knee}$ found. Known the load step time and the polynomial equations function of time, ANSYS automatically creates an Excel table and a graph (Figure 4.10) that describes for each instant how much the mechanical knee will move.
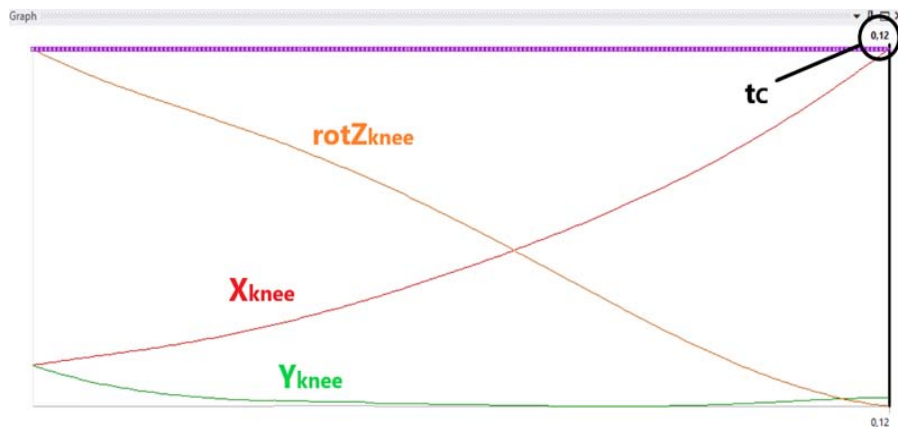
Figure 4.9: Plots of the Remote Displacement constrains in ANSYS Workbench

Then, the output to show at the end of the solutions are chosen. First the "Total deformation" of the system: in this way it is possible to evaluate if the FEM model moves in a comparable way to the real one. The ground reaction forces below the platform in the vertical (Y_G) and horizontal (X_G) direction are also plotted. Finally, the reaction moment in the Z_G direction is also measured for the calculation of the trend of the centre of pressure (COP) during the step.

Once this preprocessing phase had been carried out, the solver was launched, so the whole running step was simulated.

4.3.2 Postprocessing of the results

Before carrying on with the analysis of the numerical results, it was necessary to improve the signal acquired by the force platform during the step. As shown in the Figure 4.11, the signal has a large variation, especially at the beginning of the step, due to the platform vibrations.

Figure 4.11: Ground reaction forces in the Ground reference frame (step on platform, RUN14)

In order to clean the signal, Moving Average Filter was used. These is a simple Low Pass FIR (Finite Impulse Response) filter commonly used for regulating an array of sampled signal from unwanted noisy/vibration component. It takes N samples of input and takes the average of those to produce a single output point. As the number of points N increases, the smoothness of the output increases, whereas the data sharp modulations are made increasingly blunt. [24]
In this case N=11 points were set for the moving average. The final smooth signal is shown below in Figure 4.12.
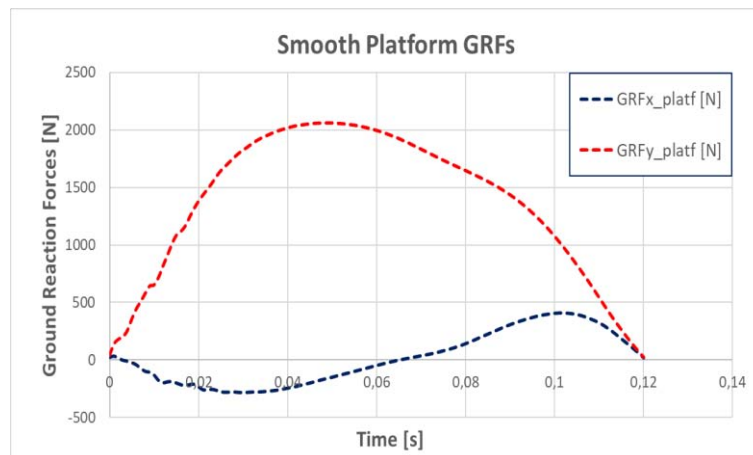

Figure 4.12: Smooth ground reaction forces (step on platform, RUN14)

In addition, six instants during the running stance phase were defined; these will be used as a reference for subsequent considerations. The description of these instants is reported in the following Table 4.2.

Instant	Description	Time [s]
t0 (HS)	Heel Strike	0
t1 (NX)	The horizontal ground reaction force reaches the maximum braking value (negative)	0.030
t2 (MY)	The vertical ground reaction force reaches the maximum value	0.050
t3 (0X)	The horizontal ground reaction force is null	0.065
t4 (PX)	The horizontal ground reaction force reaches the maximum Positive value	0.100
t5 (TO)	Toe Off	0.120

Table 4.2: Six reference instants description

Once the simulation on ANSYS was finished, the overall deformation during the step was observed. As shown in Figure 4.13, graphically the step seems very similar to the real one without showing clear differences. The instants used for the comparison are the same previously defined in Table 4.1.
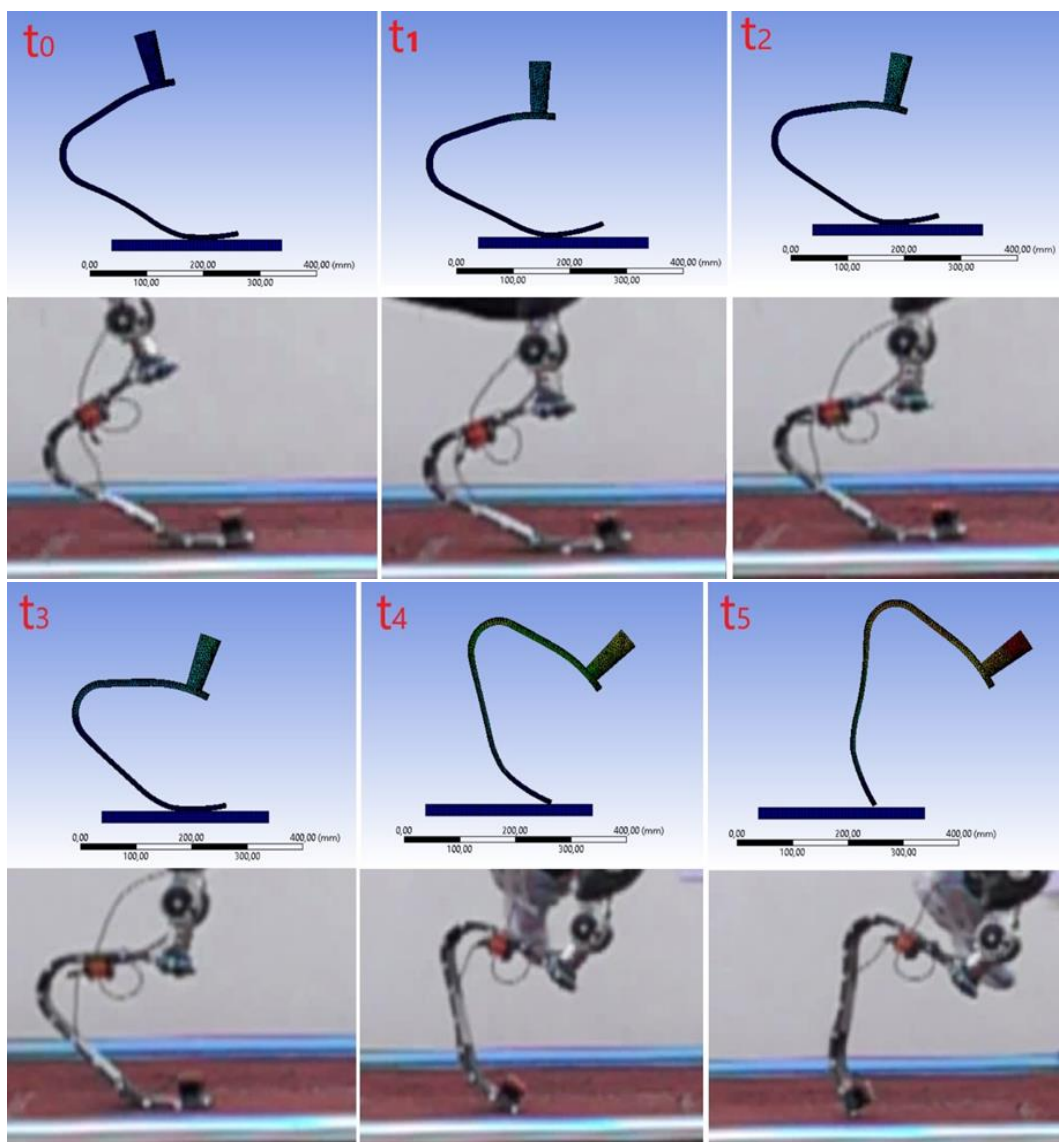

Figure 4.13: RUN14 real and numerical step sequence (t0 / t1 / t2 / t3 / t4 / t5)

In order to quantify the quality of the numerical deformation and compare it to the real one, the inclination angle of the upper straight section of the prosthesis, with respect to the horizontal, is reported below in Table 4.3 for the six defined instants: this angle, measured here with Kinovea, expresses the absolute orientation of the prosthetic foot ϑ_{Foot} (see paragraph 3.6.1).

	t0	t1	t2	t3	t4	t5
$\vartheta_{Foot,real}$ [deg]	-34	-19	-9	2	27	34
$\vartheta_{Foot,FEM}$ [deg]	-34	-20	-8	3	28	37

Table 4.3: ϑ_{Foot} angles (real and numerical) measured with Kinovea for the six instants

Another important output of interest, as it has already been said, consists in evaluating the numerical reaction forces of the ground. So, once the vertical and horizontal reaction forces were measured by ANSYS, these can be compared with the real reaction forces measured by a force platform during the athlete's run. In this way, it is possible to perform the validation of the numerical model and to understand the quality with which the FEM model can reproduce the real prosthesis behaviour during the whole step.

Validation is done by calculating the RMSE (Root Mean Square Error), for both $GRFx$ and $GRFy$, using the following equations. [15]

$$RMSE_x = \sqrt{\frac{\sum_{i=1}^{N}\left(GRFx_{platf,i}-GRFx_{FEM,i}\right)^2}{N}} \Big/ max(GRFx_{platf,i}) \qquad (4.6)$$

$$RMSE_y = \sqrt{\frac{\sum_{i=1}^{N}\left(GRFy_{platf,i}-GRFy_{FEM,i}\right)^2}{N}} \Big/ max(GRFy_{platf,i}) \qquad (4.7)$$

With

- N = sample size
- i = i-th instant of the sample
- $GRFx_{platf,i}$ = i-th horizontal Ground Reaction Force from force platform
- $GRFy_{platf,i}$ = i-th vertical Ground Reaction Force from force platform
- $GRFx_{FEM,i}$ = i-th horizontal Ground Reaction Force from FEM
- $GRFy_{FEM,i}$ = i-th vertical Ground Reaction Force from FEM

The graph with experimental (from force platform) and numerical ground reaction forces, found during the first simulations, is shown below in Figure 4.14.
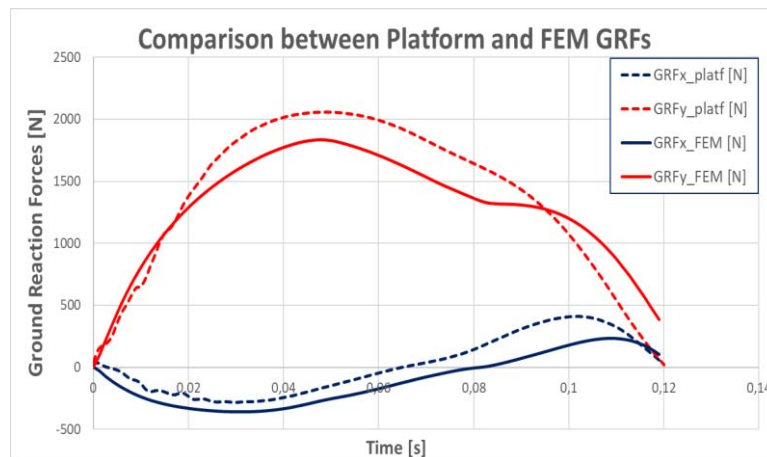

Figure 4.14: Comparison between platform (dashed lines) and numerical (continuos lines) ground reaction forces

It can be notice that, both from a graphical comparison and from the objective calculation of the RMSE, for these first simulations there is no convergence between the FEM model and experimental results. Studying Figure 4.14 it was observed that:

- The maximum value of $GRFy_{FEM}$ ($\approx$ 1840 N) is lower than the maximum value of the $GRFy_{platf}$ ($\approx$ 2060 N)
- At 0.08 s, that is the instant when the contact between the ground and the prosthesis takes place at the tip of the latter, the shape of $GRFy_{FEM}$ curve has an oscillation that the $GRFy_{platf}$ curve does not have.
- $GRFx_{FEM}$ is negative for almost the whole step and it becomes positive only in the final part.
- At the end of the contact time t_c the FEM model is still in contact with the ground. In fact, the forces measured by the FEM are not null.

If the RMSE is calculated with the equations just introduced before, the $RMSE_y$ = 11.5% while $RMSE_x$ = 33.9%, clearly too large to consider the FEM model validated. Analysing this first simulation, the total deformation of the step seems congruent with the real one, but it is not so considering the force's values involved.

However, it is needed a numerical simulation that guarantees a good convergence between FEM results and experimental data, which will be used for the following steps of this thesis.

The next step will be to understand how these results can be improved.

4.3.3 Improvement of numerical results

In order to consider the FEM model validated, the target was to find a solution that allows to obtain $RMSE_y$ <10% and $RMSE_x$ <15%. After performing many tests, three methods were found to improve the results. These methods are described below.

Method 1: change of constraint equation

Analysing Figure 4.14, as mentioned before in section 4.3.2, it was observed that at the end of the contact time the FEM model was still in contact with the ground. This means that the numerical prosthesis should move or rotate even a little more in order to detach from the platform.
Using this consideration, first the $rotZ_{knee}$ equation, found with the method explained in paragraph 4.2, was changed increasing it by a certain percentage. In this way the prosthesis was forced to rotate more.
For example, increasing the rotation by 3%, two positive point of view can be noticed (Figure 4.15). First it was observed that the numerical forces at the end of the step are equal to zero, so the prosthesis is detaching from the ground. Furthermore, the instant in which the horizontal forces change from being braking (negative values) to being propulsive (positive values) moves to the left in the graph, as for the real forces measured by the platform. This involves a reduction of $RMSE_x$, in this case equal to 11.6%.
However, there is a negative point of view: increasing the rotation FEM vertical force values decrease, causing the increase of $RMSE_y$ value, equal to 14.3%.
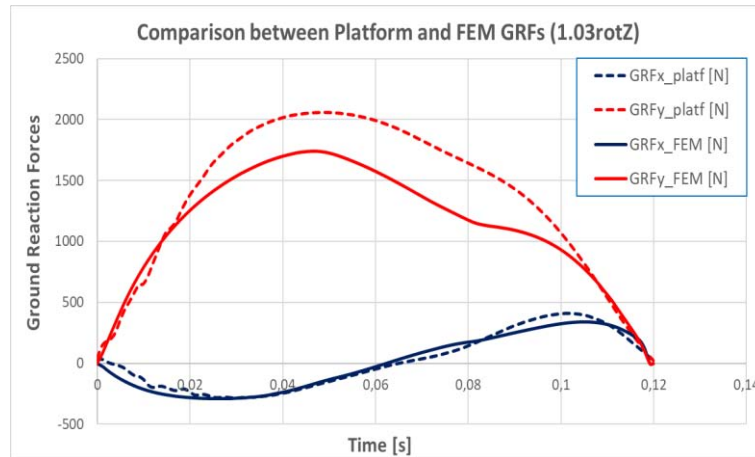
Figure 4.15: Comparison between platform and numerical ground reaction forces.
FEM forces are achieved increasing the knee rotation $rotZ_{knee}$ by 3%.

Instead, increasing only the displacement in the Y_G direction by 5%, this generates an opposite effect compared to the previous case. In fact, vertical FEM forces tend to increase (Figure 4.16) with a reduction of $RMSE_y$ value (=9.9%). However, there are two negative consequences: the horizontal force remains negative for almost the entire duration of the step and at the end of the contact time the prosthesis is still attached to the ground. This involves an increase of $RMSE_x$ (=43.2%).

 Increasing only the knee displacement in the X_G direction produces effects very similar to those just seen for the vertical displacement, but more accentuated.

Figure 4.16: Comparison between platform and numerical ground reaction
forces.FEM forces are achieved increasing the knee vertical displacement by 5%.

Observe these things, Method 1 is to find a right combination of the modified constraint equations that allows to improve the results. In this way it will be possible, for this running step, to validate the FEM model.

For example, after several attempts, a possible solution for the problem was found increasing the trajectory of the knee in the vertical direction by 9% and increasing the Z rotation by 4%. The graph of the forces found is plotted in Figure 4.17.
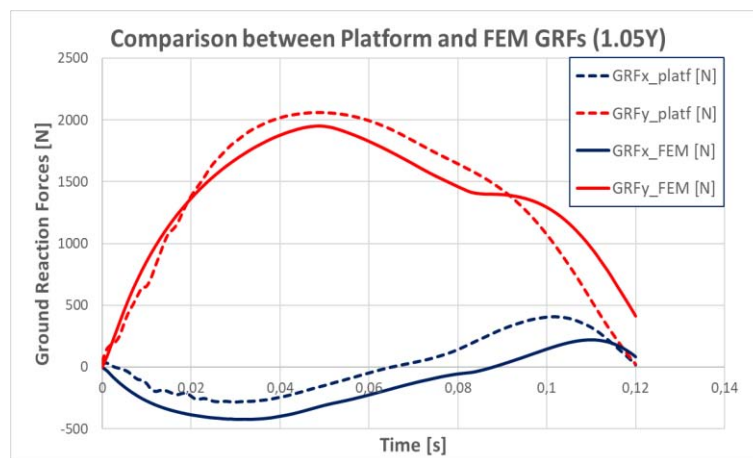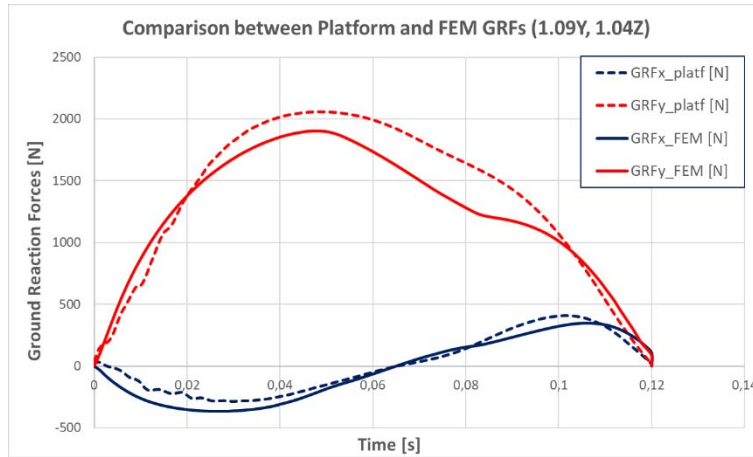
78

Figure 4.17: Comparison between platform and numerical ground reaction forces. FEM forces are achieved increasing the knee vertical displacement by 9% and knee rotation $rotZ_{knee}$ by 4%.

To validate the model, $RMSE$ is calculated. In this case $RMSE_y$ = 9.8% while $RMSE_x$ = 17.6%. These two values are closed to the target objective that it was set at the beginning of the discussion, but still remain slightly greater.

Method 2: change of constraint equations + elastic modulus $E_{dynamic}$

Here another consideration is initially made: since the X_{knee} and Y_{knee} displacements were found with Kinovea (see Section 4.2), the main source of error in their evaluation could be a mistake on the initial reference dimensional scale. This means that if, due to an error of this nature, the vertical displacement measured is wrong with respect to the real one by a certain percentage, the horizontal displacement will also be wrong by the same percentage. Therefore, it is more correct not to increase X_{knee} and Y_{knee} of two different factors as done in Method 1, but if it is decided to change them, it must be done by the same percentage.

So, for example, the test shown in Figure 4.15 is taken as reference, where the trajectory in horizontal direction is not changed but also in vertical direction. The only change concerns the rotation, increased by 3%.
However, as it was observed before, although the horizontal numerical forces are well overlapped with the real ones, in fact $RMSE_x$ <15% as desired, the vertical forces have lower values compared to the real ones.
Therefore, it was thought to carry out a modification that does not concern the constraint equations imposed, but the material of the prosthesis. As it is known if the same displacement imposed is applied and the elastic modulus is increased, the values of the forces also increase. Therefore, it was assumed that the elastic modulus found for static tests, equal to 33000 MPa, was not correct for finding the convergence between experimental and numerical forces during a complete step. It was performed, as done for static tests, the calibration of an elastic modulus that was called "dynamic" elastic modulus $E_{dynamic}$.
It is observed that, using $E_{dynamic}$ = 38000 MPa for this simulation, the results that were found are the following (Figure 4.18).
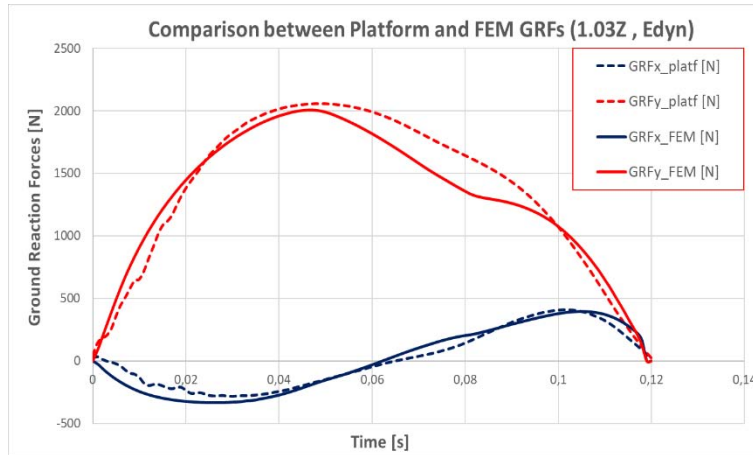
Figure 4.18: Comparison between platform and numerical ground reaction forces. FEM forces are achieved increasing the knee rotation $rotZ_{knee}$ by 3% and using $E_{dynamic}$ =38000 MPa.

In this case, the validation of the FEM model is performed using the plotted data in Figure 4.18. Calculating $RMSE$, it was observed that $RMSE_y$ = 7.4% < 10% while $RMSE_x$ = 14.2% < 15%. In these conditions the numerical model can be considered validated.

This method is interesting because, if we accept the use of a dynamic elastic modulus instead of the static one, it will be sufficient to change the rotation in the Z direction until the numerical forces are zero at the end of the contact time, without adjusting the displacement of the knee in the X and Y direction. However, this method must be verified considering other running steps different than this one which has just been examined.

Method 3: $rotZ_{knee}$ = free + elastic modulus $E_{dynamic}$

Unlike as done for the previous methods, this third solution is obtained by leaving the prosthesis free to rotate without imposing any constraint equation ($rotZ_{knee}$ = free).
With this technique the information about the rotation in the Z_G direction that the athlete, with his movement, gives to the prosthetic structure during the step are lost. The final deformation will depend only on the translation of the mechanical knee in the sagittal plane and on the contact with the ground. However, despite this method is not physically correct, it is explained because the results found are still interesting.

First a simulation is launched with only one difference: none equation in the Z direction was inserted, but the knee was "Free" to rotate.
Once the simulation is finished, the numerical forces of the ground are plotted with the real ones measured by the force platform (Figure 4.19). $RMSE$ was also calculated: you get $RMSE_y$ = 13.7% while $RMSE_x$ = 15.4%.
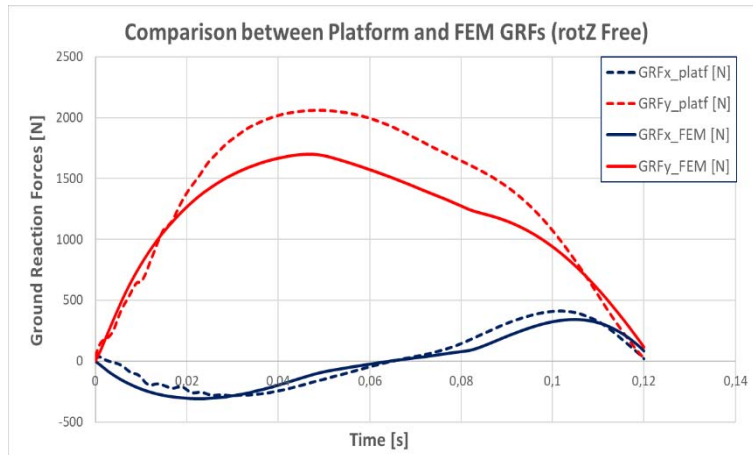
80

Figure 4.19: Comparison between platform and numerical ground reaction forces.
FEM forces are achieved leaving the knee rotation Free.

This method is interesting for the value of the $RMSE_x$, obtained without changes of trajectories, and for the shape that the numerical curves have compared to the real ones. For example, at 0.08s, the oscillation of the vertical FEM forces curve, that was explained in paragraph 4.3.2, was no longer observed. Furthermore, the curve of the horizontal FEM forces also has a shape and oscillation very similar to the real one.

Then these results were improved by following the next two steps:

1- Increase the displacement of the knee in the X_G and Y_G direction by the same percentage so that at the end of the contact time the prosthesis is about to detach from the ground. Figure 4.20 shows the results obtained by increasing the displacement in the X_G and Y_G direction by 3%.

Figure 4.20: Comparison between platform and numerical ground reaction forces. FEM forces are achieved leaving the knee rotation Free and increasing the knee horizontal and vertical displacement by 3%.

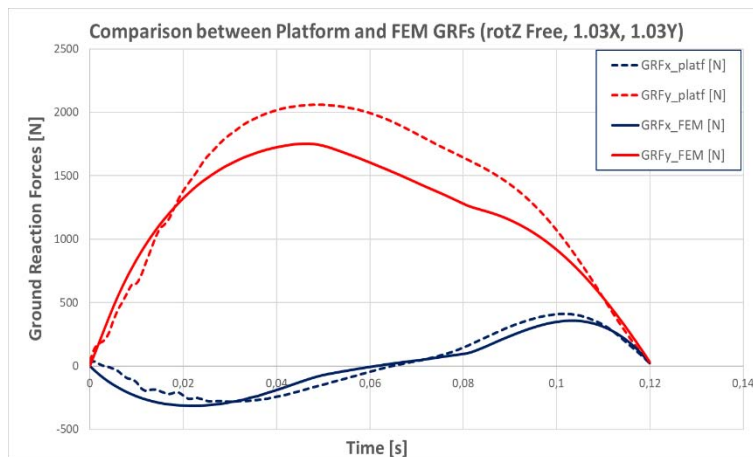2- Use the dynamic elastic modulus $E_{dynamic}$ = 38000 MPa introduced in Method 2 (Figure 4.21).
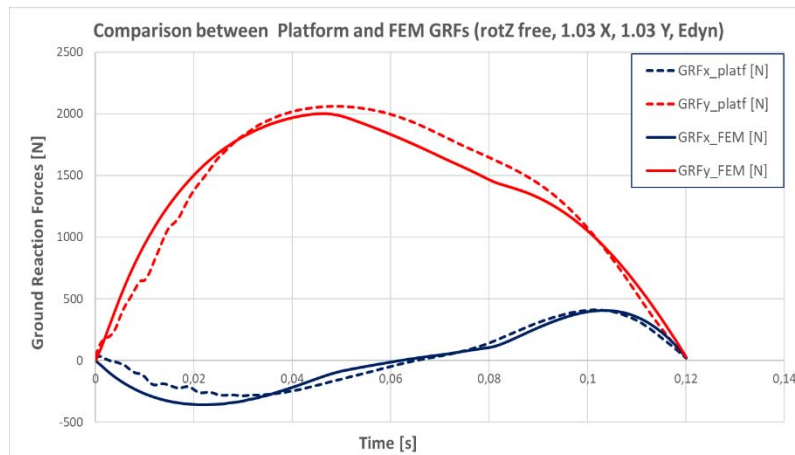

Figure 4.21: Comparison between platform and numerical ground reaction forces. FEM forces are achieved leaving the knee rotation Free, increasing the knee horizontal and vertical displacement by 3% and using E_dynamic =38000 MPa.

Here the $RMSE_y$ = 6.2% < 10% while $RMSE_x$ = 15.4% ≈ 15%. In these conditions the numerical model can be considered validated.

However, also this method must be verified considering other different running steps.

4.3.4 Evaluation of the centre of pressure displacement

In this paragraph the simulation described in Method 2 of Section 3.3 was considered. In fact, the lowest percentage values of $RMSE$ was found using this one.

The centre of pressure (COP) can be defined as the centre of the contact area between the prosthesis and the ground, where the ground reaction force vector can be visualized. The next aim consists in evaluating the trend of COP during the step (and comparing it with the real one measured by the Kistler force platform). In order to obtain this, the reaction moment M_{zz} in Z_G direction below the platform will be required, in addition to the knowledge of the numerical ground reaction forces (Figure 4.22). Since this can be chosen as an output of the simulations, it would be easily determined.
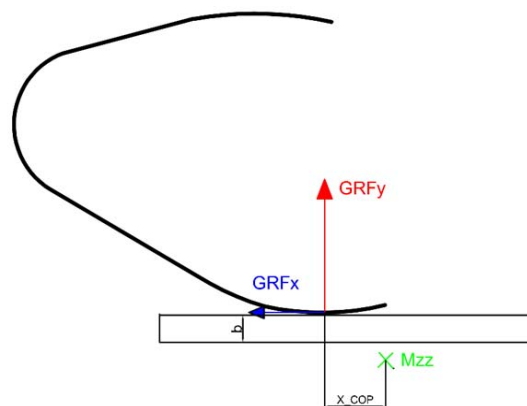

Figure 4.22: Sketch used for the evaluation of COP position X_{COP}

82

The COP displacement was calculated in the ground reference system X_G -Y_G, in which COP can only move horizontally. Thanks to FEM simulations, the values of $GRFx_{FEM}$, $GRFy_{FEM}$ and M_{zz} are always known. The arm "b" of the horizontal force, equal to the height of the platform, is also known (here 20 mm). The only unknown variable is the position X_{COP} of the centre of pressure. Therefore, it was measured using the following equation.

$$X_{COP}^G = \frac{M_{zz}+GRFx_{FEM}*b}{GRFy_{FEM}}$$
(4.8)

This technique can be applied to all simulations since the equation contains the signs of the variables.

The numerical trend of the COP found was plotted into the 'Butterfly Diagram' (Figure 4.23), particularly used during the gait analysis. This is a plot of the resultant ground reaction force vectors and is made up of successive representations of the magnitude, direction and point of application (COP) of these vectors. The resultant magnitude was calculated using the following equation.

$$GRF_{FEM} = \sqrt{GRFx_{FEM}^2 + GRFy_{FEM}^2}$$
(4.9)

In Figure 4.23 vectors are equally spaced every 10ms and between these there are six red vectors which describe the six reference instants identified previously in Table 4.2, section 4.3.2.
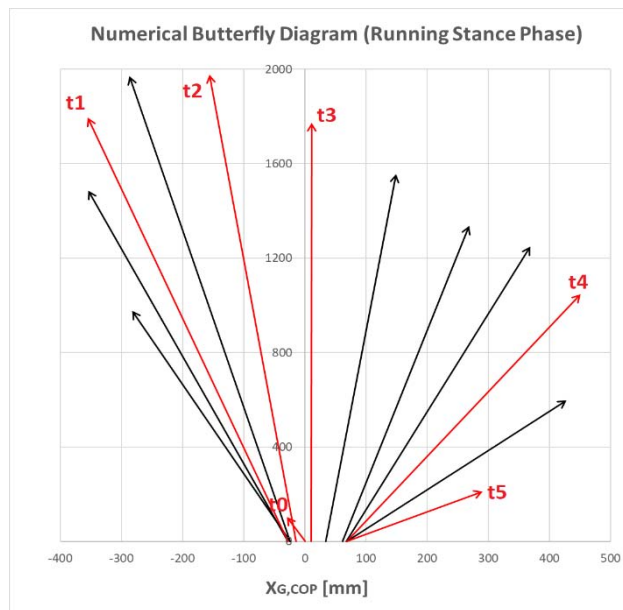

Figure 4.23: Butterfly diagram' representation of resultant ground reaction force vectors

In order to better understand this COP trend, it is also necessary to consider the total deformation of prosthesis during the step, shown in Figure 4.13. Once the prosthesis has touched the ground (t0), it flexes and rolls on it, due to the weight/load applied, the COP moves backwards respect to the initial contact point. Then, as the athlete begins to move forward, the prosthesis starts to roll in the opposite direction: the ground reaction vectors move across the diagram from left to right. In the final part of the step it was observed that the centre of pressure remains essentially fixed until the prosthesis detaches from the ground. In fact, in this phase the prosthesis rotates around its tip, which is stationary, as can be seen by analysing the total deformed shape.
Before the t3 instant, vectors are oriented to the left because the horizontal force is negative and braking. After this moment, the force vectors are directed to the right because the GRFx becomes positive.

Another representation of the numerical COP trend is shown in Figure 4.24, where the centre of pressure, in the ground reference system, is plotted on the abscissa axis; instead contact time is plotted on the ordinate axis. All instants of Table 4.2 are also reported here using red circles.
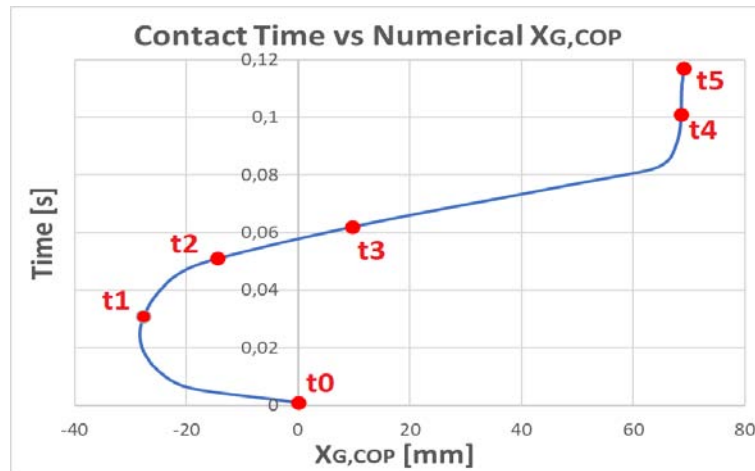

Figure 4.24: COP trend as a function of the step contact time

The Figure 4.24 shows exactly what has just been said. The COP initially tends to move backwards and then returns forward, performing a movement range of approximately 10 cm as it moves between -28 mm and +68 mm respect to the initial point of contact. It has also been observed that the instant t1, when the horizontal force of the ground reaches its maximum negative/braking value, is located near the point of maximum backward movement of the centre of pressure. Furthermore, around 0.088 s the COP stabilizes and does not change. From this moment the prosthesis is in contact with the ground only with the tip and rotates respect to it.

In Figure 4.25 the ground reaction force resultant as a function of COP trend is shown. The resultant was calculated using the equation (4.9). It can be seen from this figure that the maximum value of GRF is reached before the instant t3 (zero ground horizontal force). This is due to the fact that the maximum vertical force value is found when the horizontal force is still negative.
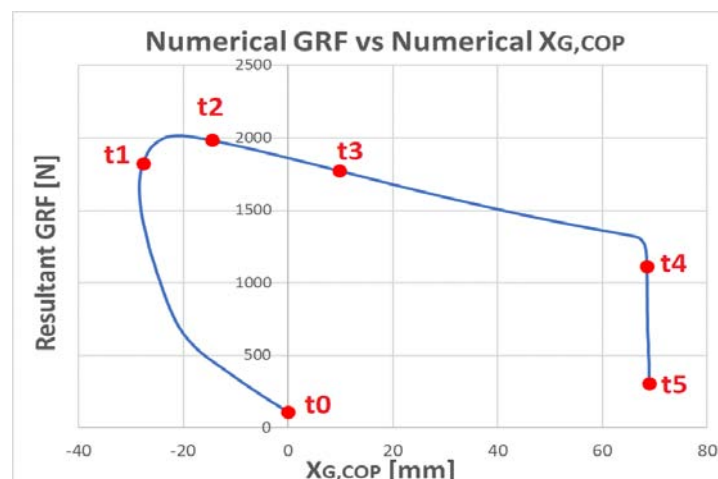

Figure 4.25: Ground reaction force resultant as a function of COP trend

Finally, the trend of the centre of pressure was compared with the real one measured by the force platform. Thanks to the Kistler force plate, it was possible to know the horizontal coordinate of the force application point. Again Moving Average Filter was used because it was necessary to improve the signal acquired during the step. However, since the raw signal had a large variation due to the platform vibrations, especially at the beginning of the step, N=30 points were set here for the moving average. The final smooth experimental signal signal was compared with the numerical COP trend of Figure 4.24. The comparison is shown in Figure 4.26.
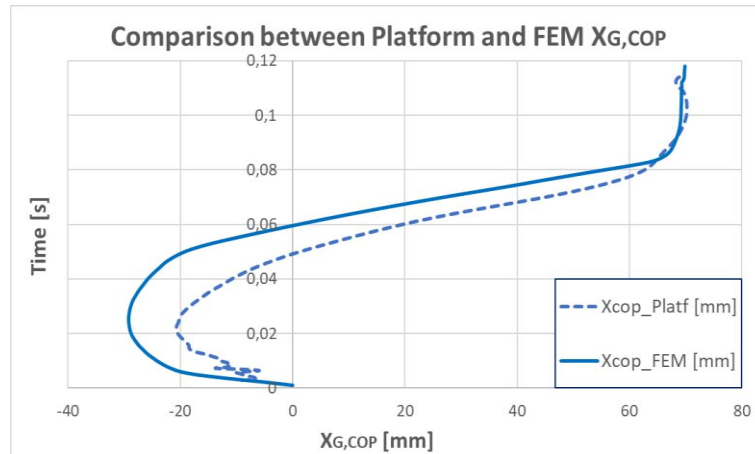
Figure 4.26: Comparison between Platform and Numerical COP trend
as a function of the step contact time

From the analysis of this graph it is possible to make the following two observations:

- The numerical model without spikes tends to roll more than the real prosthesis; this involves a greater backwards displacement of the centre of pressure, in this case 1 cm more. Perhaps this is linked to the fact that the equation describing the $rotZ_{knee}$ should be increased by 3%: in this way it is possible to recover the greater rolling of the prosthesis on the platform.

- Around 0.08 s it is observed that, both for the real prosthesis and for the FEM model, the COP remains stationary in the same point because the foot starts to rotate around its tip. This instant also coincides with that at which it was observed that strange oscillation of the numerical vertical forces plotted in Figure 4.18. This is probably due to the fact that when contact occurs along the tip of the foot, in ANSYS the contact management becomes more difficult to control.

4.3.5 Roll-over Shape (ROS)

The Roll-Over Shape (ROS) is the trajectory described by the centre of pressure expressed in a reference system integral with the prosthetic foot. The determination of the ROS, therefore, consists in a transformation of the coordinates of the COP trajectory from the ground reference system $X_G - Y_G$ (in which the COP was expressed) to this local frame. The reference system considered was the clamp reference frame $(X_C - Y_C)$, that during the step moves and rotates. The origin of this frame is located in the centre of the clamp area, the X_C axis is tangent to the clamp area surface, the Y_C axis is orthogonal to the same area and the transversal axis Z_C axis is obtained with the right-hand rule (Figure 4.27).
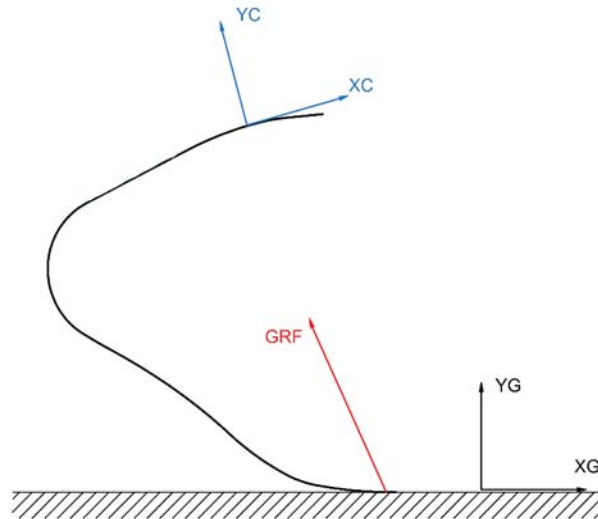

Figure 4.27: Frame systems sketch. The positions of the Clamp (blue colour)
and Ground (black colour) reference system are shown

Thanks to the numerical simulation it is possible to know in the ground reference system, at any instant of the step, the position of the clamp ($x_{G,Clamp}$ and $x_{G,Clamp}$) and the position of the centre of pressure ($x_{G,COP}$ and x=0 because the COP moves only horizontally on the platform). In order to evaluate the horizontal and vertical distance between the clamp and the COP the following two equations were used.

$$\Delta x_G = x_{G,COP} - x_{G,Clamp} \qquad (4.10)$$

$$\Delta y_G = y_{G,COP} - y_{G,Clamp} \qquad (4.11)$$

These distances were evaluated in the ground reference system during the whole stance phase. In order to know the ROS, therefore, it was necessary to transform these distances into the clamp reference frame using these two equations.

$$x_{ROS} = x_{C,COP} = \Delta x_G * \cos \vartheta_G - \Delta y_G * \sin \vartheta_G \qquad (4.12)$$

$$y_{ROS} = y_{C,COP} = \Delta x_G * \sin \vartheta_G + \Delta y_G * \cos \vartheta_G \qquad (4.13)$$

Where ϑ_G is the ground angle between the Y_C axis and Y_G axis. In Appendix C is shown a summary data table.

The trend of the COP in the clamp reference system is shown in Figure 4.28, where the six instants are also reported.
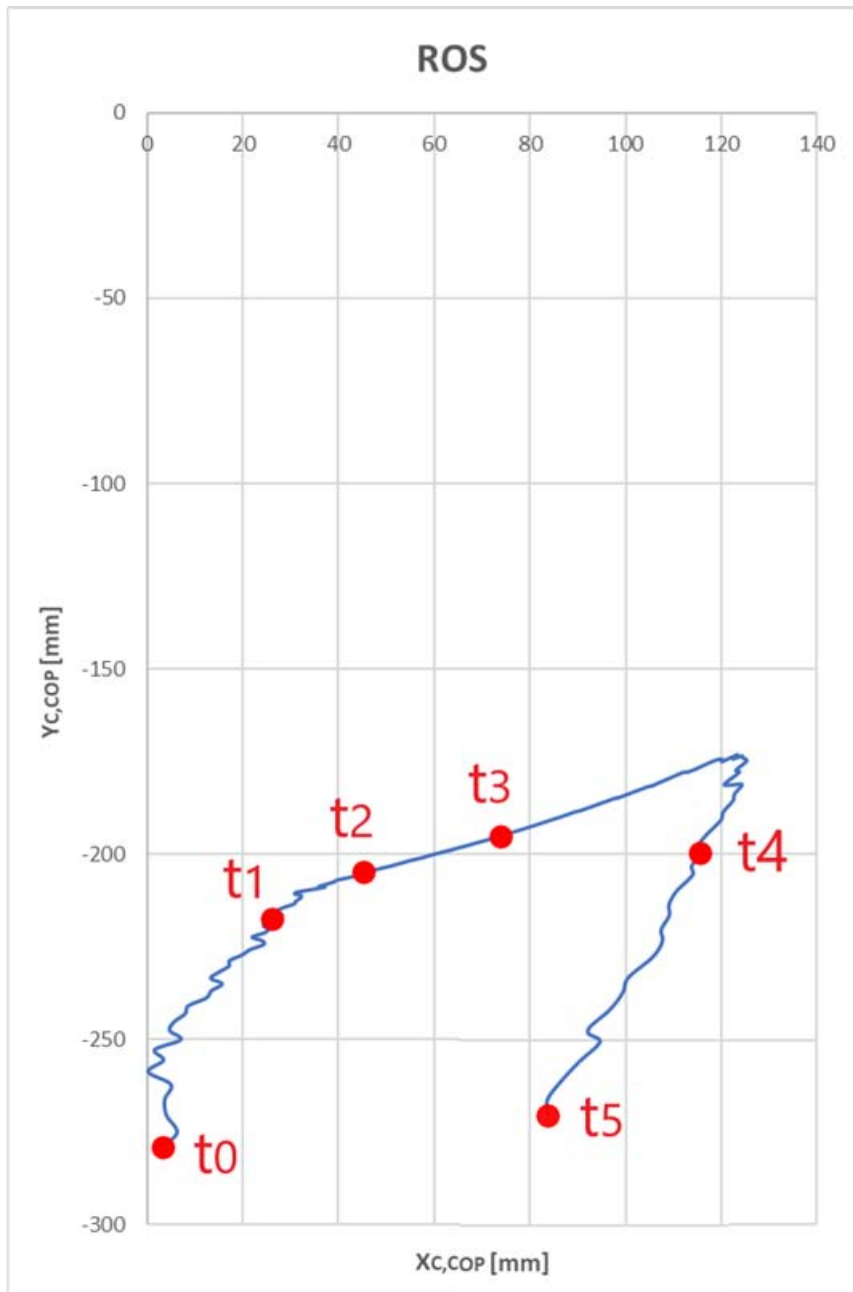
Figure 4.28: Numerical Roll-Over Shape (ROS) is the trajectory described by the centre of pressure expressed in the clamp reference system (RUN14)

4.4 Problems of the numerical step method

In paragraphs 4.2 and 4.3 the validation of the FEM model was performed considering the step on the platform recorded during RUN14 of test session n°8 (19-04-2019, Budrio, Italy). However it was necessary to understand if this method developed and used could also be repeatable, considering other running steps different than this one which has just been examined.

Therefore, another step taken by the athlete on force plate, recorded during RUN10, was chosen from test session n°8. In this case the configuration of the prosthesis was characterized by a different alignment compared to that of the RUN14, and with the clamp placed at +4°.

The procedure explained before in paragraphs 4.2, 4.3.1 and 4.3.2 was also followed in this case: analysis of the video recorded during the RUN10, determination of the equations that describe the movement and rotation of the mechanical knee in the sagittal plane, import of the geometry (with clamp at +4°) and mesh, selection of contact surfaces, imposition of constraints and loads. Once this was done, the simulation was launched and, once finished, the vertical and horizontal reaction forces measured by ANSYS were compared with the real reaction forces measured by the force platform during the athlete's run (Figure 4.29). Although here the numerical deformation is comparable to the real one too, the results found in terms of forces have very different trends compared to those observed for RUN14 (Figure 4.14).
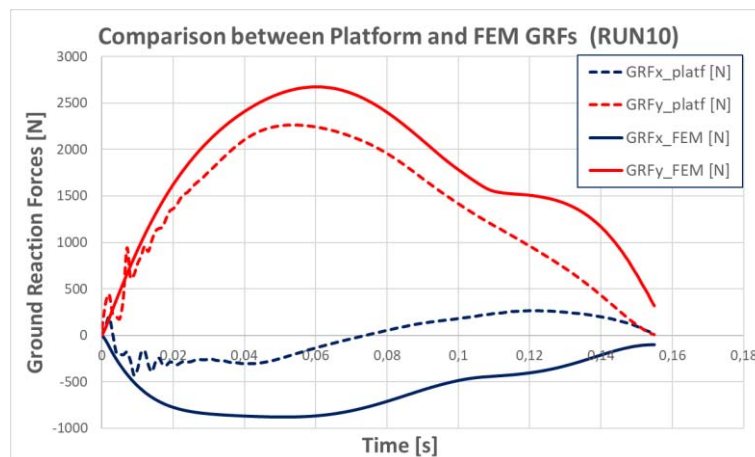
Figure 4.29: Comparison between platform (dashed lines) and numerical (continuos lines) ground reaction forces (RUN10)

As for the first simulation of RUN14, also in this case at the end of the contact time t_c the FEM model is still in contact with the ground. In fact, the forces measured by the FEM are not null. Moreover, at 0.115 s, the shape of $GRF_{y,FEM}$ curve has an oscillation that the $GRF_{y,platf}$ curve does not have. However, here the numerical vertical force is always greater than the real one (in RUN14 it was the opposite) and the horizontal reaction force is negative for the entire duration of the step, without becoming positive.

Therefore, Method 2 set out in section 4.3.3 was used as attempt to improve these results, but only trying to increase the rotation of $rotZ_{knee}$ by 3% without using the dynamic elastic modulus, thus keeping the static one. In this case the results found are shown in Figure 4.30.
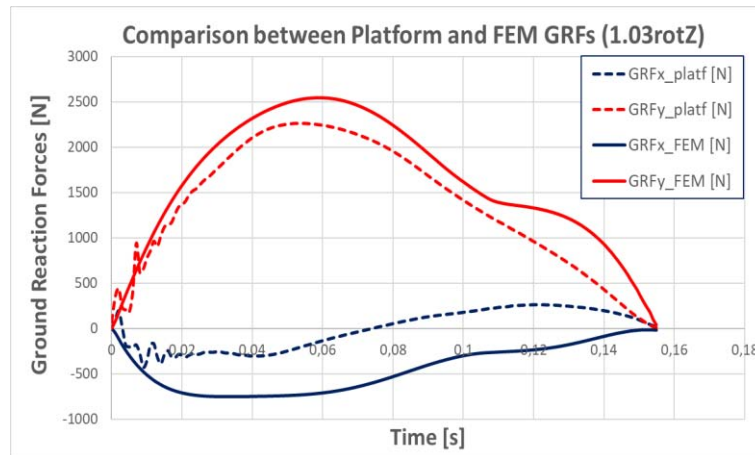
Figure 4.30: Comparison between platform and numerical ground reaction forces. FEM forces are achieved increasing the knee rotation $rotZ_{knee}$ by 3% (RUN10)

Unlike what happened for RUN14, although the forces at the end of the step are zero, the results found do not allow to validate the model also for RUN10: the vertical forces are still higher than the real ones (they would were even higher with the use of the dynamic elastic modulus which is greater than the static one) and the horizontal ones remain negative. This means that the method developed in this Chapter to simulate a complete step, using static structural analyses, is not repeatable.

However, despite of this, there is still one step available (that of RUN14) that guarantees a good convergence between FEM results and experimental data. This step will be the basis from which start for the last considerations of Chapter 5.

CHAPTER 5: THE EFFECT OF CLAMPING AND VIRTUAL SHAPING ON THE PROSTHESIS STRUCTURAL BEHAVIOUR

5.1 Introduction

In this last Chapter 5, the running step that was taken as a reference is the one of RUN14 on force platform (April 2019, Budrio), where the clamp was placed at -4°. In fact, as explained in Chapter 4, thanks to the improvement methods introduced, a satisfying simulation of this step is available that guarantees a good convergence between FEM results and experimental data.

So, using this numerical step as a starting point, in Chapter 5 it was studied:

- the effect of the clamp position, moving it from -4° to + 4°
- the effect of the shape of the prosthesis, changing the geometry of the original CAD model (which will be called Shape1 below) in order to create a different model (which will be called Shape2)

It resulted that these changes influenced the prosthesis structural behaviour by analysing the trend of the ground reaction forces (GRFs) and the trend of the centre of pressure (COP).

All following simulations were carried out using this initial *hypothesis*: the athlete maintains the same kinematics when the conditions just exposed change. This means that the displacement and rotation constraints imposed during the numerical simulations were identical to those used for the RUN14 step, without applying any modification.

This assumption is clearly very strong and has not been verified. However, it was adopted as a starting point and it can be improved further.

In the following paragraphs different GRFs were plotted: therefore the following color code, summarized in Table 5.1 were used.

Parameter	Colour
$GRFx$ (RUN14: Clamp -4°, Shape1)	
$GRFy$ (RUN14: Clamp -4°, Shape1)	
$GRFx$ (Clamp +4°, Shape1)	
$GRFy$ (Clamp +4°, Shape1)	
$GRFx$ (Clamp -4°, Shape2)	
$GRFy$ (Clamp -4°, Shape2)	

Table 5.1: Color code for the following Chapter 4 GRFs figures

5.2 Effect of clamp position during running

In this paragraph the objective is to study the effect of the clamp position during the single step on the platform, supposing to move the clamp from the -4° position (RUN14) to the +4° position. The starting point is again the analysis by Kinovea of the step, in particular of the initial instant of contact ("heel strike"), shown in Figure 5.1.

Figure 5.1: Heel Strike instant (RUN14). Note the 28° angle between the perpendicular to the ground and the segment passing through the greater trochanter (GT) and the tip of the prosthesis (TIP)

Looking at Figure 5.1, an angle of 28° was estimated between the perpendicular to the ground and the segment passing through the greater trochanter (GT), the tip of the prosthesis (TIP) and in this case, also the centre of the mechanical knee (K) and the centre of the clamp (C). It was decided to respect this condition also during the numerical simulation with the clamp at +4° (Figure 5.2). In this way, the correct alignment between the various elements of the prosthetic system was repeated again. This operation resulted in a rotation of the foot of +8° in the sagittal plane (pink angles in Figure 5.2).
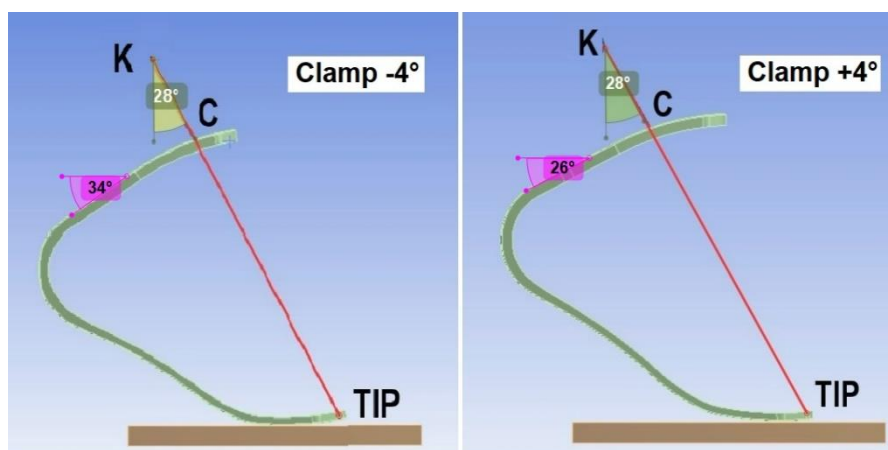

Figure 5.2: Correct alignment (Heel Strike instant). On the left the original configuration of RUN14, on the right the modified configuration with the +4° clamp

The simulation was carried out by:

- connecting the knee remote point to the +4° clamp using rigid beams (Figure 5.3)
- imposing the translation to the mechanical knee in the X_G and Y_G direction and $rotZ_{knee}$ rotation (Figure 5.3) evaluated with Kinovea in paragraph 4.2
- increasing the rotation by 3% and using the dynamic elastic modulus equal to 38000 MPa for the prosthesis (Method 2, section 4.3.3) as in previous simulations
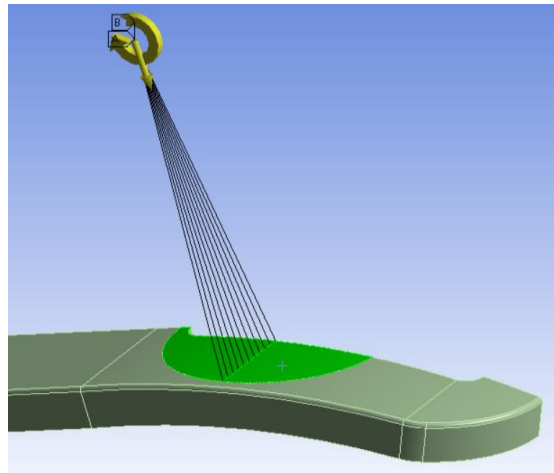

Figure 5.3: Knee remote point connected by rigid beams to the upper +4° clamp

Figure 5.4 shows the trends of the numerical ground reaction forces for this new configuration with the +4° clamp, which were compared with the original forces of RUN14. Note that, considering the same kinematics (except the clamp position of course), forces with the clamp at +4°, both vertical and horizontal, are greater in modulus and the horizontal force is braking for almost the whole duration of the step. This means that the position of the clamp at +4° involves, during the step, a stiffening of the prosthetic system.
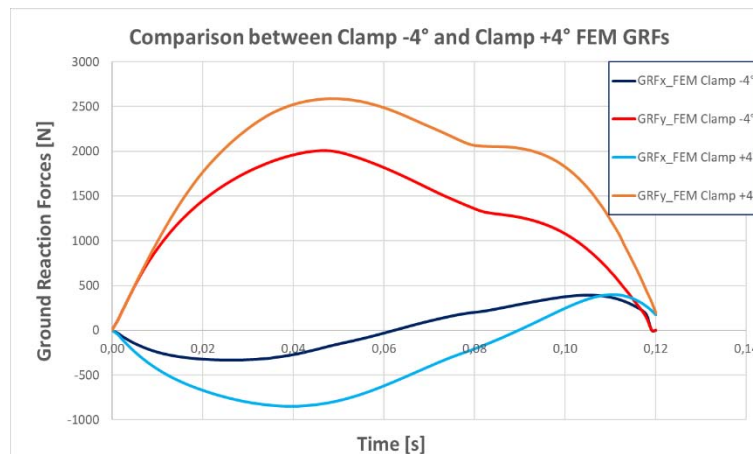
Figure 5.4: Comparison between clamp -4° and clamp +4°numerical ground reaction forces

The last curves found are not as we expected, that is with a change of the horizontal force from braking to propulsive at about half of the contact period.
The stiffening effect is in agreement with what was learned from field experience with athletes. In fact, typically athletes, during the run, perceive stiffer configurations with the clamp positioned at +4°. However, as already mentioned in paragraph 3.5, these results do not coincide with those found during bench tests where the inclination of the ground was kept fixed. In fact, during these

type of static tests, the position of the clamp does not cause any significant variation on the stiffness of the prosthetic foot.

In order to quantify this statement, Table 5.2 shows the vertical and horizontal (both braking and propulsive) GRF peaks. Moreover, given the contact time, it was possible to calculate the value of vertical and horizontal (braking, propulsive and net) impulses, using the following general equations.

$$Impulse \ = \ Time \ \times GRF \ \ [N*s] \tag{5.1}$$

$$I_{h,net} = I_{h,braking} + I_{h,propulsive} \ \ [N*s] \tag{5.2}$$

Also the percentage differences Δ, with respect to Clamp -4° configuration forces or impulses value, were calculated using the equation (5.3).

$$\Delta = \frac{I_{Clapm+4} - I_{Clamp-4}}{I_{Clamp-4}} \ \% \tag{5.3}$$

	Clamp -4°	Clamp +4°	Δ
Peak $GRFy$ [N]	2006	2585	+28.9%
Peak $GRFx_{,braking}$ [N]	-333	-848	+154.5%
Peak $GRFx_{,propulsive}$ [N]	395	398	+0.8%
I_v [Ns]	8963	13415	+49.7%
$I_{h,braking}$ [Ns]	-393	-1430	+263.9%
$I_{h,propulsive}$ [Ns]	1360	315	-76.8%
$I_{h,net}$ [Ns]	967	-1115	-215.3%

Table 5.2: Vertical and horizontal (braking and propulsive) peak forces and impulses obtained during numerical simulation of the whole step changing the clamp position.
Δ values were calculated respect to Clamp-4° values

The plot of the centre of pressure is also very interesting, in the reference system $X_G - Y_G$ of the platform for the two configurations. The six instants defined in paragraph 4.3.2 were also used here. The description of these instants is again reported in the following Table 5.3.

Instant	Description
t0 (HS)	Heel Strike
t1 (NX)	The horizontal ground reaction force reaches the maximum braking value (negative)
t2 (MY)	The vertical ground reaction force reaches the maximum value
t3 (OX)	The horizontal ground reaction force is null
t4 (PX)	The horizontal ground reaction force reaches the maximum positive value
t5 (TO)	Toe Off

Table 5.3: Six reference instants description

The two COP trends diverge in both the shape and the range of displacement (Figure 5.5):

- Clamp -4°: COP moves, relative to the point of first contact, between -28,5 mm and +68,5 mm (≈97 mm)
- Clamp +4°: COP moves, relative to the point of first contact, between -51,5 mm and +34,5 mm (≈86 mm)

This means that, in the case of clamp + 4°, once the prosthesis comes into contact with the ground, it flexes and rolls further back before starting to move in the opposite direction. Furthermore, the range of movement for clamp +4° configuration is about 1cm lower than for -4° case.
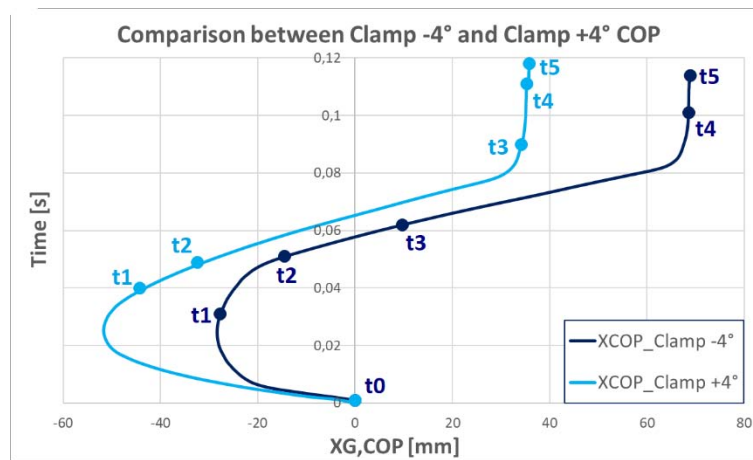

Figure 5.5: Comparison between Clamp -4° and Clamp +4° numerical COP trend as a function of the step contact time

5.3 Effect of prosthesis shape

Another potentiality that was used by working with FEM analyses was the possibility to change the geometry of the prosthesis in various shapes, which is clearly not feasible in experimental reality without high costs for the molds ang long time of development. Therefore, the effect of the foot virtual shaping on the structural behaviour of the prosthesis was studied by changing the geometry of the original CAD model (which it was called Shape1 below) in order to create a different prototype (which it was called Shape2).

As can be seen from Figure 2.14 of paragraph 2.3, the original Ottobock prosthesis (Shape1) has a double curvature in the distal part of the foot: starting from the tip (P7) it is possible to see a first section (P5-P7), divided in turn into two parts (P5-P6 and P6-P7), having a centre of curvature inside the profile of the prosthesis and a second section (P4-P5) with an external centre of curvature.
Observed this and comparing this prosthesis to an Ossur J-shape foot, another model was created, named Shape2, in which the upper/proximal part of the foot was maintained the same (P1-P3), while another shape was designed for the lower part, characterized by a single large arch of circumference between points P4.2 and P7 (Figure 5.7). The two prostheses had the same height h. In Figure 5.6 the outlines of the two geometries in the sagittal plane are shown in order to compare the original and the modified one.
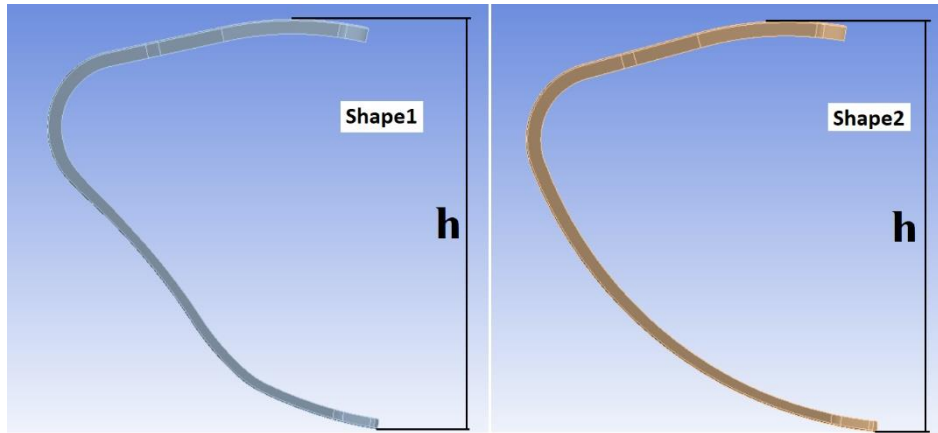
Figure 5.6: Comparison between original Ottobock standard Category 3 shape (Shape1, left) and the new model (Shape2, right)

As done for the foot Ottobock standard Category 3 (Shape1) in section 2.3, a parametric sketch of the external profile of the new prosthesis Shape 2 in the sagittal plane is shown below (Figure 5.7). The sketch was obtained by dividing it into 4 segments "S" (lines or circumference arcs) and in 5 remarkable points "P" (end points of the segments). All segments were drawn tangent to each other at the connection points. In Tables 5.3 and 5.4 the following informations were reported:

- The coordinates of the points P (Table 5.3) and the coordinates of the centres C of the circumference arcs (Table 5.4) with respect to the Clamp reference frame (X_C, Y_C) placed in the centre of the clamp when it is positioned at the buttonhole centre (clamp 0°). Note also in Figure 2.14 that the centre C1 coincides to the zero point and the radius of the segment S1 has its own centre in C1. The coordinates are reported in millimeters.
- Radius (R) of the circumference arcs and the length (L) of the straight section using the blue color (Figure 5.7 and Table 5.4). Dimensions are reported in millimeters.
- Angular dimension ($\Delta\gamma$) of the circumference arcs or inclination of the straight section with respect to the horizontal axis of the clamp using the red color (Figure 5.7 and Table 5.4).
- Thickness (in millimeters) of the prosthesis in the sagittal plane, at the points P, using the black color (Figure 5.7 and Table 5.3). Thicknesses between the various points vary linearly with the curvilinear abscissa.

Point P	Coordinates [mm]	Thickness [mm]
P1	(+59.5 ; -7)	11
P2	(-29 ; -2)	11
P3	(-136.5 ; -25)	11
P4.2	(-183.5 ; -102)	10
P7	(+66 ; -307.5)	7.5

Table 5.3: Coordinates of the points P and thicknesses of the prosthesis in the sagittal plane (in millimeters)

Segment	End points	L [mm]	R [mm]	$\Delta\gamma$ [deg]	C Coordinates [mm]
S1	P1-P2	/	280	18.2	C1 (0 ; -280)
S2	P2-P3	110	∞	12	/
S3	P3-P4.2	/	58	97.1	C3 (-129 ; -82.5)
S4	P4.2-P7	/	312	62.5	C4 (+111 ; 0)

Table 5.4: Length L, radius R, angular dimension $\Delta\gamma$ of the segments and coordinates of the centre of circumference arc segments
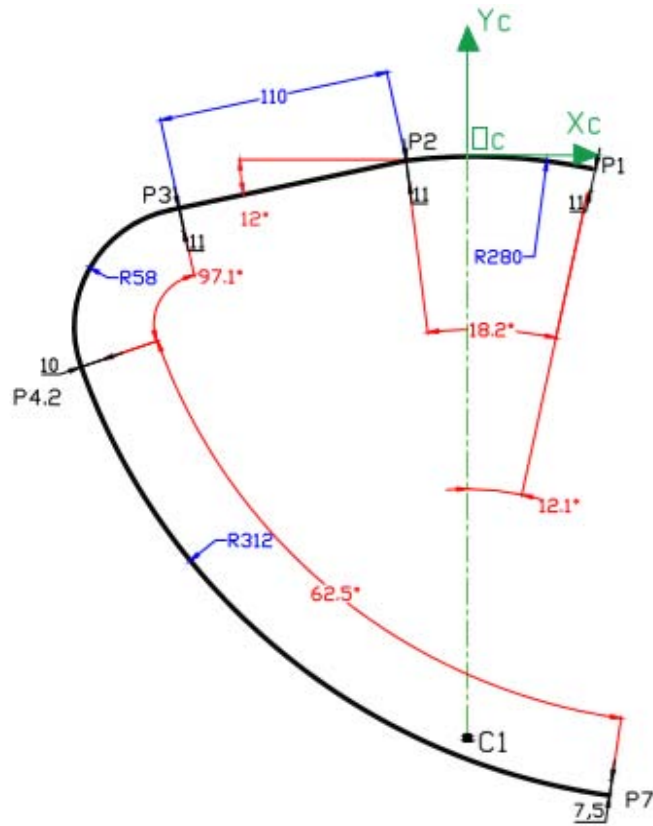
Figure 5.7: Parametric sketch of the external profile of the prosthesis Shape2 in the sagittal plane

Figure 5.8 shows the sketches of the external profiles of the two RSFs together. The two geometries are characterized by the same height h and the same length of the TAP (distance between the tip of the prosthesis and the vertical axis passing through the centre of the clamp, in this case positioned at 0°).

Figure 5.8: Comparison between the external profile of prostheses
Shape1 and Shape2. The height h and the TAP are highlighted

5.3.1 Static test

Before analysing the behavior of the Shape2 prosthesis during the complete step, static tests were performed in conditions of clamp 0°, ρ=0 and ϑ_G=0° in order to make an initial comparison with the original model.
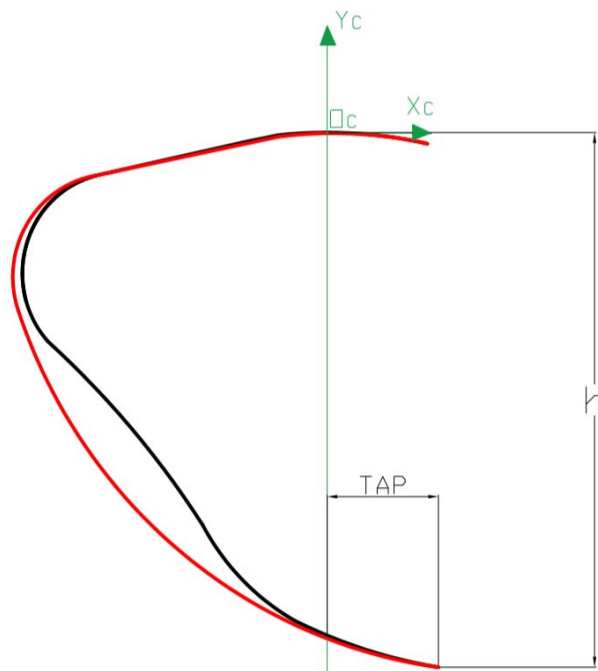
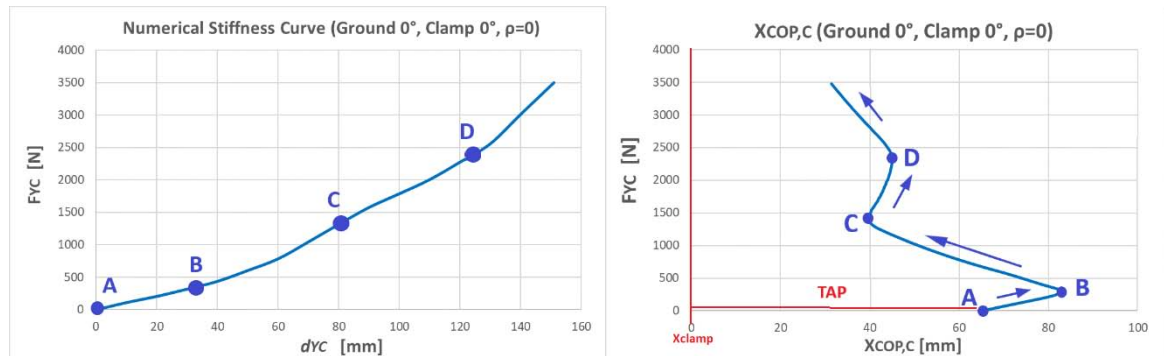In Figure 5.9 the results found in Chapter 3 for Shape1 prosthesis were reported again.

Figure 5.7: RSF Ottobock Category 3 stiffness curve (left) and trend of the COP (right)
obtained in static test in conditions of clamp 0°, ground 0°, ρ = 0

As already mentioned, this trend of the centre of pressure and the trend of the stiffness curve is due to the combination of the applied load and the portion of the prosthetic foot which is in contact with the platform. COP tends to approach the centre of the pylon/clamp when the vertical load increases. However, this undergoes a kind of stop when (it's possible to see this during FEM analysis) there is contact between the platform and the prosthesis area in correspondence with point P6 of Figure 2.14. This, in turn, causes an attenuation of the growth of stiffness, because the COP tends to move away again.

Therefore, also the behaviour of Shape2 prosthesis was studied performing the same static test, where:

- Tartan material was assigned to the platform (E=600 MPa).
- The value E=33000 MPa was taken as the equivalent isotropic elastic modulus for the prosthesis.
- The platform was free to move in the X_C direction (ρ = 0 test).
- A certain displacement d_{YC} = 152 mm is applied to the 0° clamp in the direction Y_C (negative). This displacement produced a vertical reaction load of 3500N for the Shape1 prosthesis.
- The vertical forces, in the Y_C direction, was read at the clamp area.

The results found are plotted in Figure 5.9 and Figure 5.10. For the Shape2 prosthesis, considering the same displacement applied to the clamp, the vertical forces grow up to 8000 N, more than double that the value found for the original prosthesis (Figure 5.9). In addition, a nonlinear and ever-increasing stiffness curve was observed. From the evaluation of the stiffness K_{eq}, an higher value, equal to 19.8 N/mm, was found than the value found for the Shape1 prosthesis, equal to 17.4 N/mm (percentage differences Δ=+13.8%). In particular, if we wanted to obtain a vertical reaction force of 3500 N, we had to apply a clamp displacement d_{YC} equal to 118 mm (Figure 5.10).
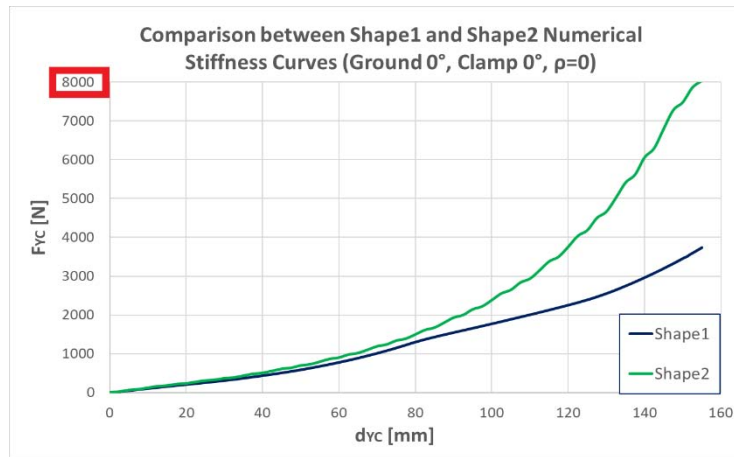
Figure 5.9: Comparison between Shape1 and Shape2 numerical stiffness curves obtained in static test with clamp 0°, ground 0°, ρ = 0
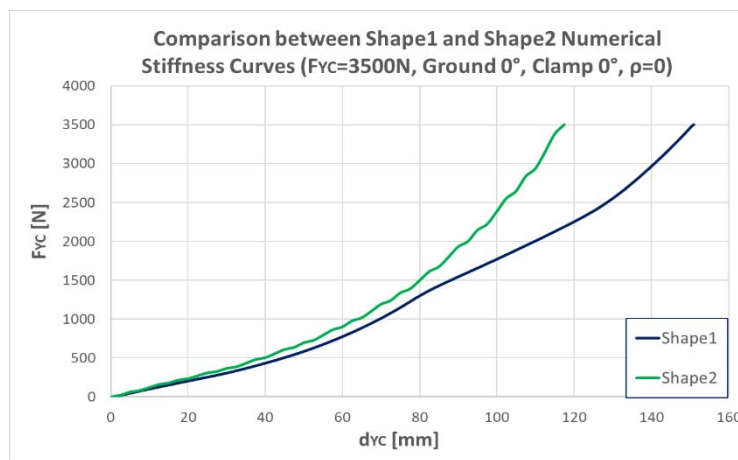
Figure 5.10: Comparison between Shape1 and Shape2 numerical stiffness curves obtained in static test with clamp 0°, ground 0°, ρ = 0 where the vertical load is equal to 3500N

This behaviour is due to the fact that this new shape does not allow to the COP to stop when the load increases. The centre of pressure tends to move due to the rolling of the prosthesis on the platform and it decreases so much that it goes beyond the centre of the pylon (negative COP values), as can be seen in Figure 5.11.

Figure 5.11: COP of Shape2 prosthesis during static tests loading with clamp 0°, ground 0°, ρ = 0. The position of the centre of the clamp is also highlighted

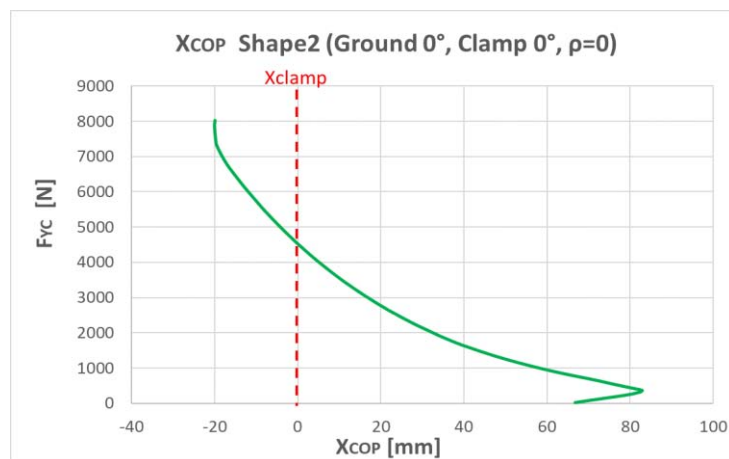This COP trend is completely different from that obtained for the Shape1 foot during the same static test (Figure 5.12).
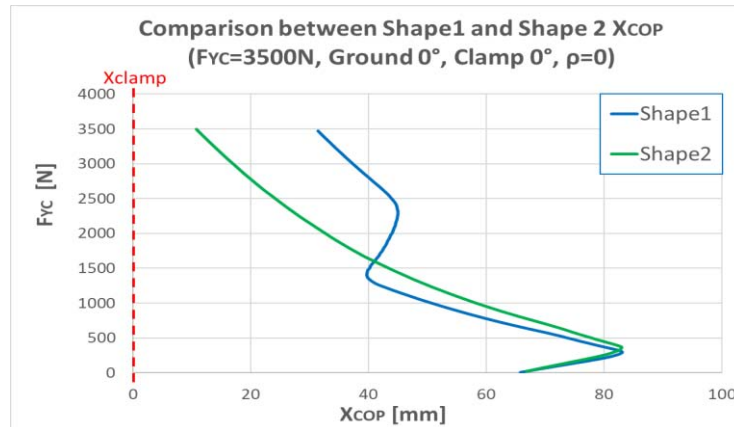
Figure 5.12: Comparison between Shape1 and Shape2 COP trend obtained in static test with clamp 0°, ground 0°, ρ = 0 where the vertical load is equal to 3500N

Therefore, as already hypothesized in paragraph 3.3, this is a clear evidence of the fact that the shape of the foot affects the trend of the centre of pressure and this, in turn, affects the stiffness curve during static tests.

5.3.2 Running step simulations

The behavior of the Shape2 prosthesis during the running step was studied here: the aim was to observe if this shape introduced significant changes even during the simulation of the whole stride. Simulations were carried out using again the RUN14 data and:

- connecting the knee remote point to the -4° clamp using rigid beams
- imposing the translation to the mechanical knee in the X_G and Y_G direction and $rotZ_{knee}$ rotation (Figure 5.3) evaluated with Kinovea in paragraph 4.2
- increasing the rotation by 3% and using the dynamic elastic modulus equal to 38000 MPa for the prosthesis (Method 2, section 4.3.3)

The graph with numerical trends of the ground reaction forces for the two geometries (Shape1 and Shape2) is shown below in Figure 5.13.

Figure 5.13: Comparison between Shape1 and Shape2 numerical ground reaction forces

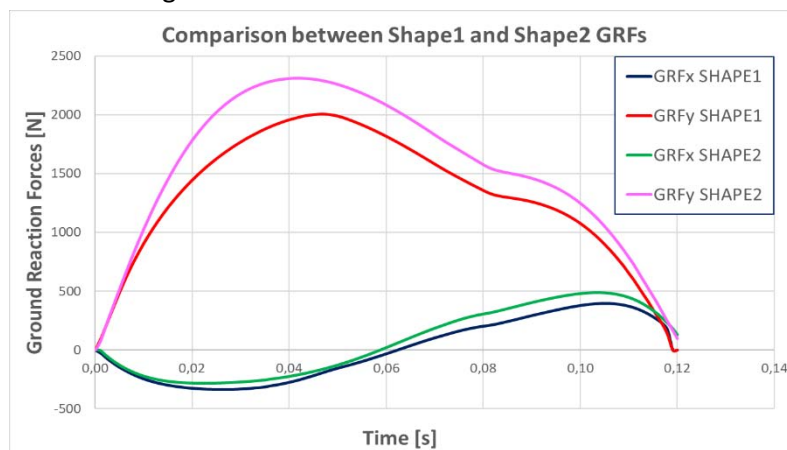Shape2 prosthesis showed a higher GRFy compared to Shape1 vertical force, with a higher peak of 300 N. Furthermore, it showed a slightly lower horizontal braking force, while the horizontal propulsive force is higher. In order to quantify this statement, values of vertical and horizontal (both braking and propulsive) peak forces were reported in Table 5.5. Moreover it was possible to calculate the value of vertical and horizontal (braking, propulsive and net) impulses, using equations (5.1) and (5.2). Also the percentage differences Δ, with respect to Shape1 impulses values, were calculated using the equation (5.4).

$$\Delta = \frac{I_{Shape2} - I_{Shape1}}{I_{Shape1}} \% \tag{5.4}$$

	Shape1	Shape2	Δ
Peak $GRFy$ [N]	2006	2313	+15.3%
Peak $GRFx_{,braking}$ [N]	-333	-285	-14.4%
Peak $GRFx_{,propulsive}$ [N]	395	486	+23%
I_v [Ns]	8963	10533	+17.5%
$I_{h,braking}$ [Ns]	-393	-320	-18.5%
$I_{h,propulsive}$ [Ns]	1360	1851	+36%
$I_{h,net}$ [Ns]	967	1531	+58.3%

Table 5.5: Vertical and horizontal peak forces and impulses obtained during numerical simulation of the whole step changing the foot shape. Δ values were calculated respect to Shape1 values

Finally, the plot of the centre of pressure, in the ground reference system $X_G - Y_G$ of the platform for the two configurations is shown in Figure 5.14. The two trends diverge in the range of COP displacement:

- Shape1: COP moves, relative to the point of first contact, between -28.5 mm and +68.5 mm (≈ 97 mm)
- Shape2: COP moves, relative to the point of first contact, between -44.5 mm and +66.5 mm (≈ 110 mm)

This means that the new Shape2, thanks to the geometry obtained with a single large arch of circumference for the lower part, tends to roll back more before moving in the forward direction.
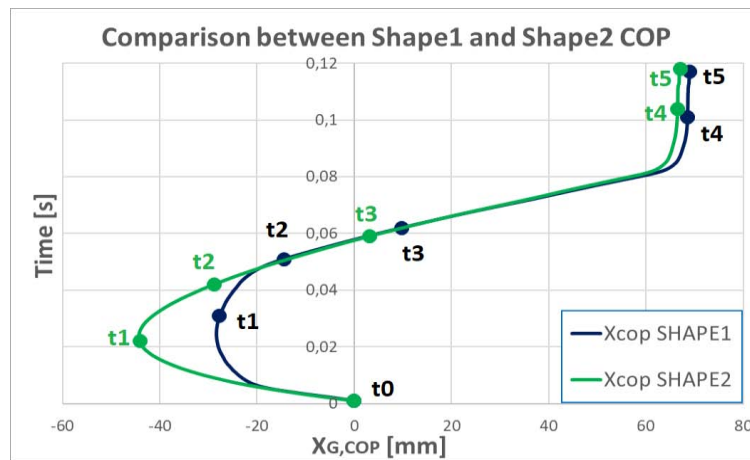
Figure 5.14: Comparison between Shape1 and Shape2 numerical COP trend as a function of the step contact time

From the analysis of results of this last paragraph 5.2 it is possible to conclude by making the following two observations:

- Although the static stiffness curves (Figure 5.9), with the same elastic modulus and displacement imposed on the clamp, show great differences due to the larger rolling of the Shape2 prosthesis on the platform, the GRFs plot (Figure 5.13) obtained during the simulation of the whole step are comparable to each other. This means that, although static stiffness curves are useful for studying and comparing various prostheses, static tests do not allow us to appreciate the true behavior of a prosthesis in real conditions of use during running.
- Assuming that the athlete maintains the same kinematics when changing prostheses, it was observed that the Shape2 foot would seem better than the original Ottobock RSF. In fact during the numerical step the Shape2 prosthesis allows to have a lower braking impulse and a greater propulsive thrust. However, we could only confirm these results by creating a real prototype with the same shape and by experimentally testing it.

CHAPTER 6: CONCLUSIONS

The aim of this thesis was to define a method for developing a 3D FEM model of a running specific prosthesis, using the ANSYS Workbench software, through which it was possible to predict and study the structural behaviour of the foot for different constraint and load conditions. Since the internal layout of carbon fibre prosthetic feet is unknown as manufacturers do not provide this information, RSF were modelled using an equivalent isotropic elastic material.

The first step of the study was to develop a procedure that allowed the calibration of the numerical model, given data collected during in-vitro static bench tests. Gianfabio Costa's bench [16], the "Colossus", was useful to realize these tests. The test bench was designed to ideally reproduce the socket of a transtibial athlete. This means that forces of the hydraulic cylinders were applied in the vertical and horizontal direction in the socket reference frame that, as the prosthesis was mounted on the bench, coincided with the clamp reference system. The bench tests were performed loading the prosthesis vertically up to 1500N and considering various configurations:

- 3 different clamp positions (-4°, 0°, + 4°)
- 4 different angles ϑ_G of the platform (-15°, 0°, +15°, +30°) in order to simulate different instants of the contact phase of the prosthesis with the ground
- 3 different load ratios applied $\rho = F_{XC}/F_{YC}$ (-0.2, 0, 0.2)

The calibration was carried out by imposing the known displacement d_{YC} on the clamp area of the prosthesis and iterating the value of the equivalent elastic modulus of the prosthesis until a satisfying match (relative error on the vertical force less than 10%) was found between the experimental known force F_{YC} and the numerical reaction force read as FEM output.
Thanks to the numerical calibration it was possible to determine a single equivalent elastic modulus value to be assigned to the material of the prosthesis Ottobock Runner Standard C-shaped Category 3, equal to 33000 MPa.

Once the model was calibrated, the foot structural behaviour was studied by evaluating the numerical mechanical stiffness loading the RSF up to 3500 N without the risk of damaging or breaking it. In order to quantify the stiffness of the prosthesis during the various static tests, two different stiffness values (K_L and K_{eq}) was proposed.
According to several literature articles, it was noticed that stiffness curves are not linear and there is a hardening progression from lower to higher vertical loads. In addition to this, thanks to the numerical analysis of the position of the centre of pressure (COP), it was possible to explain this non-linearity of the prosthesis stiffness: it was observed that the COP moved from the tip backward and tends to approach the centre of the clamp when the vertical load increases. Then, less bending moment on the RSF, due to the ground reaction force, is developed at the clamp area; if bending moment decreases also curvature decreases and stiffness increases consequently.

As further proof of the very good ability of numerical model in simulating the prosthesis behavior, the following results, validated by the static experimental tests, were observed:

- As the angle of inclination of the platform varies, changing the load ratio ρ from the negative value (-0.2) to the positive value (+0.2), the stiffness of the prosthetic foot decreases (about 20% of average changes in stiffness values from ρ=-0.2 to ρ=+0.2). The prosthesis is stiffer when ρ is negative because in this condition the horizontal force F_{XC} is a braking force.
- As the angle of inclination of the platform varies, during this type of ϑ_G=cost static test the position of the clamp does not present any significant variation on the stiffness of the prosthetic foot.
- The stiffness of the foot tends to decrease during the running stance, changing the angle of inclination of the ground from -15° to +30° (about 60% of average changes in stiffness values from -15° to +30°).

In the second part of the thesis the FEM environment was used to define another method that would guarantee to reproduce numerically the prosthesis behavior during a whole running step. Although the step is a dynamic action, it was decided to perform static structural simulations. It was hypothesized that the knowledge of the time function equations, which describe the displacement that the prosthetic system undergoes due to inertia and weight of the athlete, may allow to describe the dynamics of the step itself. Trajectories, used to define the displacement and rotation of the prosthesis during the ground contact time, and experimental GRFs, considered to validate the numerical model, were collected during an in-vivo outdoor running test session carried on by an elite paralympic athlete. Validation is done by calculating the RMSE (Root Mean Square Error), for both horizontal and vertical ground reaction forces considering experimental and numerical GRFs. In order to find a solution that allows to obtain $RMSE_y$ <10% and $RMSE_x$ <15%, three methods were found to improve the results.

Considering the model validated with the second method, it was also possible to estimate the displacement of the COP during the step, which is slightly overestimated by the numerical model without spikes, because it tends to roll more than the real prosthesis; this involves a greater backwards displacement of the centre of pressure (1 cm more).

However there is a negative aspect: this method is not repeatable to date. This means that, by analysing another step of a different run, it is not possible to find a good convergence between the GRF measures from the force platform and those valued numerically. Therefore, this method requires an improvement in the future.

Finally, since we still had a numerical running step available that guaranteed a good convergence between FEM results and experimental data, the last analyses were focused on the effect produced on the mechanical behaviour by changing the clamp position and by virtual shaping of the prosthesis, modifying the original geometry and creating a new prototype (called Shape2). In order to obtain these it was assumed that the athlete maintains the same kinematics during running when conditions just exposed change.

It was noticed that changing the position of the clamp from -4° to +4° involved, during the running step, a stiffening of the prosthetic system. This effect disagrees with results of static ϑ_G=cost bench tests, but it is in agreement with what was learned from field experience with athletes. In fact, typically athletes, during the run, perceive stiffer configurations with the clamp positioned at +4°.

More interesting results were found by changing the original geometry of the prosthesis by creating a new model (Shape2) in which the upper part of the foot was kept the same, while another shape was designed for the lower part, characterized by a single large arch of circumference. First, it was observed that, although the stiffness curves obtained in static tests shown great differences due to the larger rolling of the Shape2 prosthesis on the platform, the GRFs plot obtained during the simulation of the whole step are comparable to each other. This means that static stiffness curves are useful for studying and comparing various prostheses, but static tests do not allow us to appreciate the true behavior of a prosthesis in real conditions of use during running.

Second, it was examined that the Shape2 foot would seem better than the original Ottobock RSF. In fact, looking at the impulses, during the numerical step the Shape2 prosthesis allows to have a lower braking impulse and a higher vertical and horizontal propulsive thrust.

Clearly there is no experimental proof of this: we should have the possibility of creating a real prototype having the same shape to confirm or not such results, which can however be considered of interest.

BIBLIOGRAPHY

[1] J. Ventura e G. Shvo, «Yellow as "Non-Black": Prosthetics, Semiotics, Hermeneutics, Freedom and Function,» *The Design Journal,* 2017.

[2] A. Staros, «The SACH (solid-ankle cushion-heel) foot,» *Ortho Pros Appl J,* 1957.

[3] H. Hobara, «Running-specific prostheses: The history, mechanics, and controversy,» *Journal of the Society of Biomechanisms,* 2014.

[4] O. N. Beck, P. Taboga e A. M. Grabowski, «How do prosthetic stiffness, height and running speed affect the biomechanics of athletes with bilateral transtibial amputations?,» *Journal of The Royal Society Interface,* 2017.

[5] R. Blickhan, «The spring–mass model for running and hopping,» *J. Biomech,* 1989.

[6] R. Alexander, «Energy-saving mechanisms in walking and running,» *J. Exp. Biol.,* 1991.

[7] C. Farley, J. Glasheen e T. McMahon, «Running springs: speed and animal size,» *J. Exp. Biol.,* 1993.

[8] G. Cavagna, F. Saibene e R. Margaria, «Mechanical work in running,» *J Appl Physiol,* 1964.

[9] O. N. Beck, P. Taboga e A. M. Grabowski, «Characterizing the Mechanical Properties of Running-Specific Prostheses,» *Plos One,* 2016.

[10] J. Czernieck, A. Gitter e C. Munro, «Joint moment and muscle power output characteristics of below knee amputees during running: the influence of energy storing prosthetic feet,» *Journal of biomechanics,* 1991.

[11] Y. Sano, A. Makimoto, S. Hashizume, A. Muraia, Y. Kobayashi, H. Takemura e H. Hobara, «Leg stiffness during sprinting in transfemoral amputees with runningspecific prosthesis,» *Gait & Posture,* 2017.

[12] C. McGowan, A. Grabowski, W. McDermott, H. Herr e R. Kram, «Leg stiffness of sprinters using running-specific prostheses,» *J. R. Soc. Interface 9,* 2012.

[13] A. Grabowski, C. McGowan, W. McDermott, M. T. Beale, R. Kram e H. Herr, «Running-specific prostheses limit ground-force during sprinting.,» *Biol. Lett. 6,* 2010.

[14] A. Makimoto, Y. Sano, S. Hashizume, A. Murai, Y. Kobayashi, H. Takemura e H. Hobara, «Ground Reaction Forces During Sprinting in Unilateral Transfemoral Amputees,» *Journal of applied biomechanics,* 2017.

[15] A. Gri, «The effect of socket alignment on the running performance of elite Paralympic athletes during indoor and outdoor tests using an instrumented Running Prosthetic Foot,» 2019.

[16] G. Costa, «Design and construction of a multichannel bench test for running specific prostheses,» 2018.

[17] L. Mazzanti, «Developement of experimental methods for the static and dynamic structural characterization of running specific prostheses,» 2020.

[18] G. Meneghetti e F. Maggio, «Ansys Workbench Training,» 2017.

[19] «ANSYS Training Manual, Advanced Contact,» 2005.

[20] «ANSYS.com,» [Online]. Available: https://www.ansys.com.

[21] S. C. Bloch, Excel per Ingegneri, Apogeo, 2001.

[22] N. Petrone, G. Costa, G. Foscan, A. Gri, R. Boekestijn, G. Migliore e A. Cutti., «Collection of Structural Loads Acting on Instrumented Running Specific Prostheses during Field Tests on Elite Athletes,» 2020.

[23] G. Foscan, «Structural analysis and functional behaviour of Running Specific Prosthesis during in-vivo field tests and laboratory bench tests,» 2018.

[24] N. Petrone, «Analisi dei segnali bioingegneristici».

[25] A. B. Wilson, «Recent Advances in Above-Knee Prosthetics».

[26] Ottobock, «1E91 Runner, 1E93 Runner junior manual».

APPENDIX

Appendix A: Further numerical curves obtained during static tests

Appendix A.1: Second derivative of RSF static stiffness curves and COP trend

Clamp 0°, Ground -15°, ρ=0

Figure 1: RSP Ottobock Category 3 stiffness curve ($F_y - d_{YC}$) obtained in static test in conditions of clamp 0°, ground -15°, ρ = 0

Figure 2: Plot of the second derivative as a function of the vertical load F_{YC} (ground -15°, clamp 0°, ρ=0)

Figure 3: COP during static tests loading with clamp 0°, ground -15°, ρ = 0.

Clamp 0°, Ground +15°, ρ=0

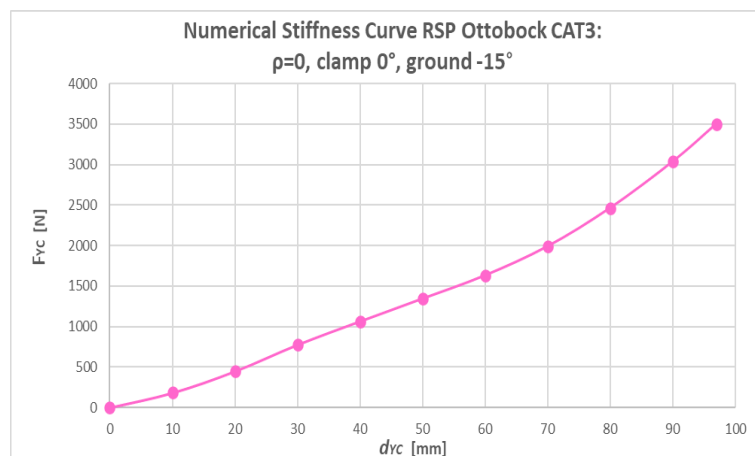*Figure 4: RSP Ottobock Category 3 stiffness curve ($F_y - d_{YC}$)*
obtained in static test in conditions of clamp 0°, ground +15°, ρ = 0

Figure 5: Plot of the second derivative as a function of the vertical
load F_{YC} (ground +15°, clamp 0°, ρ=0)

110

Figure 6: COP during static tests loading with clamp 0°, ground +15°, ρ = 0.

Clamp 0°, Ground +30°, ρ=0

Figure 7: RSP Ottobock Category 3 stiffness curve ($F_y - d_{YC}$)
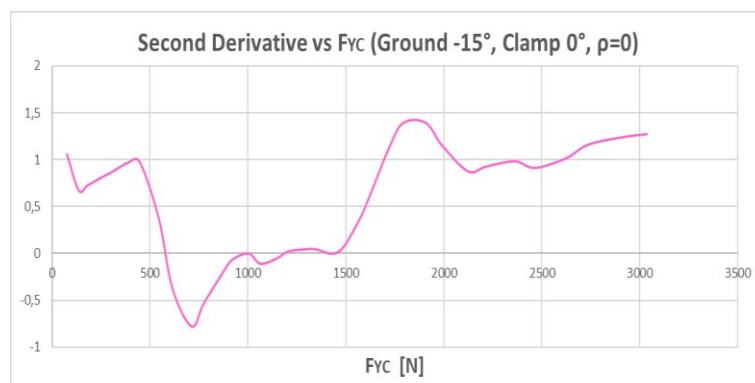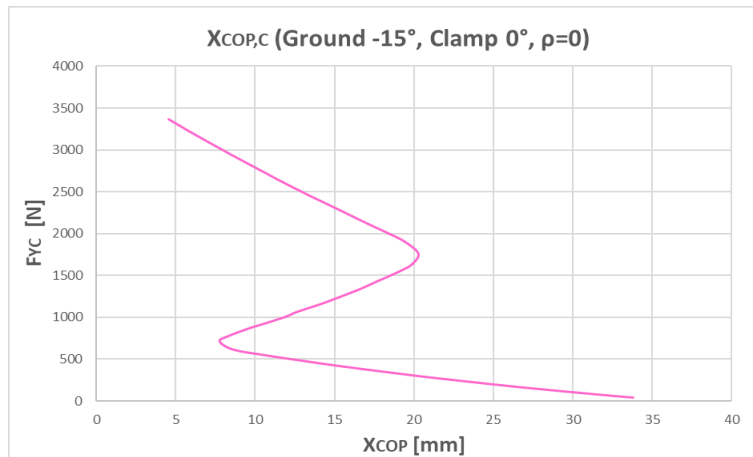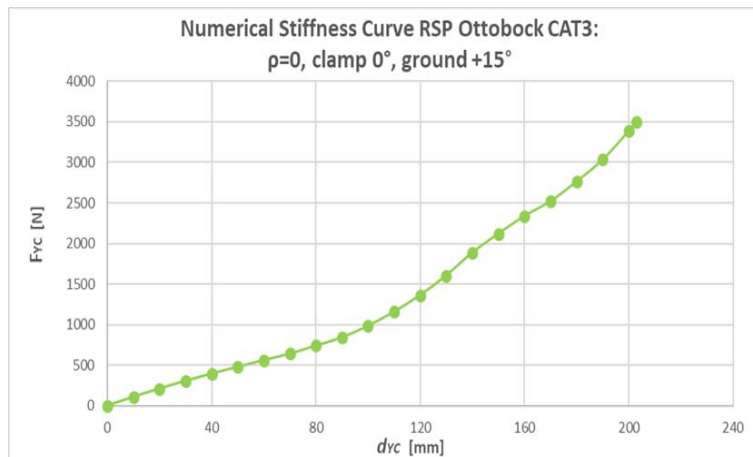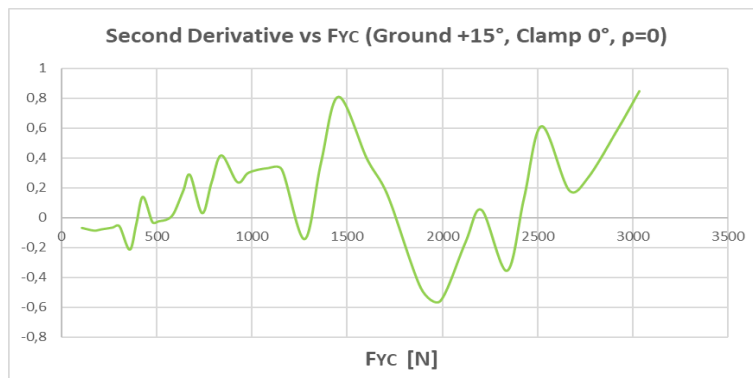obtained in static test in conditions of clamp 0°, ground +30°, ρ = 0

Figure 8: Plot of the second derivative as a function of the vertical
load F_{YC} (ground +30°, clamp 0°, ρ=0)

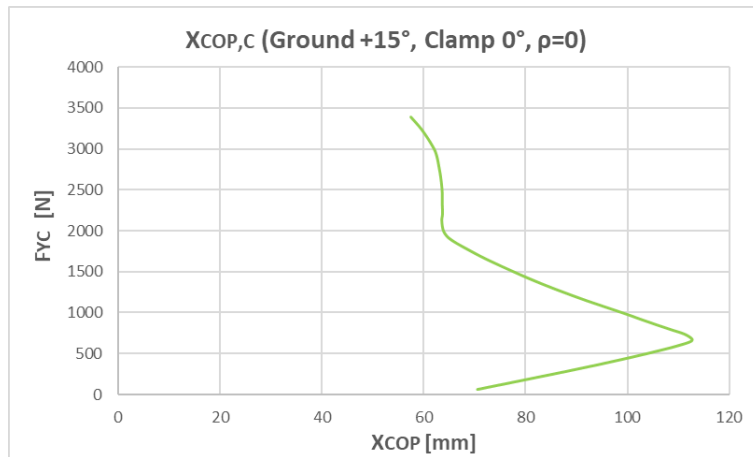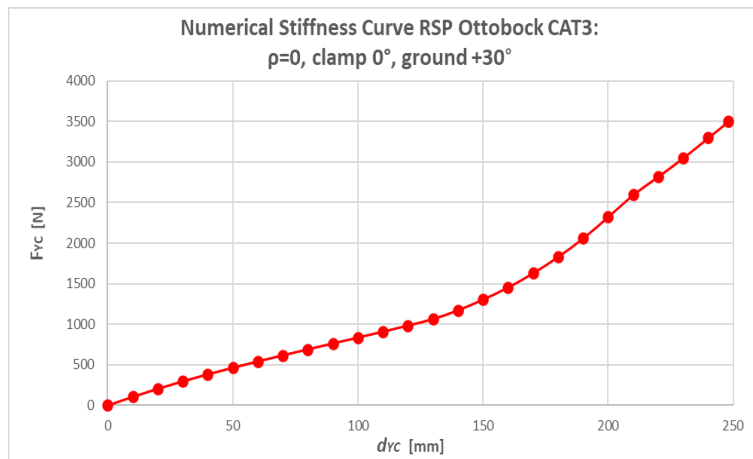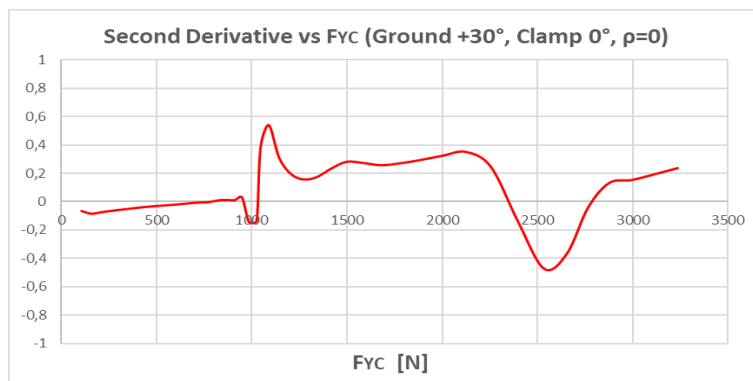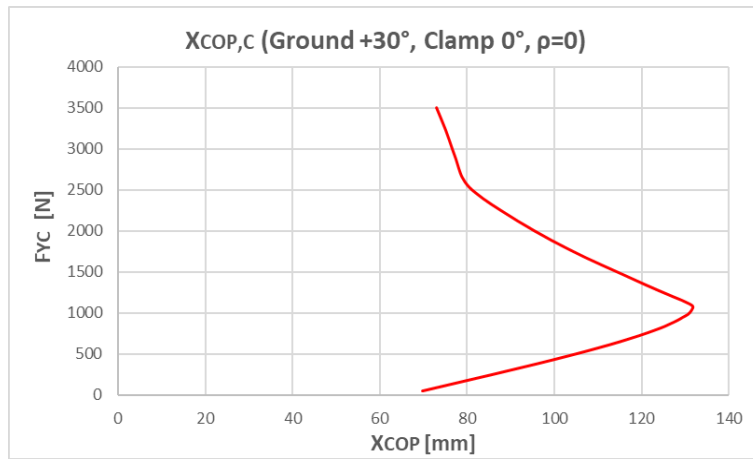*Figure 9: COP during static tests loading with clamp 0°, ground +30°, ρ = 0.*

Appendix A.2: RSF stiffness curves obtained changing the load ratio ρ (clamp 0°)

Clamp 0°, Ground -15°

Figure 10: RSP Ottobock Category 3 numerical stiffness curves ($F_{YC} - d_{YC}$) obtained in static test in conditions of clamp 0° and ground -15° when the load ratio ρ changes. Note that the prosthesis stiffness decreases from ρ=-0.2 to ρ=+0.2

ϑ_G =-15°, Clamp 0°	$\rho = -0.2$	$\rho = 0$	$\rho = +0.2$
K_L [N/mm]	35.69 (R²=0.981)	31.42 (R²=0.971)	27.15 (R²=0.954)
Δ_L[%]	+13.6	/	-13.6
K_{eq} [N/mm]	35.53	29.23	24.27
Δ_{eq}[%]	+21.6	/	-16.9

Table 1: K_L and K_{eq} values obtained in numerical static test in conditions of clamp 0° and ground -15° when the load ratio ρ changes. Δ values were calculated respect to the stiffness obtained in the case ρ=0

Clamp 0°, Ground +15°

Figure 11: RSP Ottobock Category 3 numerical stiffness curves ($F_{YC} - d_{YC}$) obtained in static test in conditions of clamp 0° and ground +15° when the load ratio ρ changes. Note that the prosthesis stiffness decreases from ρ=-0.2 to ρ=+0.2

ϑ_G =+15°, Clamp 0°	$\rho = -0.2$	$\rho = 0$	$\rho = +0.2$
K_L [N/mm]	14.89 (R^2=0.995)	14.36 (R^2=0.986)	12.90 (R^2=0.971)
Δ_L[%]	+3.7	/	-10.2
K_{eq} [N/mm]	14.29	13.04	11.45
Δ_{eq}[%]	+9.6	/	-12.2

Table 2: K_L and K_{eq} values obtained in numerical static test in conditions of clamp 0° and ground +15° when the load ratio ρ changes. Δ values were calculated respect to the stiffness obtained in the case ρ=0
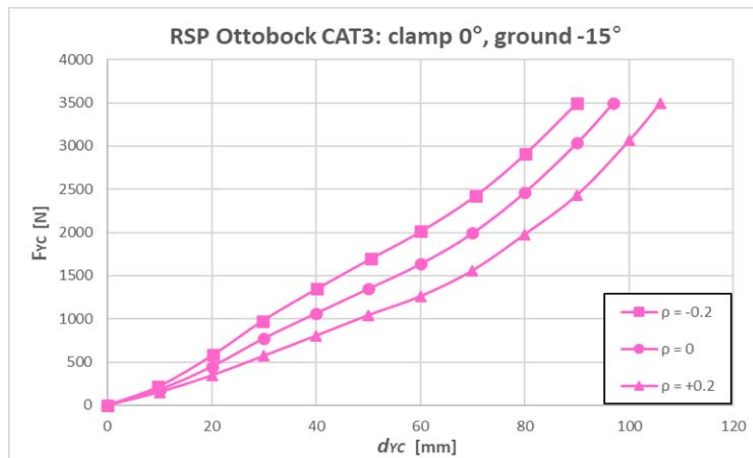
Clamp 0°, Ground +30°

Figure 12: RSP Ottobock Category 3 numerical stiffness curves ($F_{YC} - d_{YC}$) obtained in static test in conditions of clamp 0° and ground +30° when the load ratio ρ changes. Note that the prosthesis stiffness decreases from ρ=-0.2 to ρ=+0.2

ϑ_G =+30°, Clamp 0°	$\rho = -0.2$	$\rho = 0$	$\rho = +0.2$
K_L [N/mm]	12.34 (R^2=0.978)	11.68 (R^2=0.966)	10.76 (R^2=0.957)
Δ_L[%]	+5.6	/	-7.9
K_{eq} [N/mm]	11.62	10.42	9.14
Δ_{eq}[%]	+11.5	/	-12.3

Table 3: K_L and K_{eq} values obtained in numerical static test in conditions of clamp 0° and ground +30° when the load ratio ρ changes. Δ values were calculated respect to the stiffness obtained in the case ρ=0

Appendix A.3: RSF stiffness curves obtained changing the clamp position (ρ=0)
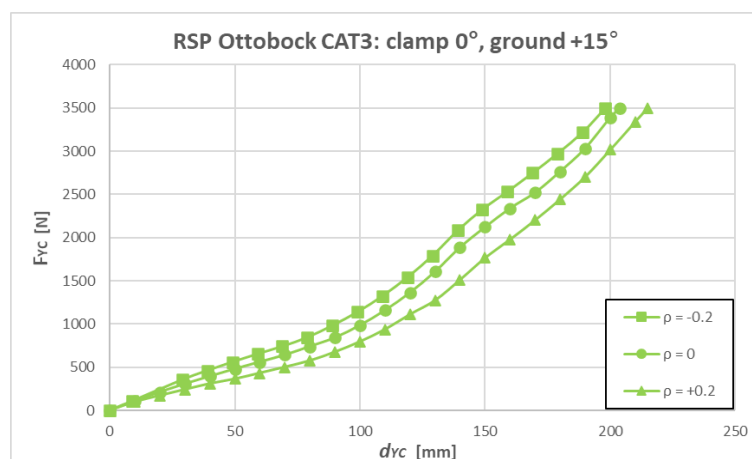
ρ=0*, Ground -15°*

Figure 13: RSP Ottobock Category 3 numerical stiffness curves (F_{YC} - d_{YC})
obtained in numerical static test in conditions of ρ=0 and ground -15° when
the clamp position changes.

ϑ_G =-15°, ρ=0	$clamp + 4°$	$clamp\ 0°$	$clamp - 4°$
K_L [N/mm]	30.75 (R²=0.988)	31.42 (R²=0.986)	33.16 (R²=0.986)
Δ_L [%]	-2.1	/	+5.5
K_{eq} [N/mm]	28.72	29.23	31.8
Δ_{eq} [%]	-1.7	/	+8.8

Table 4: K_L and K_{eq} values obtained in numerical static test in conditions of ρ=0 and ground -15° when the
clamp position changes. Δ values were calculated respect to the stiffness obtained for clamp 0°
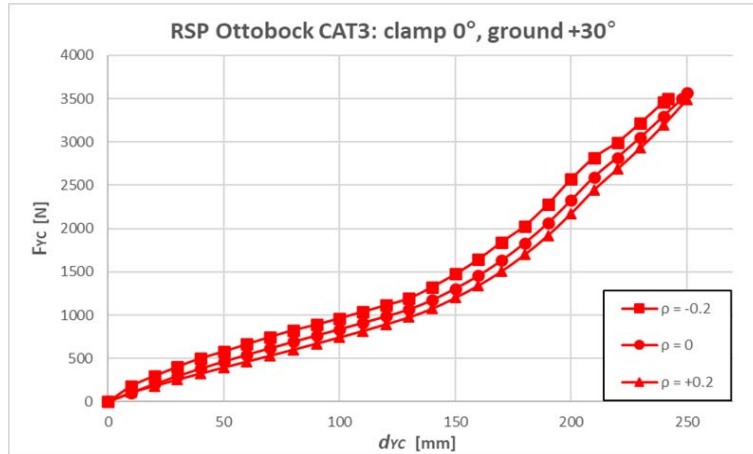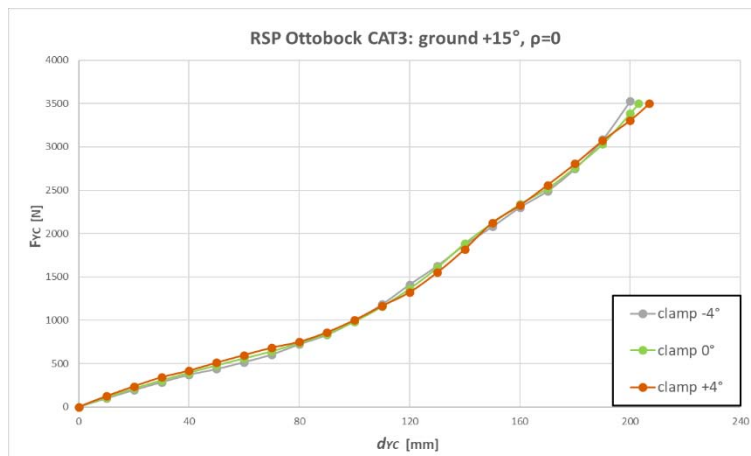
ρ=0*, Ground +15°*

Figure 14: RSP Ottobock Category 3 numerical stiffness curves (F_{YC} - d_{YC})
obtained in numerical static test in conditions of ρ=0 and ground +15° when
the clamp position changes.

ϑ_G =+15°, ρ=0	$clamp + 4°$	$clamp\ 0°$	$clamp - 4°$
K_L [N/mm]	14.32 (R²=0.973)	14.36 (R²=0.971)	14 (R²=0.967)
Δ_L[%]	-0.3	/	-2.5
K_{eq} [N/mm]	13.22	13.04	12.8
Δ_{eq}[%]	+1.4	/	-1.8

Table 5: K_L and K_{eq} values obtained in numerical static test in conditions of ρ=0 and ground +15° when the clamp position changes. Δ values were calculated respect to the stiffness obtained for clamp 0°
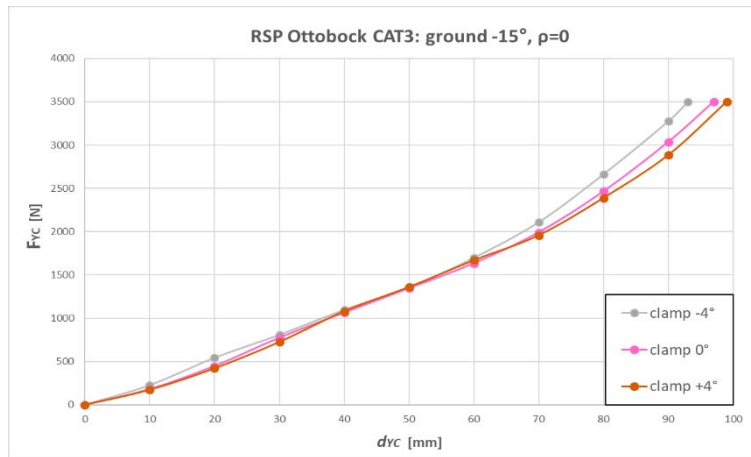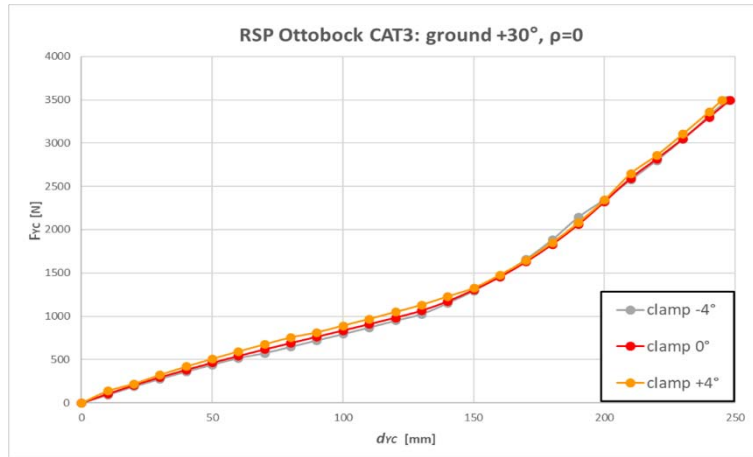
ρ=0*, Ground +30°*

Figure 15: RSP Ottobock Category 3 numerical stiffness curves (F_{YC} - d_{YC})
obtained in numerical static test in conditions of ρ=0 and ground +30°
when the clamp position changes.

ϑ_G =+30°, ρ=0	$clamp + 4°$	$clamp\ 0°$	$clamp - 4°$
K_L [N/mm]	11.63 (R²=0.970)	11.38 (R²=0.965)	11.38 (R²=0.967)
Δ_L[%]	+2.2	/	0
K_{eq} [N/mm]	10.83	10.42	10.45
Δ_{eq}[%]	+3.9	/	+0.3

Table 6: K_L and K_{eq} values obtained in numerical static test in conditions of ρ=0 and ground +30° when the clamp position changes. Δ values were calculated respect to the stiffness obtained for clamp 0°

## Appendix A.4: Further maps of numerical stiffness curves

Clamp 0°, ρ=-0.2

Figure 16: Map of numerical stiffness curves ($F_{YC} - d_{YC}$) obtained in static test in conditions of clamp 0° and ρ=-0.2 when the ground inclination changes. Both the numerical curves (continuos line) and the experimental curves (dashed line) are reported

ϑ_G [deg]	d_{YC} [mm]	$F_{YC,exp}$ [N]	$F_{YC,FEM}$ [N]	$err_{F_{YC}}$ [%]
-15	20.2	528	592	12.1
-15	34.3	1027	1120	9.06
-15	47.6	1512	1588	5.03
0	38.8	505	530	4.95
0	62	1016	1067	5.02
0	79.5	1520	1560	2.63
+15	41.2	481	491	2.08
+15	85.1	972	917	5.66
+15	114.2	1500	1448	3.47
+30	39.8	471	500	6.16
+30	99	932	960	3.00

Table 7: Summary table of $err_{F_{YC}}$ calculated considering numerical and experimental values of F_{YC} for a given clamp displacement d_{YC} (clamp 0°, ρ=-0.2)

Average percentage error $\overline{err_{F_{YC}}}$ = 5.4%.

Figure 17: Map of numerical stiffness curves ($F_{YC} - d_{YC}$) obtained in static test in conditions of clamp 0° and ρ=+0.2 when the ground inclination changes. Both the numerical curves (continuos line) and the experimental curves (dashed line) are reported

ϑ_G [deg]	d_{YC} [mm]	$F_{YC,exp}$ [N]	$F_{YC,FEM}$ [N]	$err_{F_{YC}}$ [%]
-15	26.3	523	510	2.49
-15	46.6	1008	993	1.49
-15	63.7	1524	1456	4.46
0	48.7	480	417	13.1
0	76.2	1005	930	7.46
0	97.5	1505	1412	6.18
+15	55.1	472	415	12.0
+15	102.1	971	851	12.3
+15	130.8	1483	1393	6.07
+30	57.5	478	462	3.35
+30	120.8	940	888	5.53

Table 8: Summary table of $err_{F_{YC}}$ calculated considering numerical and experimental values of F_{YC} for a given clamp displacement d_{YC} (clamp 0°, ρ=+0.2)

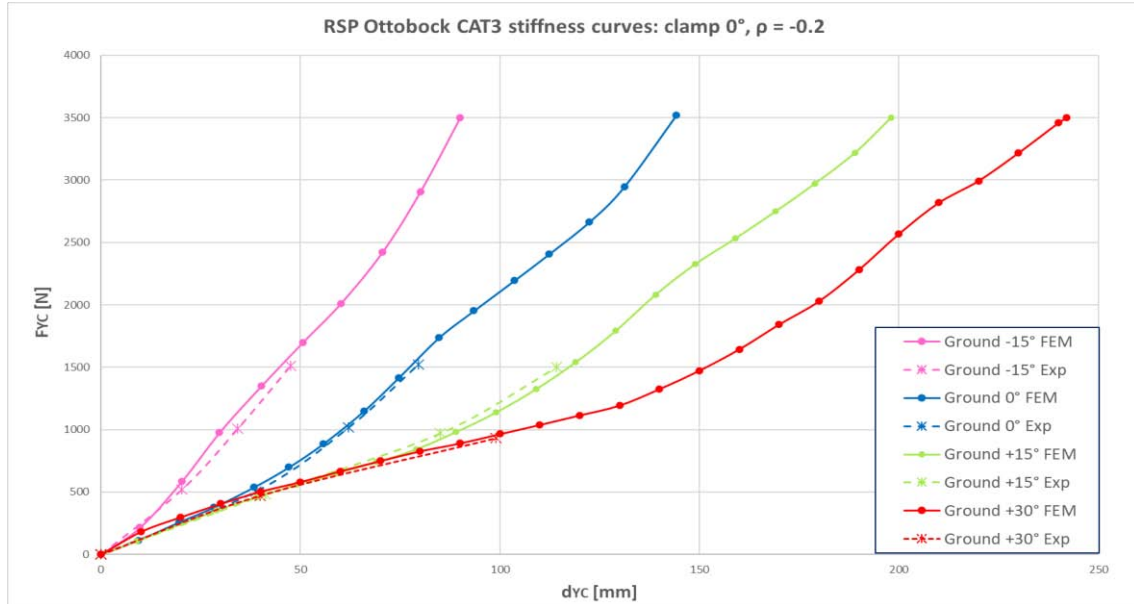Average percentage error $\overline{err_{F_{YC}}}$ = 6.8%.

Clamp -4°, ρ=0

Figure 18: Map of numerical stiffness curves ($F_{YC} - d_{YC}$) obtained in static test in conditions of clamp -4° and ρ=0 when the ground inclination changes. Both the numerical curves (continuos line) and the experimental curves (dashed line) are reported

ϑ_G [deg]	d_{YC} [mm]	$F_{YC,exp}$ [N]	$F_{YC,FEM}$ [N]	$err_{F_{YC}}$ [%]
-15	22.5	521	608	16.7
-15	40.6	1011	1101	8.9
-15	57.2	1519	1592	4.8
0	59.4	783	829	5.8
0	68.9	1000	1079	7.9
0	90.2	1513	1568	3.6
+15	50.4	476	446	6.3
+15	94.3	957	904	5.5
+15	121.7	1480	1443	2.5
+30	53.5	480	481	0.2
+30	117.2	948	910	4

Table 9: Summary table of $err_{F_{YC}}$ calculated considering numerical and experimental values of F_{YC} for a given clamp displacement d_{YC} (clamp -4°, ρ=0)
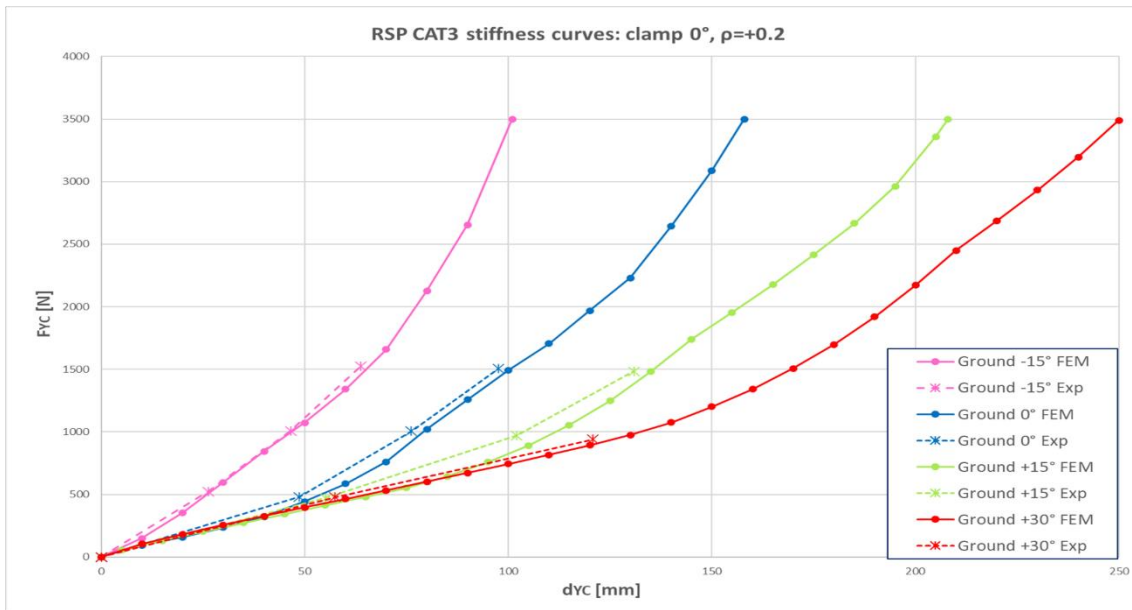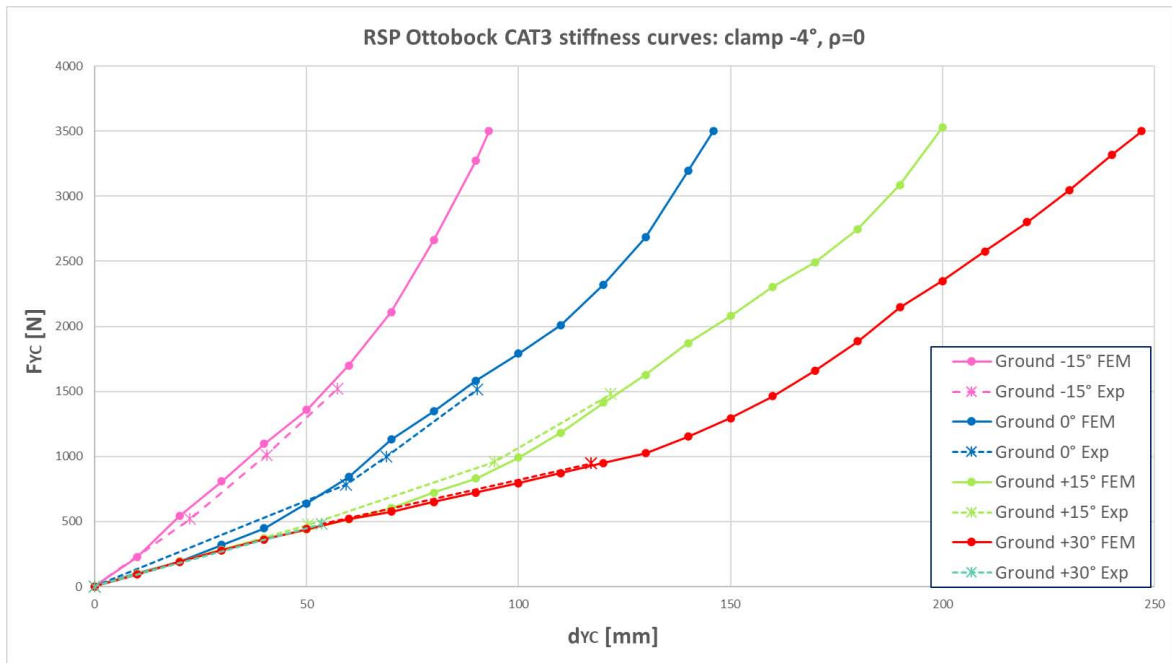
Average percentage error $\overline{err_{F_{YC}}}$ = 6%.
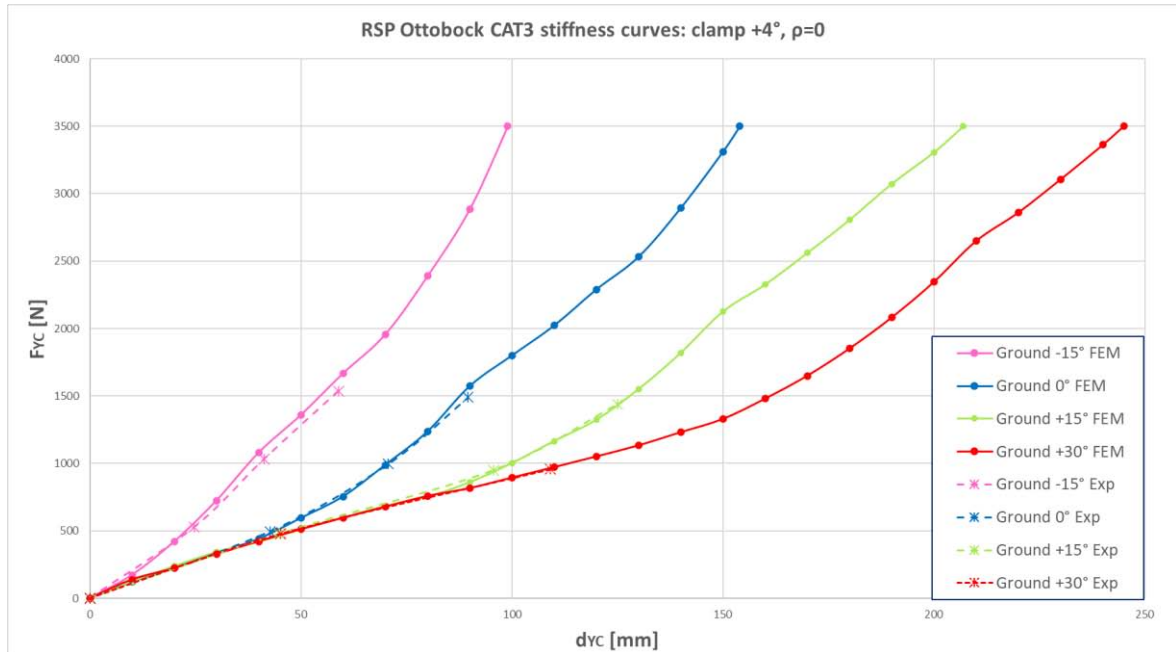
Figure 19: Map of numerical stiffness curves ($F_{YC} - d_{YC}$) obtained in static test in conditions of clamp +4° and ρ=0 when the ground inclination changes. Both the numerical curves (continuos line) and the experimental curves (dashed line) are reported

ϑ_G [deg]	d_{YC} [mm]	$F_{YC,exp}$ [N]	$F_{YC,FEM}$ [N]	$err_{F_{YC}}$ [%]
-15	24.7	526	532	1.1
-15	41.3	1032	1077	4.4
-15	58.9	1536	1582	3
0	42.7	496	479	3.4
0	70.7	997	986	1.1
0	89.6	1491	1530	2.6
+15	44.8	477	478	0.2
+15	95.6	949	930	2
+15	125.1	1438	1464	1.8
+30	45.2	477	473	0.8
+30	109.1	957	956	0.1

Table 10: Summary table of $err_{F_{YC}}$ calculated considering numerical and experimental values of F_{YC} for a given clamp displacement d_{YC} (clamp +4°, ρ=0)

Average percentage error $\overline{err_{F_{YC}}}$ = 1.9%.

Appendix B

| time [s]	$GRFx$ [N]	$GRFy$ [N]	ϑ_{Foot} [deg]	ϑ_G [deg]	F_{XC} [N]	F_{YC} [N]	ρ
0	-104	-58	-28,5	-20,5	-117	-18	6,45
0,005	-204	493	-26,4	-19,1	-32	533	-0,06
0,01	-249	853	-24,4	-17,5	20	888	0,02
0,015	-274	1177	-22,5	-16,0	62	1207	0,05
0,02	-265	1417	-20,7	-14,5	99	1438	0,07
0,025	-234	1630	-19,0	-13,0	138	1641	0,08
0,03	-211	1801	-17,4	-11,5	152	1807	0,08
0,035	-211	1915	-15,9	-10,0	123	1922	0,06
0,04	-194	2002	-14,4	-8,5	102	2008	0,05
0,045	-163	2053	-12,9	-6,9	86	2058	0,04
0,05	-108	2063	-11,4	-5,4	88	2064	0,04
0,055	-68	2020	-9,9	-3,9	69	2020	0,03
0,06	-48	1937	-8,3	-2,4	33	1938	0,02
0,065	2	1856	-6,9	-0,9	30	1856	0,02
0,07	27	1742	-5,5	0,6	7	1742	0,00
0,075	53	1639	-4,1	2,2	-8	1640	-0,01
0,08	79	1541	-2,7	3,7	-20	1543	-0,01
0,085	94	1421	-1,4	5,2	-35	1423	-0,02
0,09	124	1316	0,0	6,7	-31	1322	-0,02
0,095	151	1200	1,5	8,2	-22	1209	-0,02
0,1	149	1044	3,0	9,7	-29	1054	-0,03
0,105	159	892	4,6	11,3	-18	906	-0,02
0,11	162	732	6,2	12,8	-4	749	0,00
0,115	134	525	7,8	14,3	0	542	0,00
0,12	116	322	9,3	15,8	24	341	0,07
0,125	65	103	10,9	17,3	31	118	0,27
0,129	5	-55	12,2	18,5	22	-50	-0,44

Table 11: Summary Table of step number 8 of the RUN9 registered on 19/04/2019. The forces F_{YC} and F_{XC} shown in the Table are those reported in the clamp reference system (+4° configuration).

Appendix C

Time [s]	ϑ_G [deg]	$x_{G,Clamp}$ [mm]	$y_{G,Clamp}$ [mm]	$x_{G,COP}$ [mm]	$y_{G,COP}$ [mm]	x_{ROS} [mm]	y_{ROS} [mm]
0,000	-17,1	-80,6	265,6	4,7	0	3,3	-278,9
0,005	-13,7	-78,7	253,5	-11,7	0	4,9	-262,2
0,010	-12,3	-76,4	241,0	-19,1	0	4,6	-247,6
0,015	-9,4	-73,5	231,6	-21,8	0	13,3	-236,9
0,021	-7,4	-69,7	224,6	-23,3	0	17,1	-228,7
0,025	-4,8	-65,8	220,5	-23,7	0	23,8	-223,2
0,030	-2,9	-59,9	216,7	-23,4	0	25,6	-218,2
0,035	-0,5	-52,9	214,0	-22,2	0	28,7	-214,2
0,040	2,1	-44,8	212,0	-20,5	0	32,0	-211,0
0,045	5,3	-36,0	210,6	-18,0	0	37,5	-208,0
0,050	8,5	-26,4	209,6	-13,1	0	44,2	-205,3
0,055	11,4	-16,2	208,8	-3,7	0	53,4	-202,2
0,061	14,2	-5,4	208,3	7,4	0	63,5	-198,8
0,065	19,1	3,6	208,1	16,9	0	80,6	-192,3
0,070	21,6	15,5	208,3	29,9	0	89,9	-188,4
0,075	25,0	28,4	208,9	43,9	0	102,2	-182,9
0,080	28,6	42,3	210,2	57,4	0	113,8	-177,4
0,085	32,3	57,8	212,2	69,4	0	123,3	-173,1
0,090	36,5	75,1	215,0	71,9	0	125,3	-174,8
0,095	40,2	94,6	218,6	72,8	0	124,3	-181,1
0,101	42,1	116,6	222,8	73,2	0	117,0	-194,5
0,105	44,5	136,2	226,5	73,3	0	114,0	-205,6
0,110	47,0	163,2	231,1	73,3	0	107,7	-223,4
0,115	47,4	193,1	235,4	73,4	0	92,1	-247,5
0,120	49,7	225,6	238,5	73,7	0	83,7	-270,0

Table 12: Summary Data Table for ROS numerical evaluation (RUN14)

RINGRAZIAMENTI

Con la scrittura di questa ultima pagina giunge al termine il mio percorso universitario.

Vorrei ringraziare in primo luogo tutta la mia famiglia, in particolare i miei genitori e mia sorella Valentina, che mi hanno dato l'opportunità di studiare e intraprendere questa esperienza che sarà sicuramente fondamentale per il mio futuro. Sono certo che continueranno a gioire per ogni obiettivo che raggiungerò, come hanno sempre fatto in tutti questi anni.

Ringrazio Barbara che mi ha sempre sostenuto, spronato ed è riuscita a tirate fuori il meglio di me in questi anni insieme, accompagnandomi verso questo importante traguardo.

Voglio ringraziare gli amici di una vita Campa, Toni, Marco, Fede, Luca e Andrea che per me sono sempre fondamentali, nonostante i meno frequenti momenti di incontro.

Ringrazio i coinquilini Albri e Toppy con cui ho trascorso cinque anni bellissimi in appartamento a Padova. Non dimenticherò mai tutti i momenti felici e sereni che abbiamo trascorso cucinando insieme, facendoci scherzi e guardando centinaia di serie tv diverse.

Grazie ai compagni di corso Nicola, Matteo e Michele con cui ho condiviso questa avventura universitaria, tra libri e appunti, gioie e dolori, ma anche aperitivi, pizze e grandi risate.

Questo lavoro probabilmente non sarebbe mai nato senza l'aiuto del professore Petrone, relatore di questa tesi. Lo ringrazio per la sua gentilezza, le sue intuizioni e osservazioni che mi hanno permesso di cambiare spesso il punto di vista da cui osservare il problema. Grazie a lei ho davvero imparato molto.

Infine ringrazio tutti i ragazzi del laboratorio di Costruzione di Macchine per i preziosi consigli e i momenti di confronto durante lo svolgimento della tesi, ma anche per tutte le chiacchiere e i momenti di svago.